EFFECTS OF CONTROL HYSTERESIS

ON THE SPACE SHUTTLE ORBITER'S ENTRY

By

Richard Wayne Powell

B.S. in Aerospace Engineering

Virginia Polytechnic Institute

June 1970

A Thesis submitted to

the Faculty of

The School of Engineering and Applied Science

of The George Washington University in partial satisfaction

of the requirements for the degree of Master of Science

(NASA-TM-X-74681) EFFECTS OF CONTROL HYSTERESIS ON THE SPACE SHUTTLE ORBITER'S ENTRY M.S. Thesis - George Washington Univ. (NASA) 109 p HC A06/MF A01 CSCL 22C N77-21139 Unclas G3/13 22867

June 1975

Thesis directed by

Dr. Manuel J. Queijo

ACKNOWLEDGEMENTS

The author is indebted to the National Aeronautics and Space Administration for permission to use Space Shuttle program-related research material in this thesis. The author wishes to express his sincere appreciation to Mr. Howard W. Stone of the Langley Research Center for his guidance in the inception of this project, and to Dr. Manuel J. Queijo for his assistance in the preparation of this thesis. Special thanks are extended to Mrs. Carol M. Forrest and Mrs. JoAnn W. Hudgins for their invaluable assistance in the typing of and figure preparation for the manuscript.

TABLE OF CONTENTS

I. LIST OF FIGURES

II. LIST OF TABLES

III. LIST OF SYMBOLS

SYMBOL	UNIT	DEFINITION
b	m	wing span
$\bar{c}$	m	reference chord
C_ℓ	n.d.	rolling moment coefficient $[L/(\bar{q}Sb)]$
C_m	n.d.	pitching moment coefficient $[M/(\bar{q}S\bar{c})]$
C1	n.d.	"control hysteresis" coefficient
C2	deg	"control hysteresis" equivalent aileron deflection
g	m/sec^2	acceleration of gravity
k_p		multiplier in $\delta_{a,c}$ block diagram
L	N·m	rolling moment
M	n.d.	Mach number
M	N·m	pitching moment
n.d.		non-dimensional
p	deg/sec	roll rate about the body axis
Pa	N/m^2	Pascal
$\bar{q}$	Pa	dynamic pressure
r	deg/sec	yaw rate about the body axis
r'	deg/sec	$r-(180\ g \sin(\phi) \cos(\theta))/V$
s		Laplacian operator
S	m^2	wing reference area

t	sec	time
V	m/sec	velocity
α	deg	angle-of-attack
β	deg	sideslip angle
δ_a	deg	aileron deflection
$\dot{\delta}_a$	deg/sec	$d\delta a/dt$
$\delta_{a,c}$	deg	commanded aileron deflection
$\delta_{a,UD}$	deg	aileron deflection from up-down counter
θ	deg	pitch angle about the body axis
ϕ	deg	roll angle about the body axis

IV. INTRODUCTION

An aerodynamic phenomena which sometimes occurs is a variation of an aerodynamic force with control surface deflection which depends on the control direction of motion of the surface. This effect, which can appear as illustrated in the following sketch, is referred to as "control hysteresis."

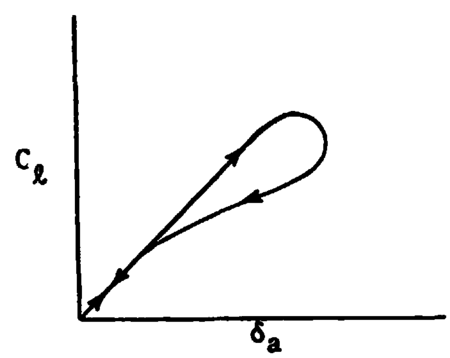

Arrows indicate direction of control deflection.

Using wind-tunnel data from early shuttle configurations and simplified wing-body shapes, J. Peter Reding and Lars E. Ericson of the Lockheed Missiles and Space Company, under a contract for the NASA Johnson Space Center, identified "control hysteresis" as a possible problem area for the space shuttle orbiter's entry (reference 1). They showed that regions of shock-induced separated flow might be expected to exist on the leeward wing surface, and that upward deflected control surfaces affect the extent of the separation. Bow shock-control surface shock interactions can take place ahead of the elevon deflected downward into the wind. Also, movement of a control surface into a wing leading edge, wing fillet, or nose vortex can cause the vortex to burst. Lags in re-establishing flow field equilibrium may result from these phenomena and thus "control hysteresis" or a dependency upon the direction of control surface deflection may exist. Before discussing the possible ramifications of "control hysteresis," an examination of the orbiter's control philosophy is needed.

In the normal operational mode, the space shuttle orbiter entry is directed by on-board computers from deorbit through landing. Attitude is controlled by both aerodynamic control surfaces and a reaction control system (RCS) consisting of twenty (20) 4000 N (900 lb) thrust, hypergolic-fueled rockets. The aerodynamic surfaces include elevons (acting as both elevators and ailerons), rudder, speed brakes, and body flap. The speed brake and body flap deflections are determined from preset tables. The elevons, as elevators, are used for longitudinal control; as ailerons, they are used either for turn coordination (angle of attack (α) > 18° or Mach number (M) > 5), or for roll attitude control (α < 18° and M < 5). When the ailerons are being used for roll attitude control, the rudder is used for turn coordination, otherwise it is inoperative. The RCS provides rolling, pitching, and yawing moments. The roll RCS, operative until a dynamic pressure of 479 Pa (10 psf) is sensed, aids the ailerons in turn coordination. The pitch RCS, operative until a dynamic pressure of 958 Pa (20 psf) is sensed, aids the elevators in longitudinal control. The yaw RCS is used in two modes. For α > 18° or M > 5, the yaw RCS is used for roll attitude control. This is done by using the yaw thrusters to produce sideslip and then allowing the orbiter's positive dihedral effect to roll the vehicle. When $\alpha \leq 18°$ and M ≤ 5, the yaw RCS augments the rudder. If "control hysteresis" is present in the ailerons, the most active aerodynamic control during entry, two possible situations exist, depending on the flight conditions. If α > 18° or M > 5, the ailerons may be unable to properly coordinate the turn, because as the ailerons deflect, moving first one direction and then the other, "hysteresis" will result in different aerodynamic moments for the same deflection angle.

In addition, at these flight conditions, a lateral trim network is fed to the commanded aileron circuit to minimize RCS propellant consumption due to lateral center-of-gravity offsets and cross-wind effects. This network causes slight uncoordination of a roll maneuver resulting in the ailerons overshooting the proper position and therefore requiring a reversal in the direction of the surface movement. Thus, the error signal in the commanded aileron circuit will oscillate about zero. If this oscillation is larger than any built-in deadband, the ailerons will also oscillate. Since the turn coordination signal is also fed to the roll thrusters, while they are operational, and yaw rate and roll angle error signals are fed to the yaw thrusters, "hysteresis" in the ailerons aerodynamic moments could result in alternate (positive then negative) thruster firings, and sharply increase fuel consumption. When the ailerons are used for roll control ($\alpha \leq 18°$ and $M \leq 5$), hysteresis could result in the orbiter continuously hunting to reach the commanded roll angle, i.e. orbiter oscillating about the commanded roll angle, and since turn coordination is the responsibility of the rudder augmented by the yaw thrusters, this oscillation cou d produce alternate yaw thruster firings. Thus, the major effect of "control hysteresis" was expected to be an increase in the amount of RCS fuel required for entry. Since the amount of fuel that is carried is limited, this increase could result in poor control of the orbiter, and limit its maneuverability.

Wind-tunnel tests using a remotely controlled elevon model were conducted in the NASA-Langley Research Center's Continuous Flow Hypersonic Tunnel at a Mach number of 10.3. ..'ta, taken at 40 frames/sec as the elevons were driven through their operational range, revealed some evidence of hysteresis. The low Strouhal number (the model elevon rate of seven (7) deg/sec corresponds to a full-scale rate of only 0.175 deg/sec), and low Reynolds number (1.0×10^6 based on length for the model as compared to approximately 5.0×10^6 full scale), made the determination of the amount of full-scale "control hysteresis" impossible. Consequently, a six (6)-degree-of-freedom analysis was conducted to determine the system tolerance to hysteresis.

Hysteresis was modeled by offsetting and/or modifying the slope of the roll due to aileron such that the values of the rolling moment changed with the direction of control surface travel.

In mid 1973, development of a simulator to examine automated spacecraft entries was begun by the author, et al, specifically to examine this and other problems associated with the space shuttle orbiter's entry. It is a six (6)-degree-of-freedom, interactive simulator known as the Automatic Flight Dynamics Simulator, ARFDS (reference 2). ARFDS was modified to include "control hysteresis" and an analysis of the entry was made to examine the impact of this potential problem. This analysis is the subject of this thesis.

V. SPACE SHUTTLE SYSTEM DESCRIPTION

The physical characteristics of the space shuttle that were used are summarized in Table 1. The guidance scheme utilized is described in Appendix A, and the control system is described in Appendix B. The control and guidance scheme are applicable from deorbit to the Terminal Area Energy Management (TAEM) interface which occurs at 457.2 m/sec (1500 fps) and an altitude of 21.3 km (70 000 ft).

The entry in the automatic mode is directed entirely by on-board computers. The guidance system software produces a series of angle-of-attack and roll attitude commands that the control system software utilizes to direct the RCS and surface deflections.

VI. WIND TUNNEL RESULTS

Wind-tunnel tests were conducted in the NASA Langley Research Center's Continuous Flow Hypersonic Tunnel of a space shuttle orbiter model with remotely controlled elevons (both left and right elevons move together). Data were taken at 40 frames/sec. as the elevon was driven between its limits (-40° to 15° to -40°) at seven (7) degs/sec. Figure 1 shows pitching moment (C_m) data fairings from these tests which indicate that "control hysteresis" may be present. The "control hysteresis" observed in the data is very close to the balance accuracy; however, these trends repeated for all cases that were run, indicating a strong possibility that "control hysteresis" did exist.

Test parameters including a low Strouhal number (model elevon rate scaled to a full scale rate of only 0.175 deg/sec.) and a low Reynolds number (1.0×10^6 based on length as compared to 5.0×10^6 full scale) made it impossible to predict the amount of full-scale "control hyste-hysteresis" that might be expected. Therefore, some analysis of the system tolerance to control hysteresis was needed.

VII. AUTOMATIC REENTRY FLIGHT DYNAMICS SIMULATOR (ARFDS) DESCRIPTION

In mid 1973, development was begun on a new interactive simulator capable of handling studies of automated spacecraft entries, namely, space shuttle. Up to that time, studies had been made at the NASA Johnson Space Center (JSC) and by the author using a batch mode computer program known as G.E. Mass.* The new simulator was developed by personnel of the Analysis and Computation Division of the NASA Langley Research Center after being provided suitable equations and overall program logic by the author. The simulator is known as the Automatic Reentry Flight Dynamics Simulator, ARFDS, (see reference 2), and it has the following advantages over G.E. Mass:

1. Interactive capability.

2. Faster integration and table look-up capability.

3. Separate time channels for guidance, control, and the equations of motion.

4. Entry states can be observed on strip charts as well as printed output.

The checkout of ARFDS was the responsibility of the author. To do this, the G.E. Mass Program was modified to simulate a typical shuttle entry problem. The author independently programed the control scheme, adapted a

---

*Written under contract to the Manned Spacecraft Center and was available in 1963.

guidance system routine* obtained from the shuttle program office at JSC, added an appropriate viscous aerodynamic model, added a reaction control system model complete with aerodynamic interference effects, and modified the integration routines to allow for a one (1) pass method for integration of the filters in the control system.

The analysis described herein was performed on the checked out version of ARFDS to take advantage of the speed, ease of modification, and strip charts. For this analysis, models to simulate aerodynamic control hysteresis were added to ARFDS.

*The guidance routine was rewritten for ARFDS to increase efficiency - see Appendix A.

VIII. SIMULATION APPROACH

Since nominal entry runs had indicated that the elevons are more active as ailerons than as elevons, an investigation was made with ARFDS where "control hysteresis" was added to the rolling moment (C_ℓ) due to aileron deflection (δ_a). This moment was chosen because:

(1) Possible causes of "control hysteresis" such as separation and vortex burst would predominantly effect wing lift or normal force which determines the amount of rolling moment produced.

(2) The rolling moment is the primary control output of the aileron for which the control system is designed.

"Control hysteresis" was added to C_ℓ due to δ_a in two (2) different manners as shown in figure 2. Figure 2a shows the first method where if the aileron deflection is increasing ($\dot{\delta}_a$ positive), the nominal value of C_ℓ is used; if the deflection is decreasing ($\dot{\delta}_a$ negative), the nominal value of C_ℓ is multiplied by C1. This changes the slope of the C_ℓ vs. δ_a values. C1 was varied from 0.5 to 1.5, providing a $\pm$ 50 percent change in the slope. For small values of δ_a, C1 would have little effect on C_ℓ, as this method allows for no displacement of the origin. To correct this deficiency, an increment, C2 (figure 2b), was added to the nominal value if $\dot{\delta}_a$ was negative. C2 was expressed as an equivalent aileron deflection, e.g. C2 was equal to x° of aileron and therefore C2 was a function of M and α. C2 was varied between $\pm$ 5° of aileron (the maximum δ_a experienced in any of these cases was less than 10°). Figure 2c shows the range of hysteresis covered by this study for Mach four (4) and Mach numbers greater than ten (10). This range was felt to be greater than would be experienced by the orbiter.

The aileron deflection remains zero (0) until a dynamic pressure ($\bar{q}$) of 96 Pa (2 psf) is reached (nominally 320 seconds after deorbit). The simulation on ARFDS was initiated at this point and continued until the TAEM interface conditions are encountered.

IX. DISCUSSION OF RESULTS

The results of simulations for the nominal conditions (C1 = 1, C2 = 0) with a guidance system sampling time of 0.32 seconds and a control system sampling time of 0.04 seconds is shown on time history strip charts shown in figure 3. As indicated previously and in Appendix B, the ailerons are used for turn coordination until α is reduced to 18°, ≈1720 seconds from deorbit. After that time, the ailerons are used for Φ control, and the rudder assumes the coordination role. Times of increased aileron activity, namely between 400 and 500 seconds where Φ increases from -15° to -75° and after 1500 seconds where roll reversals occur, are times of increased RCS firings. Thus, it was expected that adding hysteresis would increase the RCS firings at these points and result in more fuel consumption. Figures 4 and 5 show the effect of reducing C1 to 0.7 and 0.5, respectively. Neither of these cases are significantly different from the nominal, either in the δ_a or the RCS thruster history. Returning C1 to its nominal value of 1.0 and applying C2 values of -2° (figure 6) and -5° (figure 7) produced similar results as did the combination of C1 = 0.5 and C2 = -5 (figure 8). On a batch version of ARFDS (no strip charts), cases for C1 = 1.5 with C2 = 0, and C1 = 1 with C2 = 5, were also run. Table II shows the RCS fuel consumption for all these cases and they fall within six (6) percent of the nominal.

During the time of the present study, it became evident to the NASA Johnson Space Center and the contractor that the on-board-computers could become over-burdened by the many assigned tasks (flight control, guidance and navigation functions, redundancy management, etc.). It appeared desirable therefore to require guidance calculations infrequently as possible. Guidance system design studies at NASA Johnson Space Center had shown that guidance system sampling every 2.0 seconds was sufficient for proper targeting. When the guidance system sampling time was increased from 0.32 seconds to 2.0 seconds, the author, et al, in reference 3, found that the RCS yaw thrusters would limit cycle causing the RCS fuel consumption to double. Three (3) system changes were identified that eliminate this limit cycling and actually result in a 37 percent reduction in fuel consumption from 320 seconds in the entry to the TAEM interface over the nominal case identified earlier. The three system changes are:

1. Replacement of the step changes in commanded angle-of-attack and roll attitude with a linear variation (ramp-like).

2. Modification of two (2) gains in the control circuit.

Figures 9-14 show the results of applying "control hysteresis" to the simulation with the revised system, and again "control hysteresis" makes little difference in control surface and vehicle motion time histories. Table III shows the fuel consumption due to hysteresis with revised guidance.

Examination of the time history strip charts for both the nominal (0.32 second sampling time) and revised guidance (2.00 seconds sampling time with system change) cases reveals that for most of the entry, $\dot{\delta}_a$ is zero (0). Examination of the $\delta_{a,c}$ block diagram, figure 15, reveals that this must be due to the error signal remaining within the deadband for most of the entry, and this is probably preventing the "control hysteresis" from having any significant effect. Consequently, this filter was removed from the circuit, and both a nominal (C1 = 1, C2 = 0) case, and a "control hysteresis" case (C1 = 0.5, C2 = -5) were run (figures 16 and 17) with the nominal guidance (0.32 second sampling time). The aileron without the deadband becomes a continuously moving control, and hysteresis results in significant increases in RCS fuel consumption (see Table IV, where a C1 of 0.5 and C2 of -5 results in a 37 percent increase in fuel consumption over the C1 of 1.0 and C2 of 0 case). Thus, the deadband filter in the aileron circuit is acting to suppress the effects of any "control hysteresis" over the range of C1 and C2 tested. There is no deadband filter in the elevator circuit, but since the elevator moves so slowly and pitch rates are quite small during the nominal entry, there is probably no problem. If, however, due to mission change, or in the presence of wind gusts, etc., the elevator becomes a more active control, a deadband filter will probably be required to suppress the effects of control hysteresis. This possibility should be the subject of a future study.

X. CONCLUDING REMARKS

A study by J. Peter Reding and Lars E. Ericson of the Lockheed Missiles and Space Company identified "control hysteresis" as a possible problem area for the space shuttle orbiter's entry. This "control hysteresis" phenomena was detected in the NASA Langley Research Center's Continuous Flow Hypersonic Tunnel using a remotely controlled elevon model. Consequently, a six (6)-degree-of-freedom-simulation examination was conducted on the space shuttle orbiter's entry to determine if "control hysteresis" in the rolling moment due to aileron deflection has any major effects on the controllability of the orbiter or required reaction control system fuel consumption. "Control hysteresis" was modeled by offsetting and/or modifying the slope of the roll due to aileron such that the value of the rolling moment changed with the direction of control surface travel.

The simulations indicated that the orbiter system can tolerate "control hysteresis" that produces a 50 percent change in the nominal characteristics, or an offset in the nominal characteristics equivalent to a five (5) degree aileron deflection with little increase in the required reaction control system's fuel consumption. This tolerance was traced to a deadband filter in the commanded aileron circuit. Removal of this filter results in significant increases in fuel consumption. Thus, "control hysteresis" in roll due to aileron is not a problem with the present control system for the range of hysteresis magnitude tested If conditions exist that make the elevator a more active control, a deadband filter should be added to suppress the effects of "control hysteresis." A study should be made to determine if a deadband filter should be added to the elevator signal.

XI. REFERENCES

1. Reding, J. P.; and Ericsson, L. E.: Review of Delta Wing Space Shuttle Vehicle Dynamics. NASA TM X-2508, December 1971.

2. Kaylor, J. T.; Rowell, L. F.; and Powell, R. W.: A Real-Time Digital Computer Program for the Simulation of Automatic Spacecraft Entries. Proposed NASA TM X.

3. Powell, R. W.; Stone, H. W.; and Rowell, L. F.: Simulation Results of Modifications to the Shuttle's Entry/Guidance Control System Interface. Proposed NASA TM X.

4. Harrold, J. C.: Analytic Drag Control Entry Guidance System. JSC Internal Note No. 74-FM-25,75.

TABLE I.- PHYSICAL CHARACTERISTICS OF SPACE SHUTTLE ORBITER

	Mass Properties
MASS	83 001 kg (182 986 lb)
I_{XX}	1 029 066 kg-m^2 (759 000 slug-ft^2)
I_{YY}	7 816 290 kg-m^2 (5 765 000 slug-ft^2)
I_{ZZ}	8 015 596 kg-m^2 (5 912 000 slug-ft^2)
I_{XZ}	177 612 kg-m^2 (131 000 slug-ft^2)
$I_{XY} = I_{YZ} = 0$	
	WING
Reference Area	249.91 m^2 (2690.0 ft^2)
Chord	12.06 m (39.57 ft)
Span	23.79 m (78.06 ft)
	ELEVON
Reference Area	19.51 m^2 (210.0 ft^2)
Chord	2.30 m (7.56 ft)
	RUDDER
Reference Area	9.30 m^2 (100.15 ft^2)
Chord	1.86 m (6.1 ft)
	BODY FLAP
Reference Area	12.54 m^2 (135.0 ft^2)
Chord	2.06 m (6.75 ft)

TABLE II

RCS FUEL CONSUMPTION FOR THE NOMINAL GUIDANCE

WITH A SAMPLING TIME OF 0.32 SECONDS

C1	C2	FUEL CONSUMPTION, kg (lb)
1	0	176 (388)
0.7	0	171 (378)
0.5	0	185 (408)
1.5	0	174 (385)*
1	-2	173 (382)
1	-5	181 (399)
1	+5	176 (389)*
0.5	-5	178 (393)

*Cases were run on batch version of ARFDS so strip charts are not available.

TABLE III

RCS FUEL CONSUMPTION FOR THE REVISED GUIDANCE

WITH A SAMPLING TIME OF 2.00 SECONDS

C1	C2	FUEL CONSUMPTION, kg (lb)
1	0	111 (245)
0.7	0	112 (246)
0.5	0	110 (243)
1	-2	111 (245)
1	-5	127 (280)
0.5	-5	124 (274)

TABLE IV

RCS FUEL CONSUMPTION FOR THE NOMINAL GUIDANCE WITH A SAMPLING TIME OF 0.32 SECONDS WITH THE AILERON DEADBAND FILTER REMOVED

C1	C2	FUEL CONSUMPTION, kg (lb)
1	0	156 (343)
0.5	-5	213 (470)

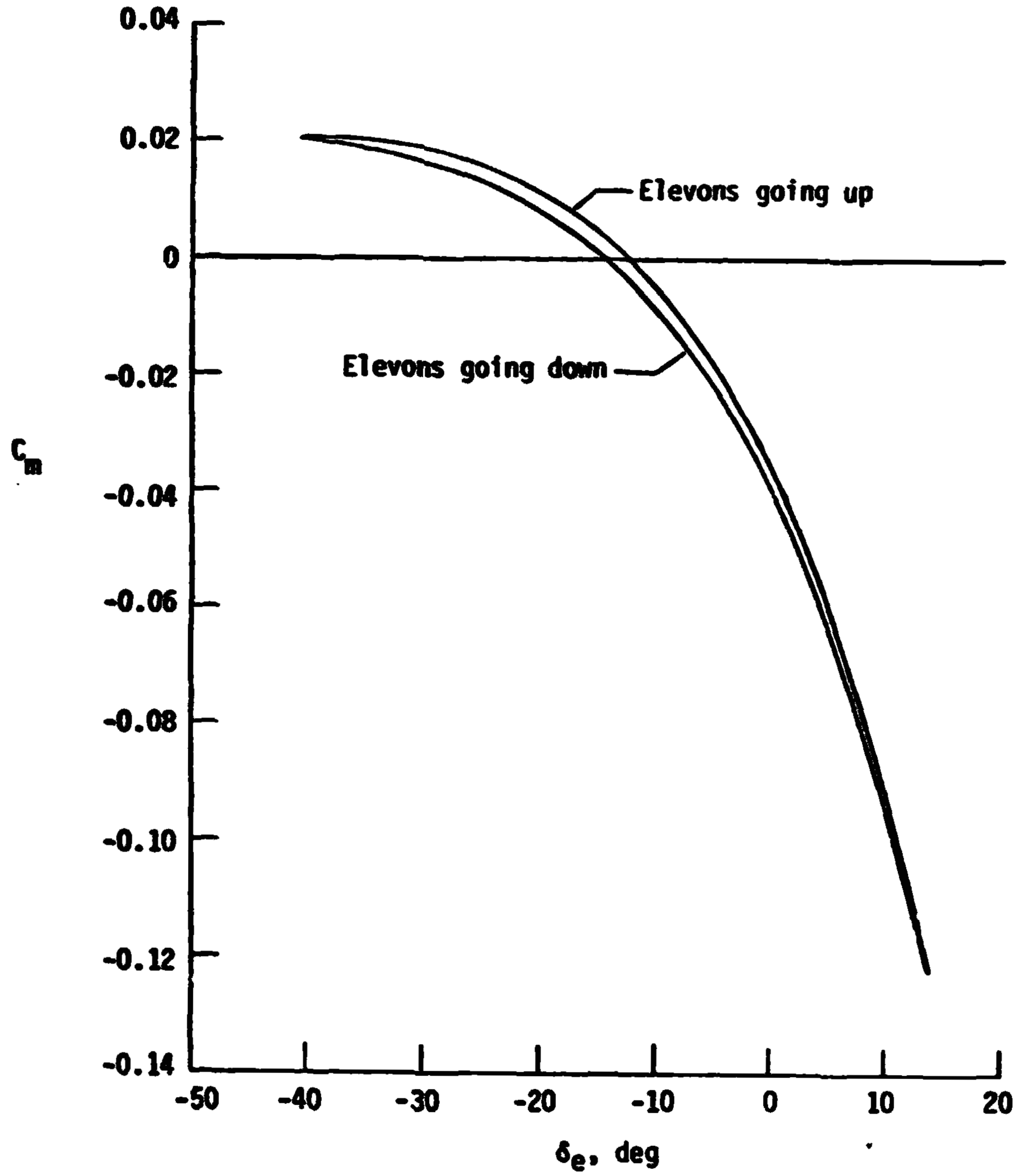

Figure 1. Pitching Moment Data for a Space Shuttle Orbiter Model With Remotely Controlled Elevons From the NASA Langley Research Center's Continuous Flow Hypersonic Tunnel.

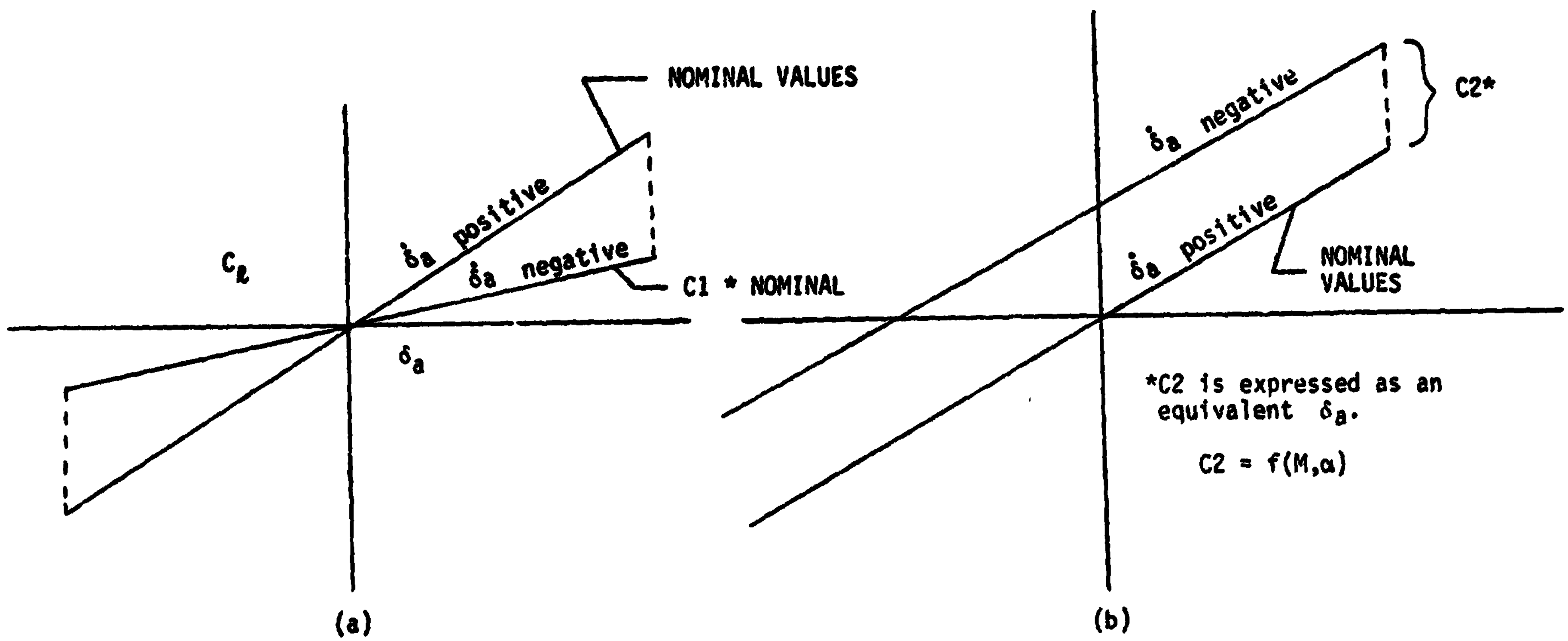

Figure 2. Hysteresis Models.

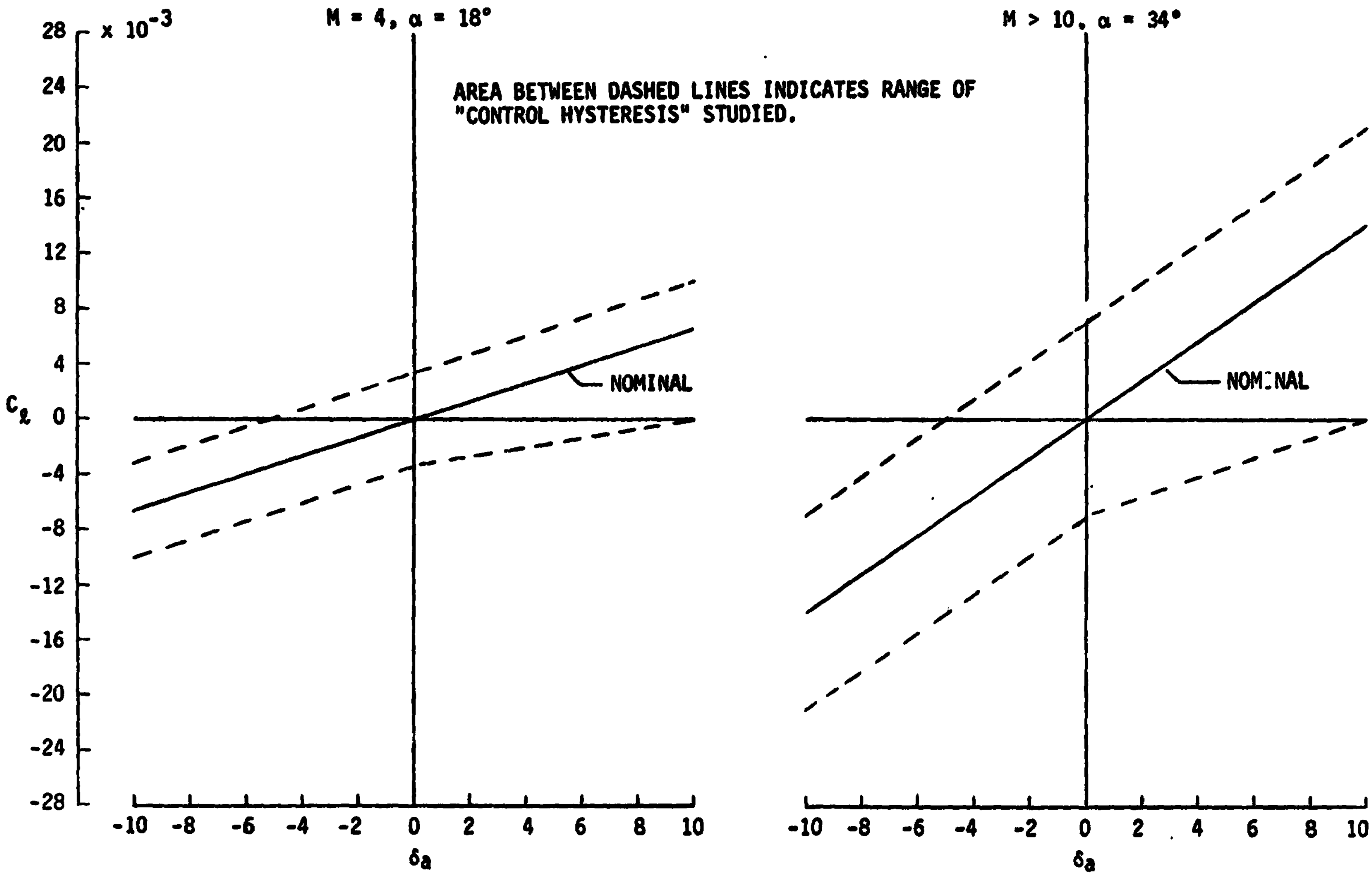

(c) Range of "control hysteresis" studied.

Figure 2.- Concluded.

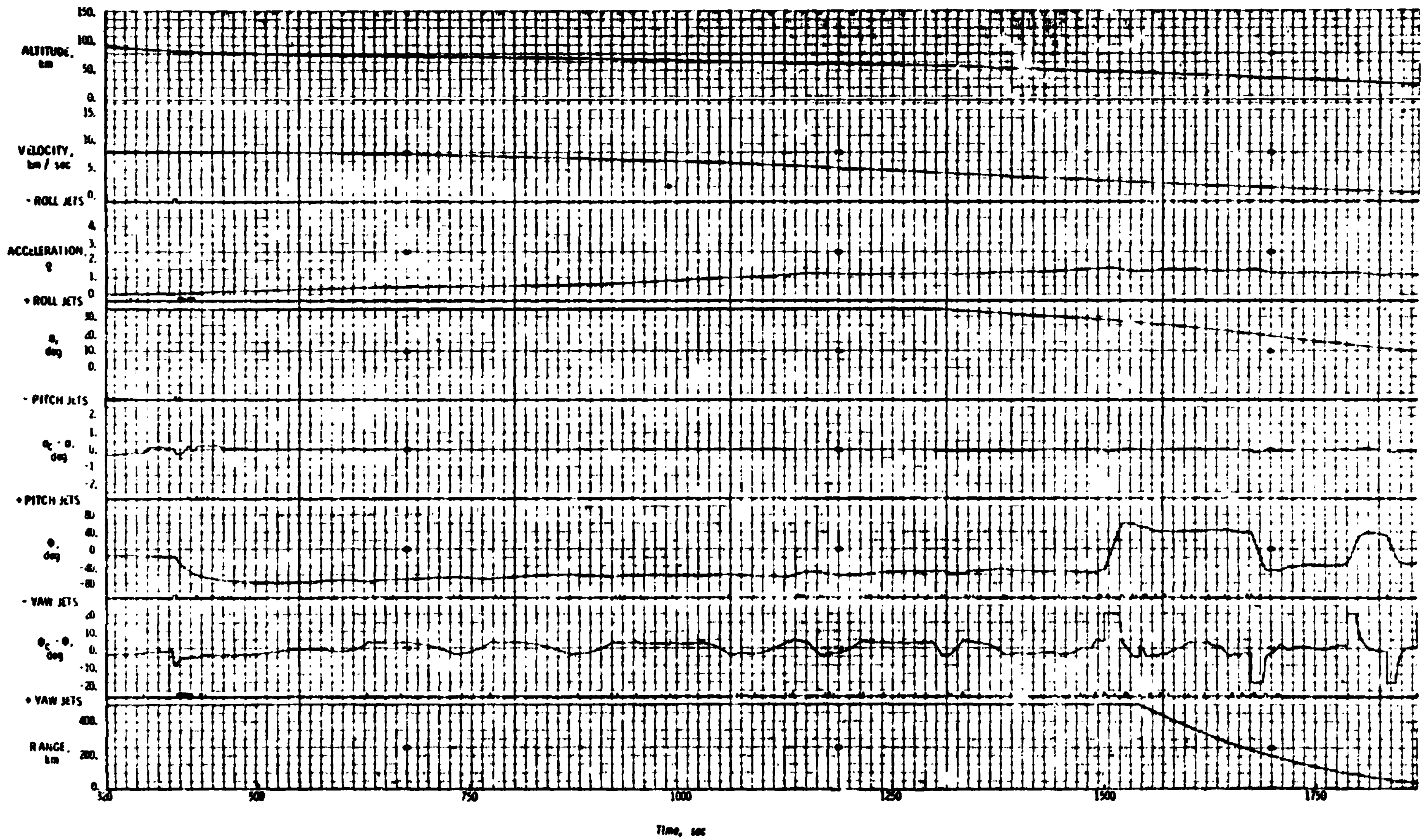

Figure 3. NOMINAL GUIDANCE - NO HYSTERESIS

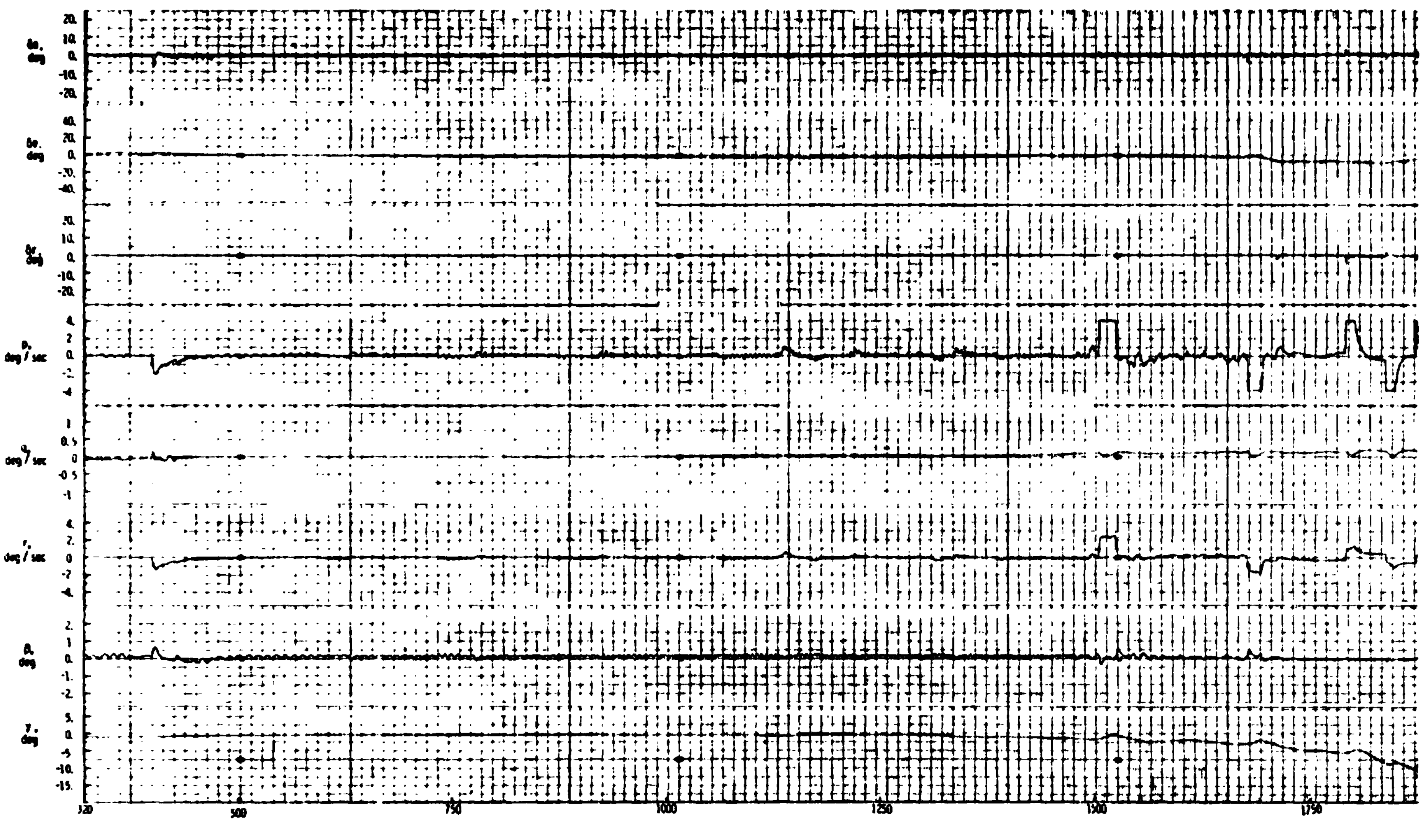

Figure 3. Concluded

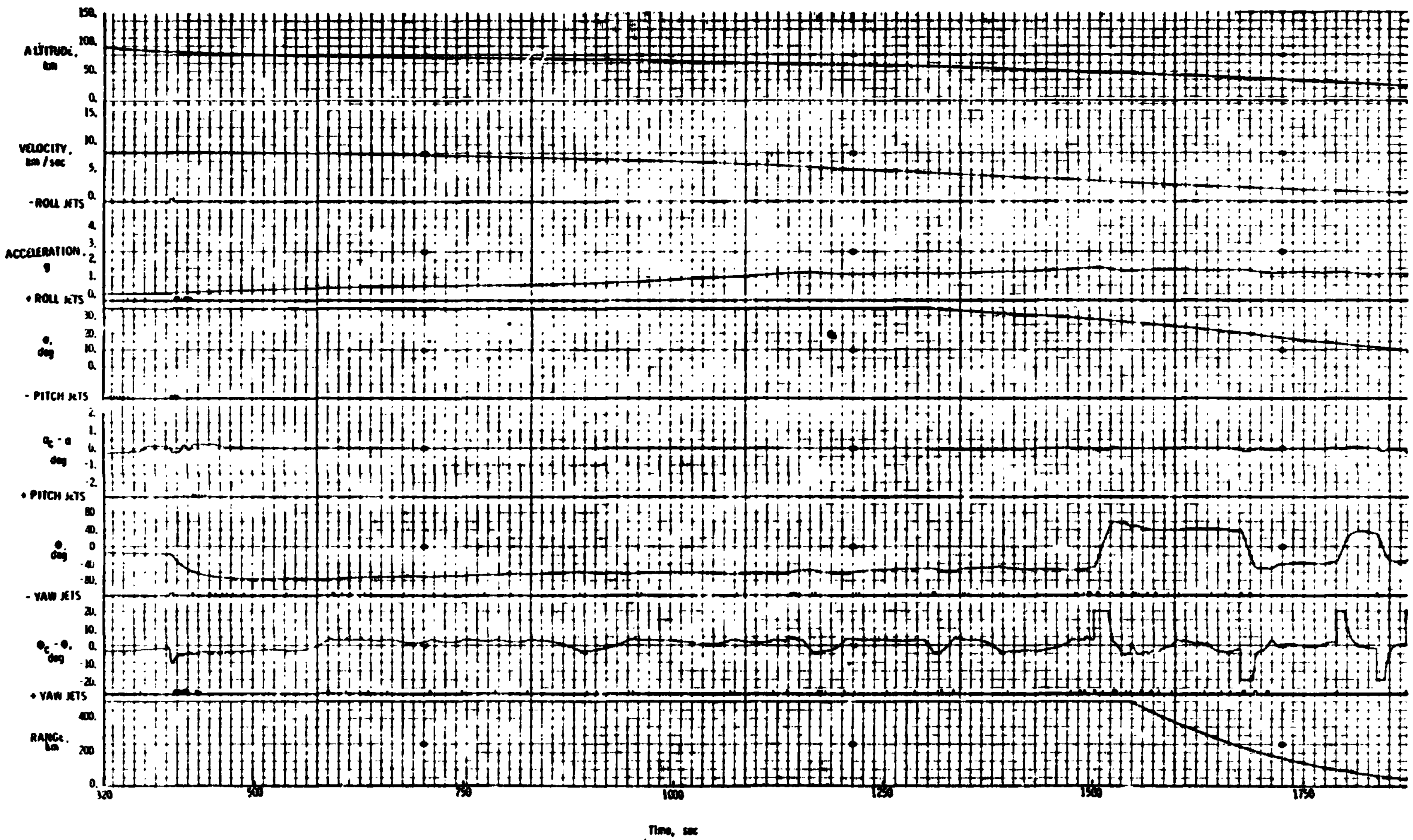

Figure 4. NOMINAL GUIDANCE - HYSTERESIS FACTORS C1 = 0.7, C2 = 0

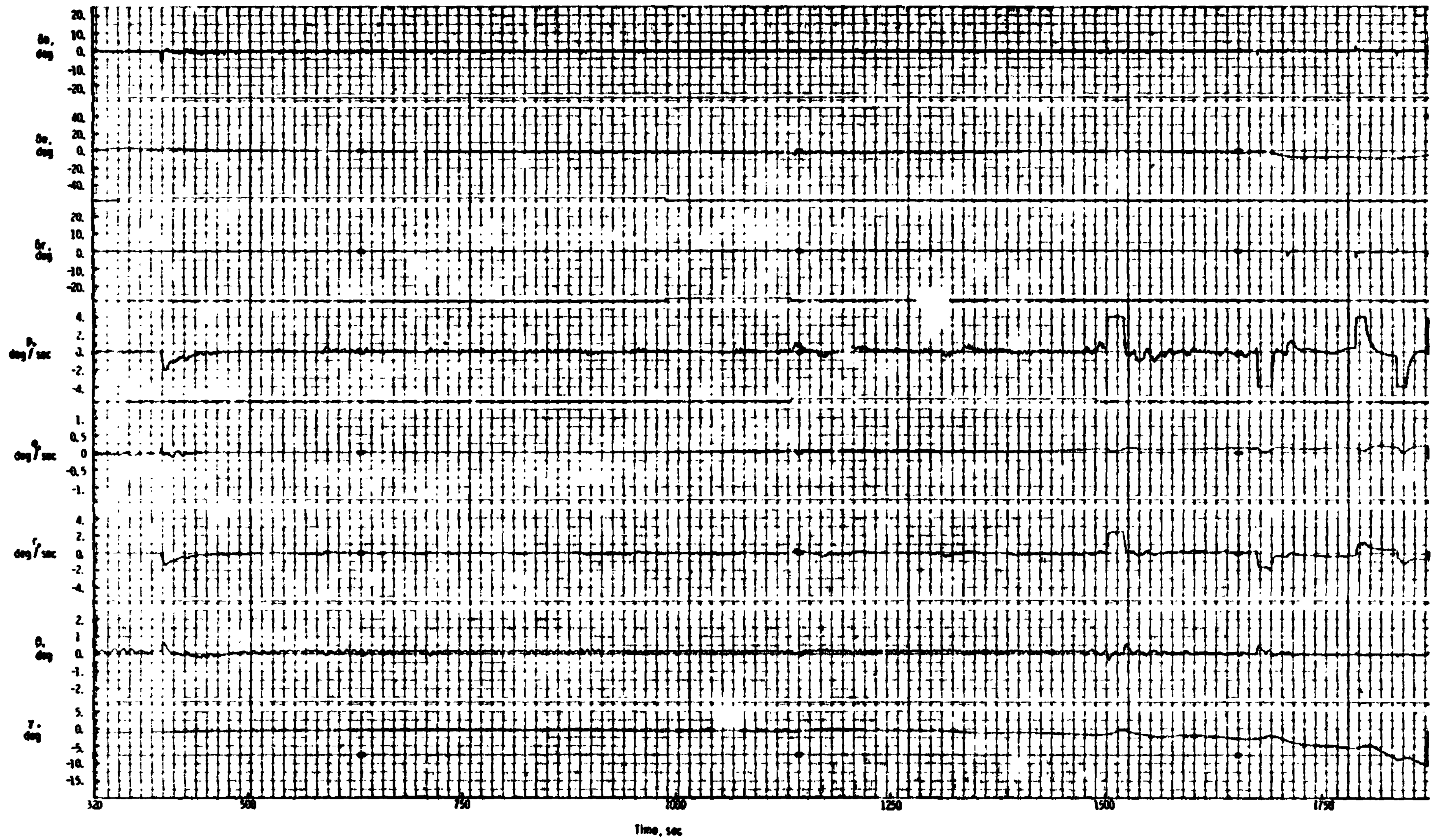

Figure 4. Concluded

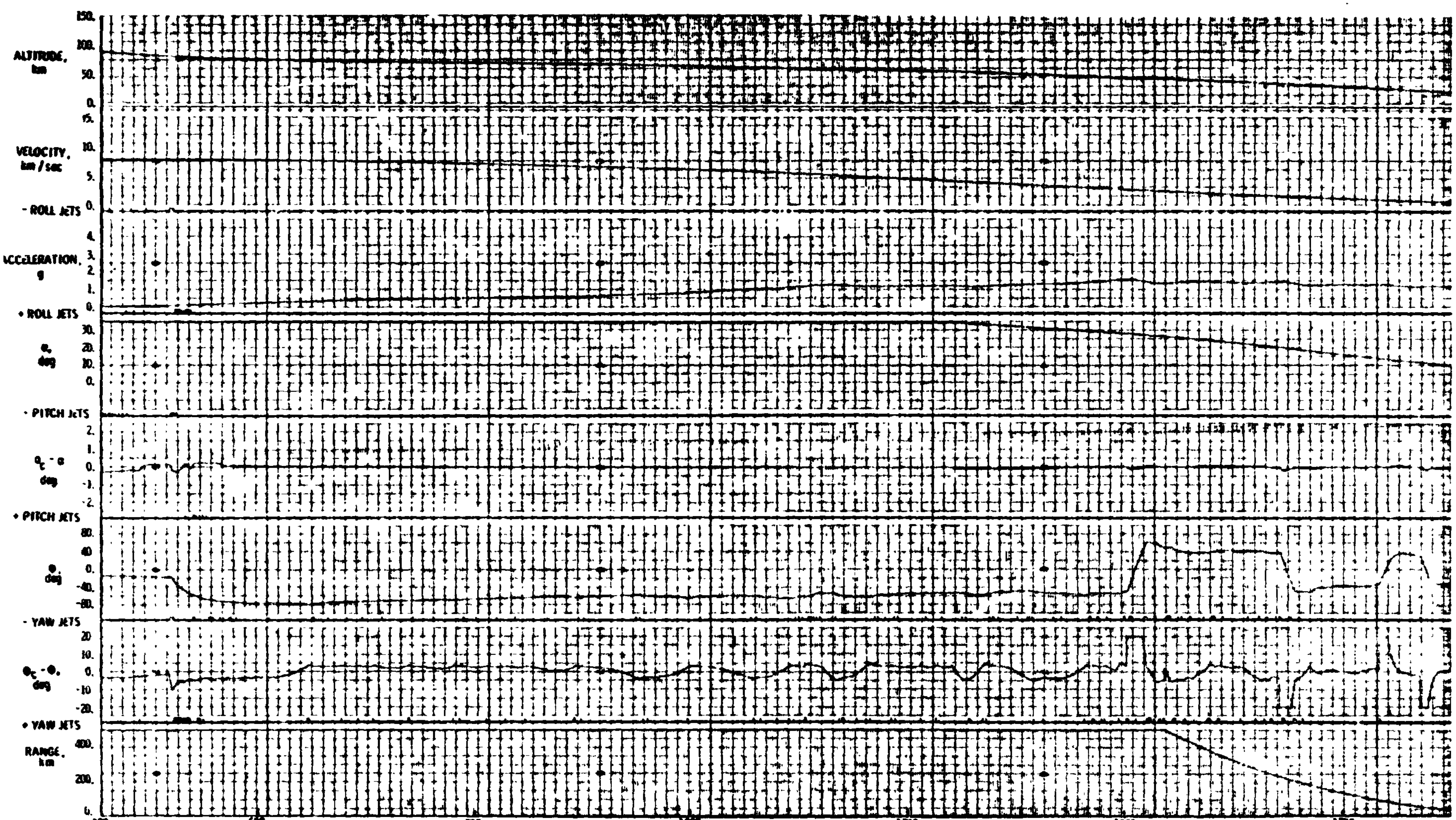

Figure 5. NOMINAL GUIDANCE - HYSTERESIS FACTORS C1 = 0.5, C2 = 0

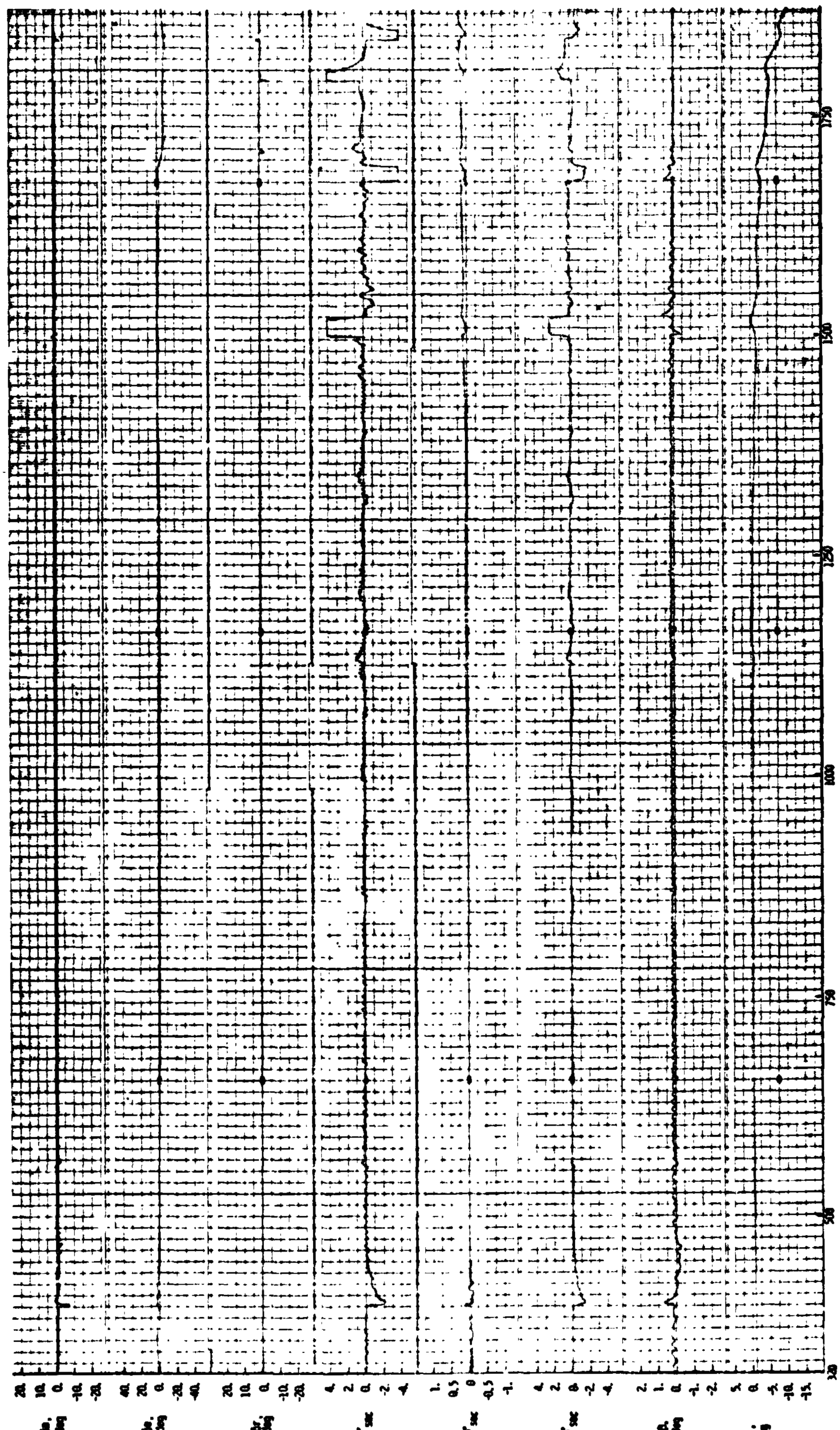

Figure 5. Concluded

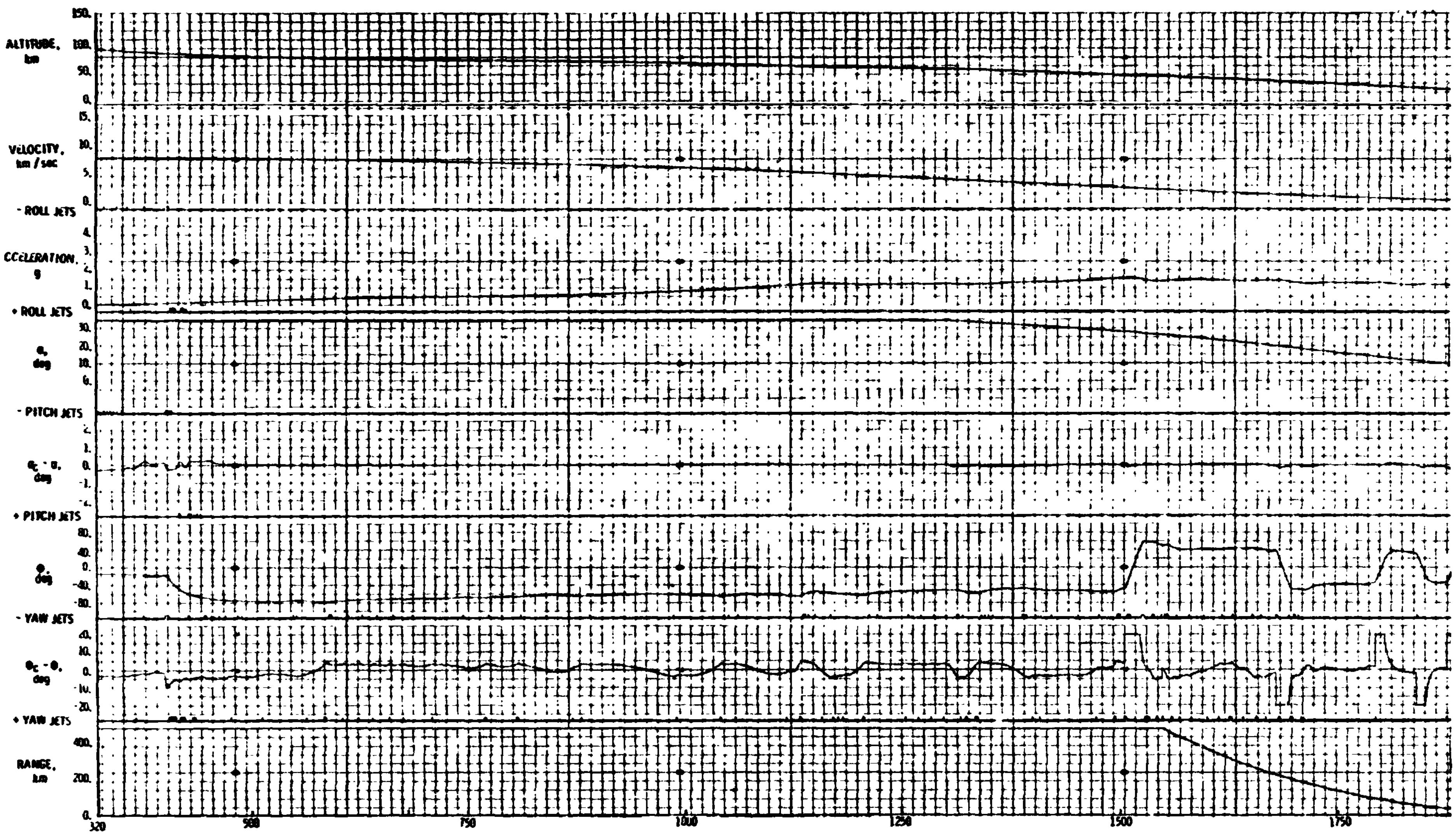

Figure 6. NOMINAL GUIDANCE - HYSTERESIS FACTORS C1 = 1.0, C2 = -2

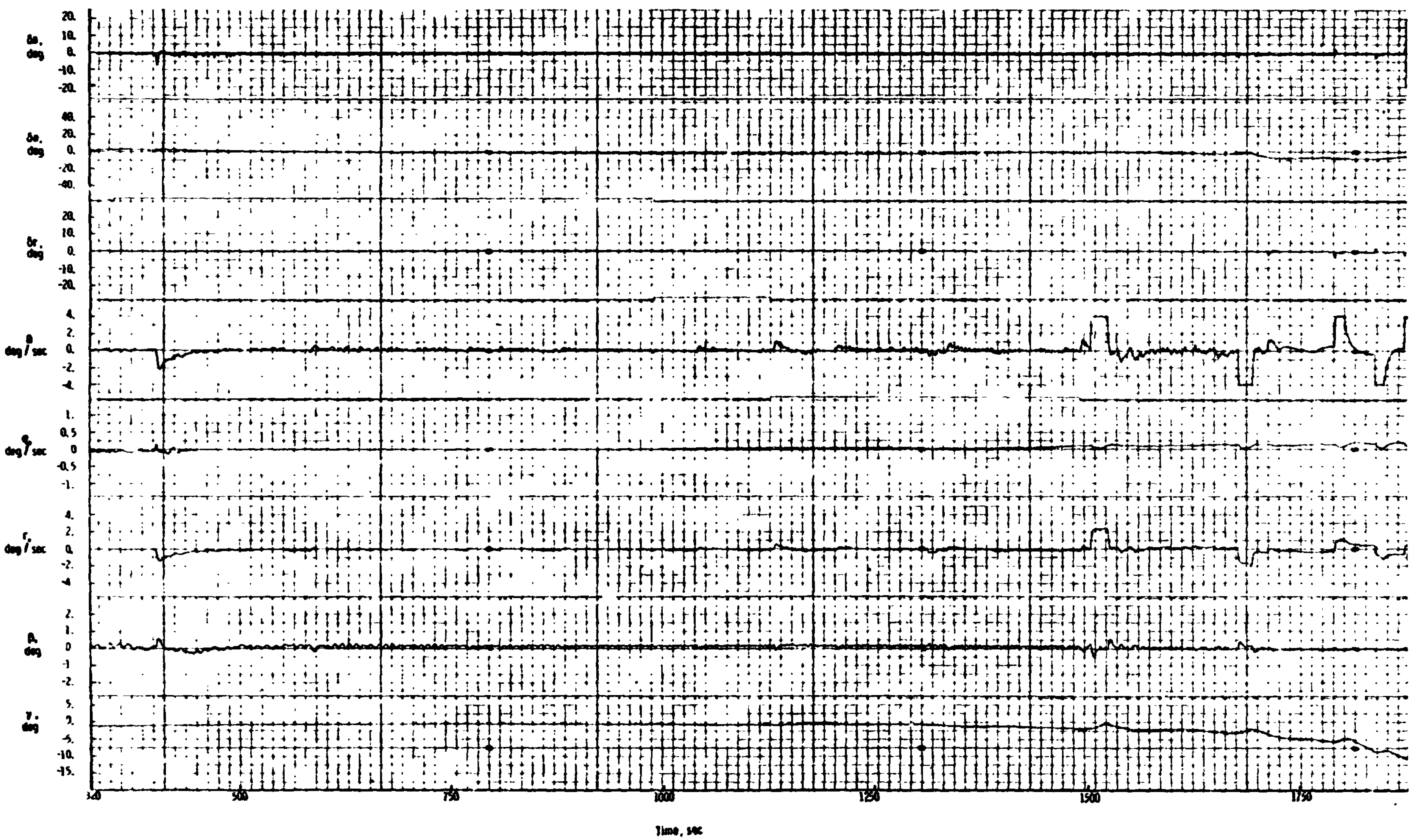

Figure 6. Concluded

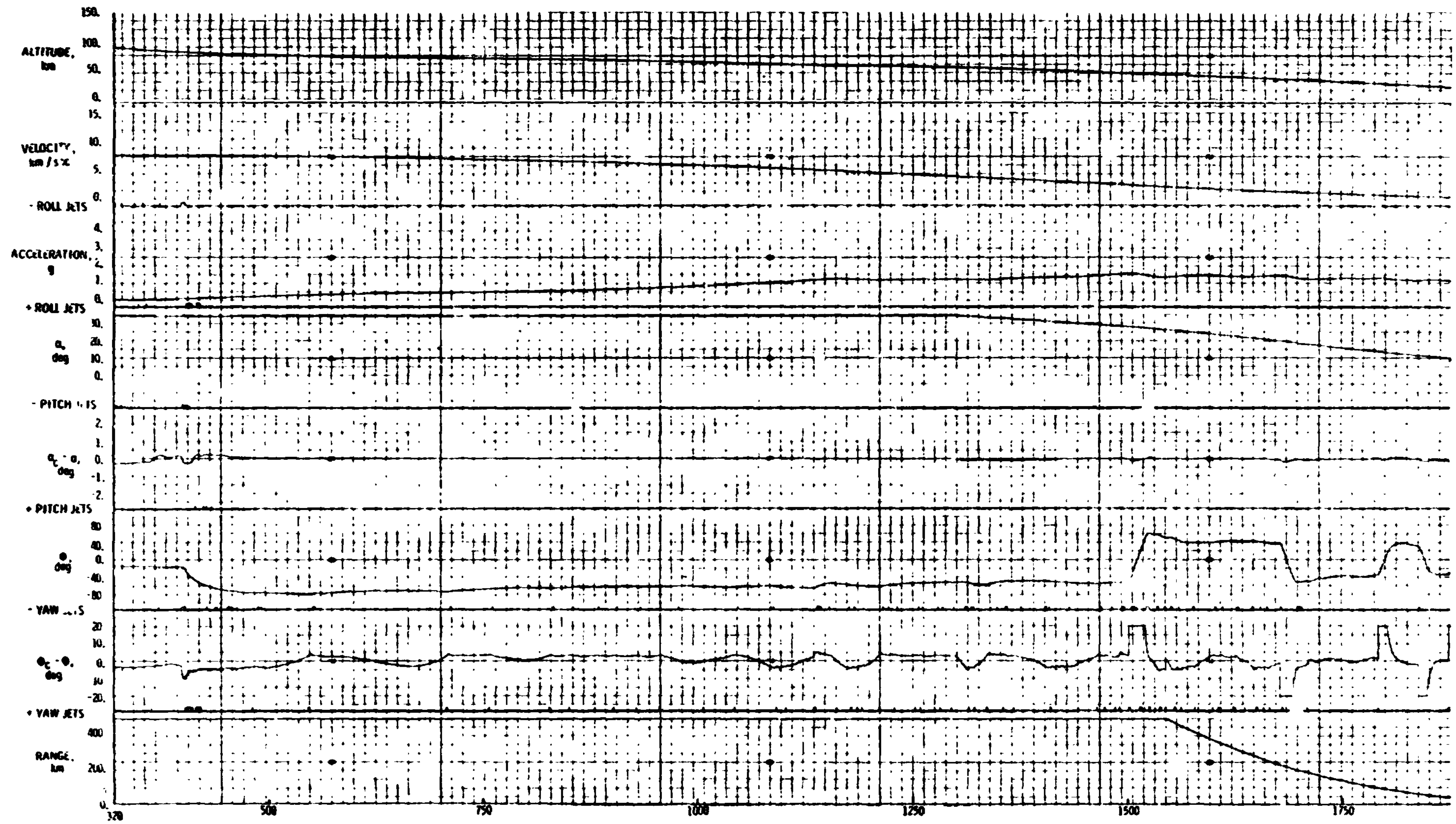

Time, sec

Figure 7. NOMINAL GUIDANCE - HYSTERESIS FACTORS C1 = 1.0, C2 = -5

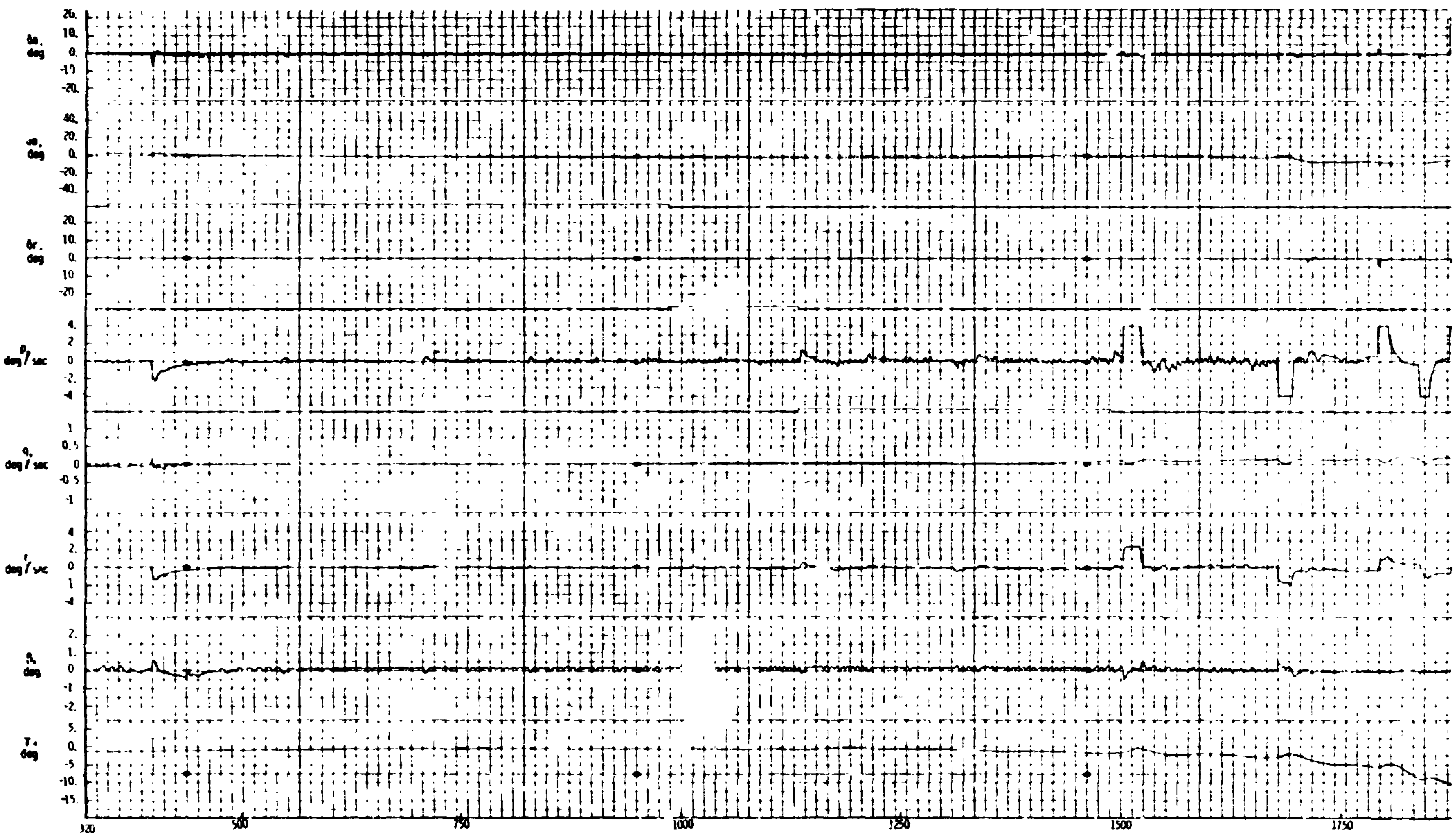

Figure 7. Concluded

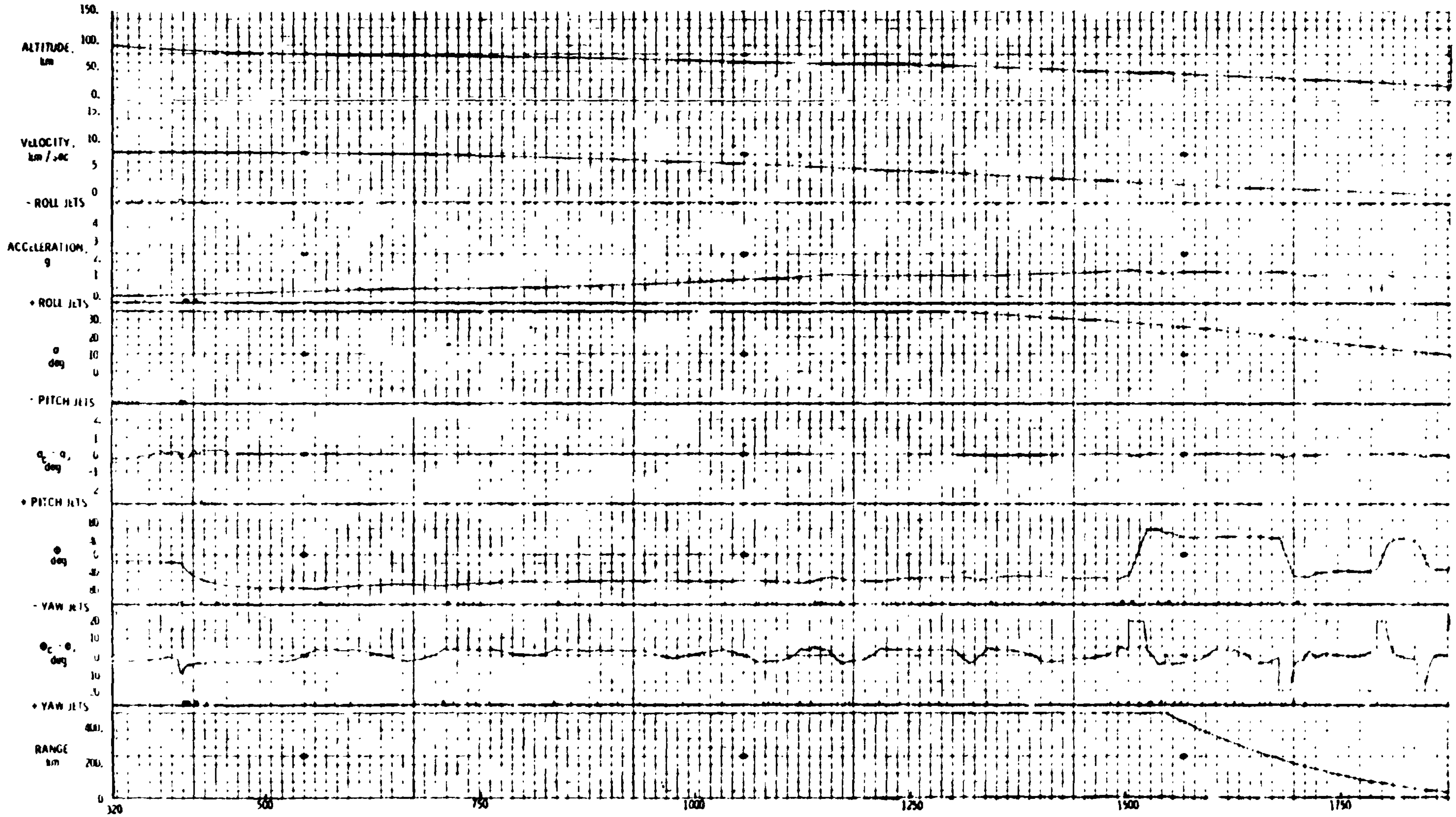

Figure 8. NOMINAL GUIDANCE - HYSTERESIS FACTORS C1 = 0.5, C2 = -5

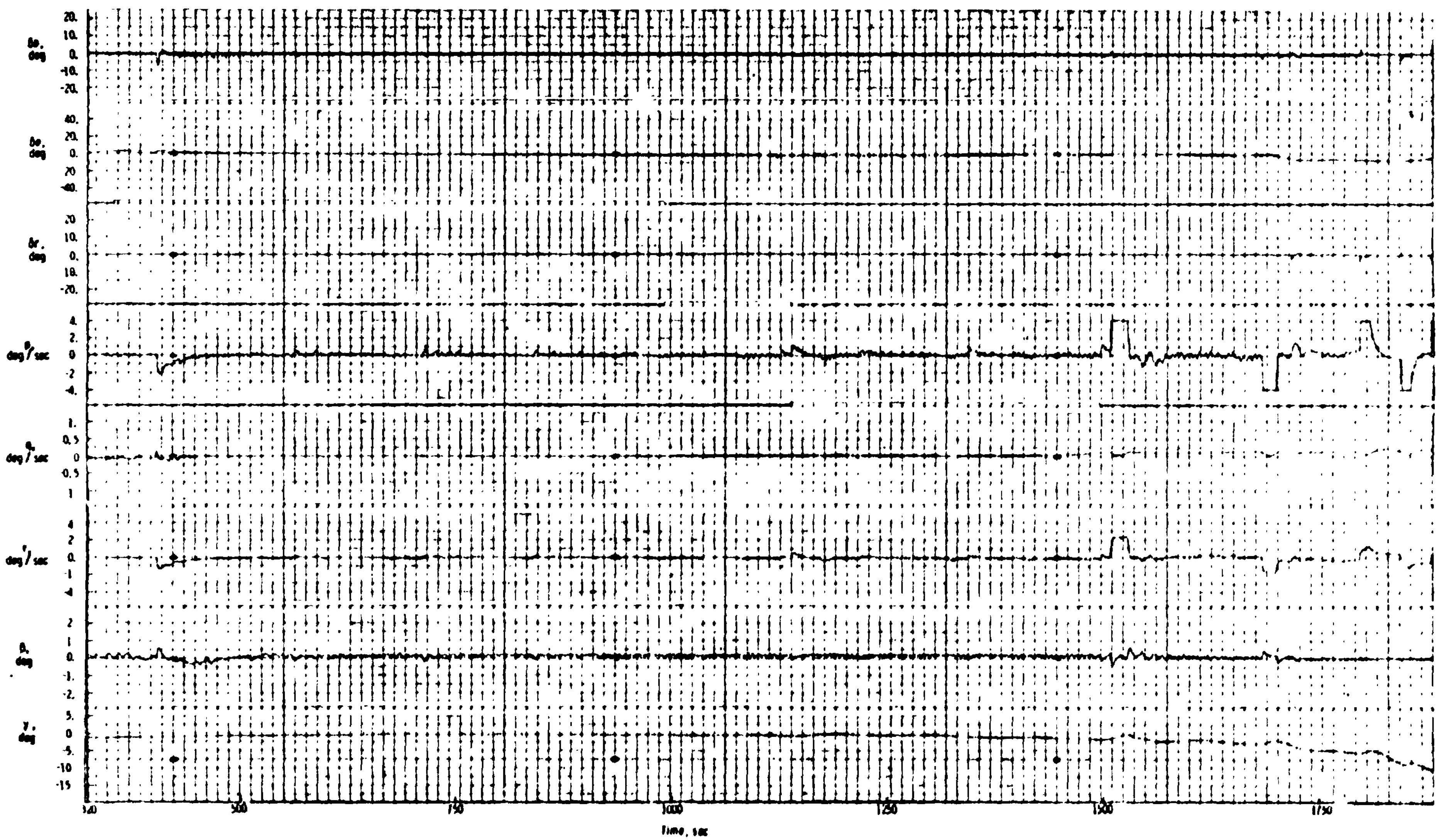

Figure 8. Concluded

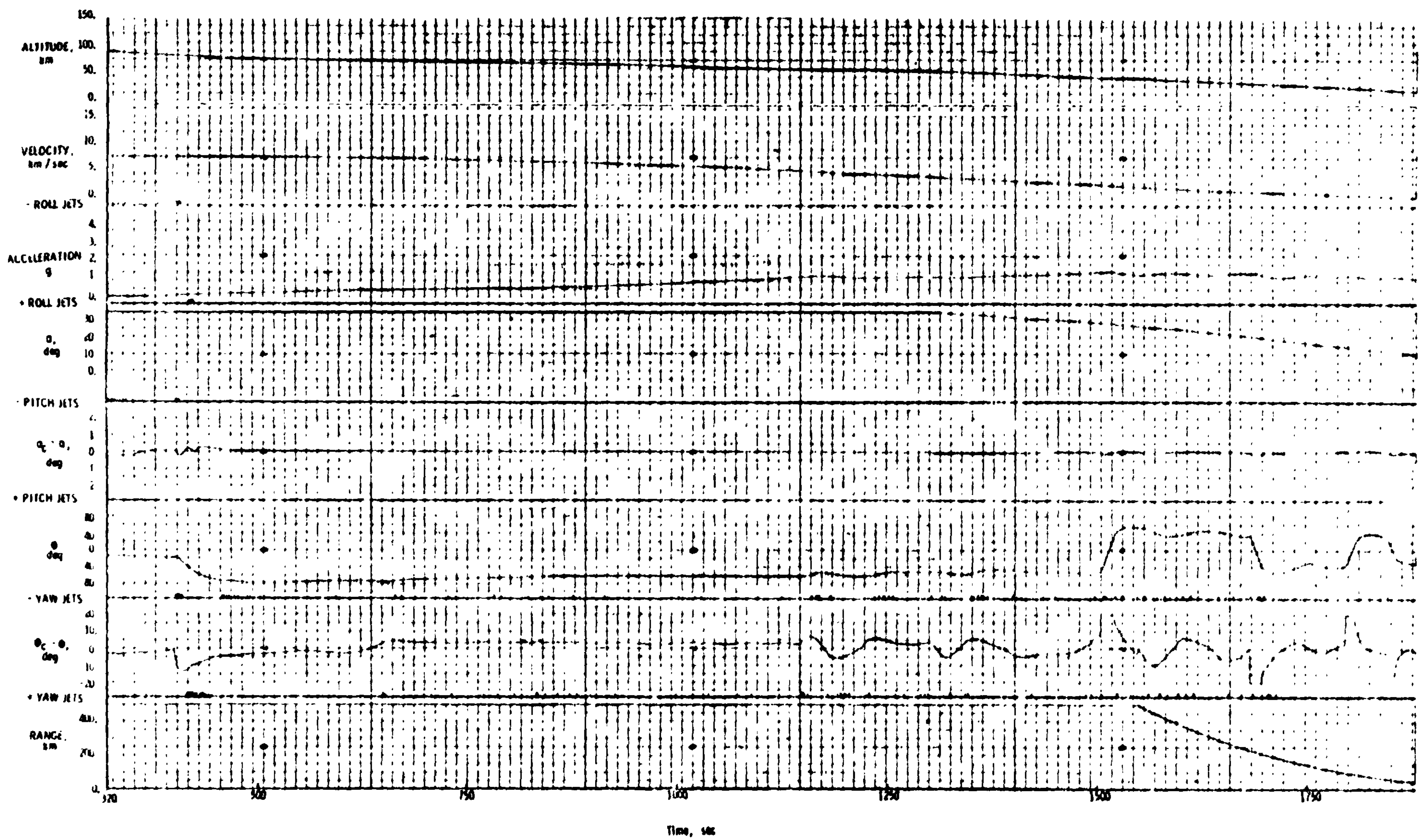

Figure 9. REVISED GUIDANCE - NO HYSTERESIS

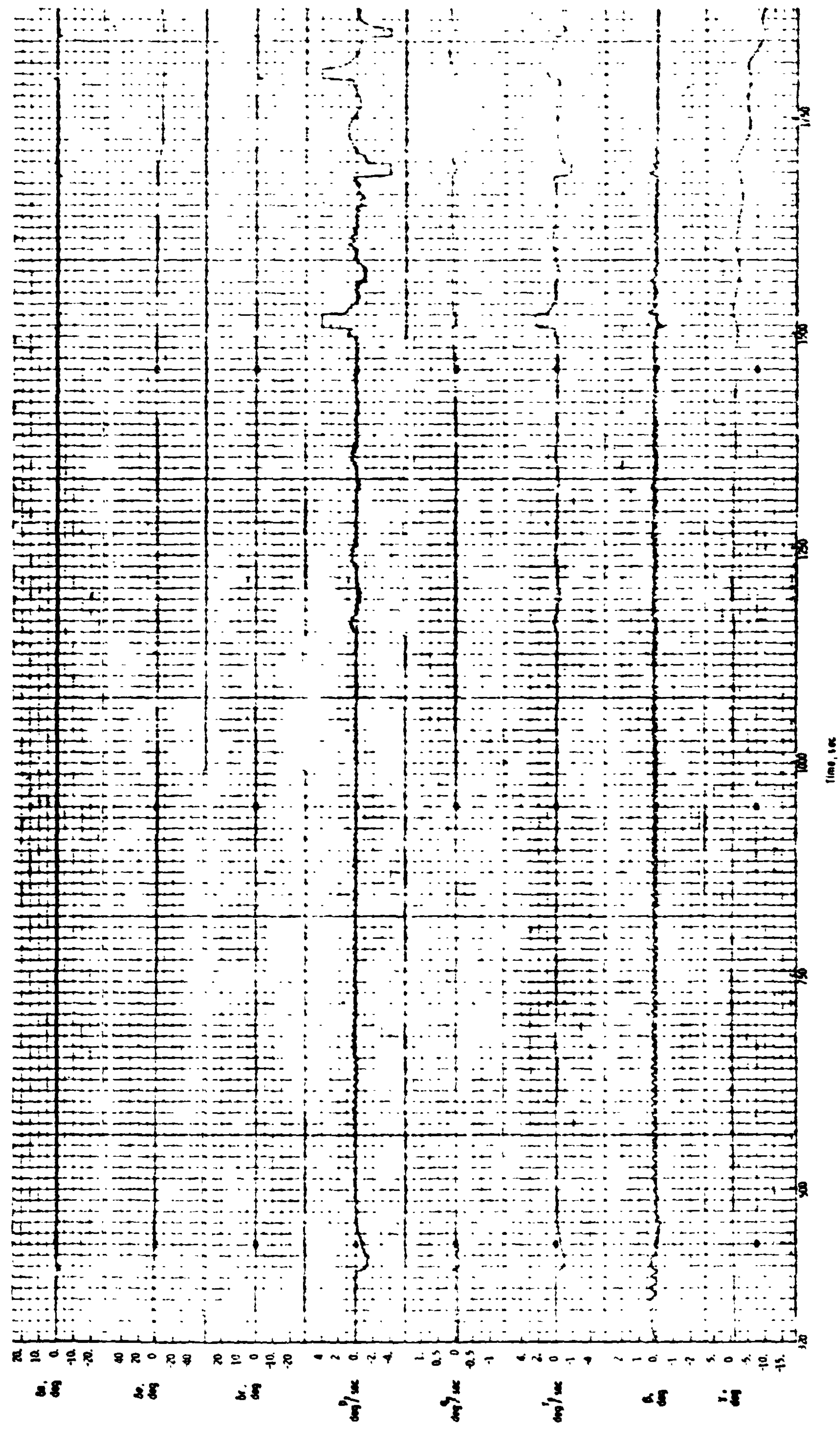

Figure 9. Concluded.

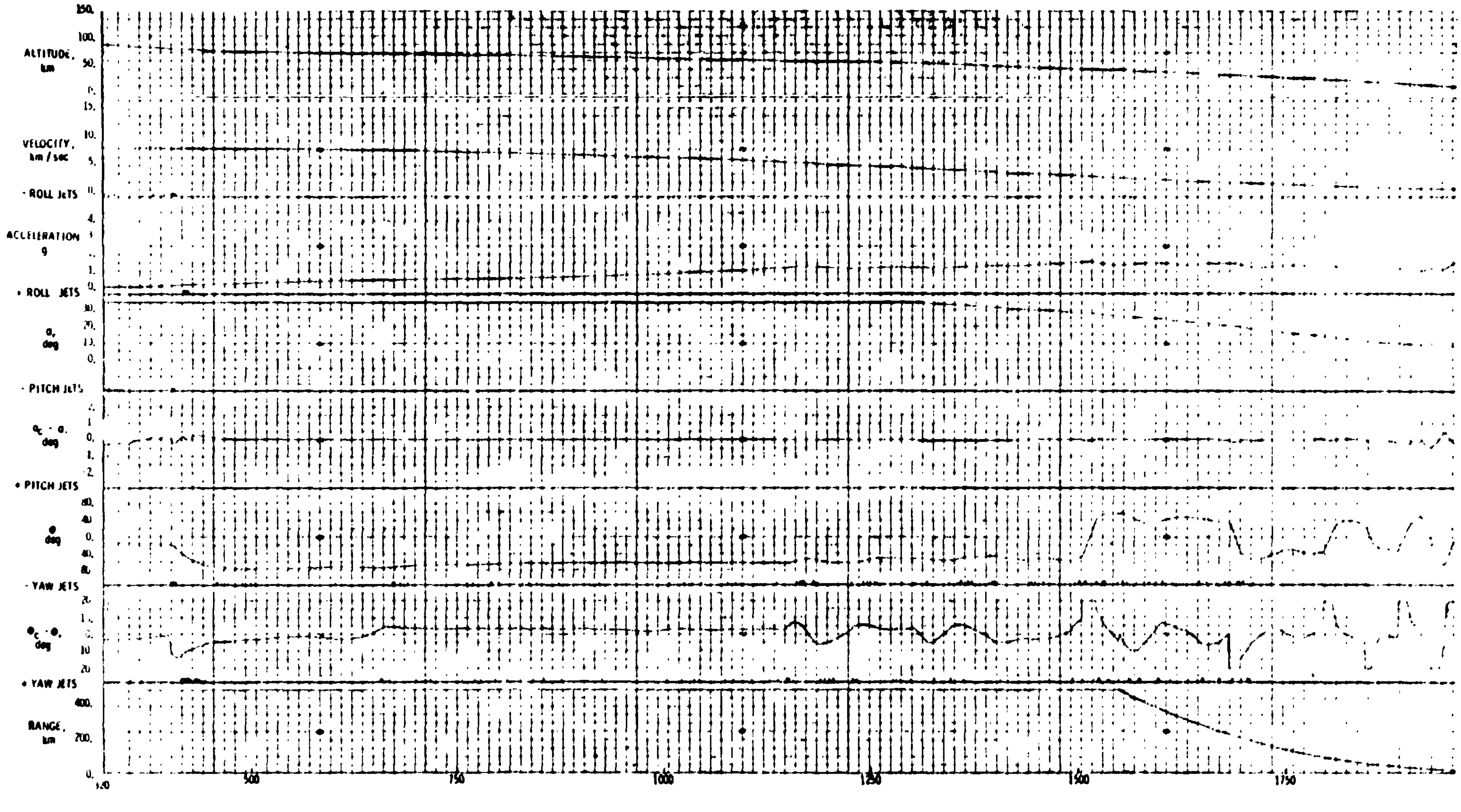

Figure 10. REVISED GUIDANCE - HYSTERESIS FACTORS C1 = 0.7, C2 = 0

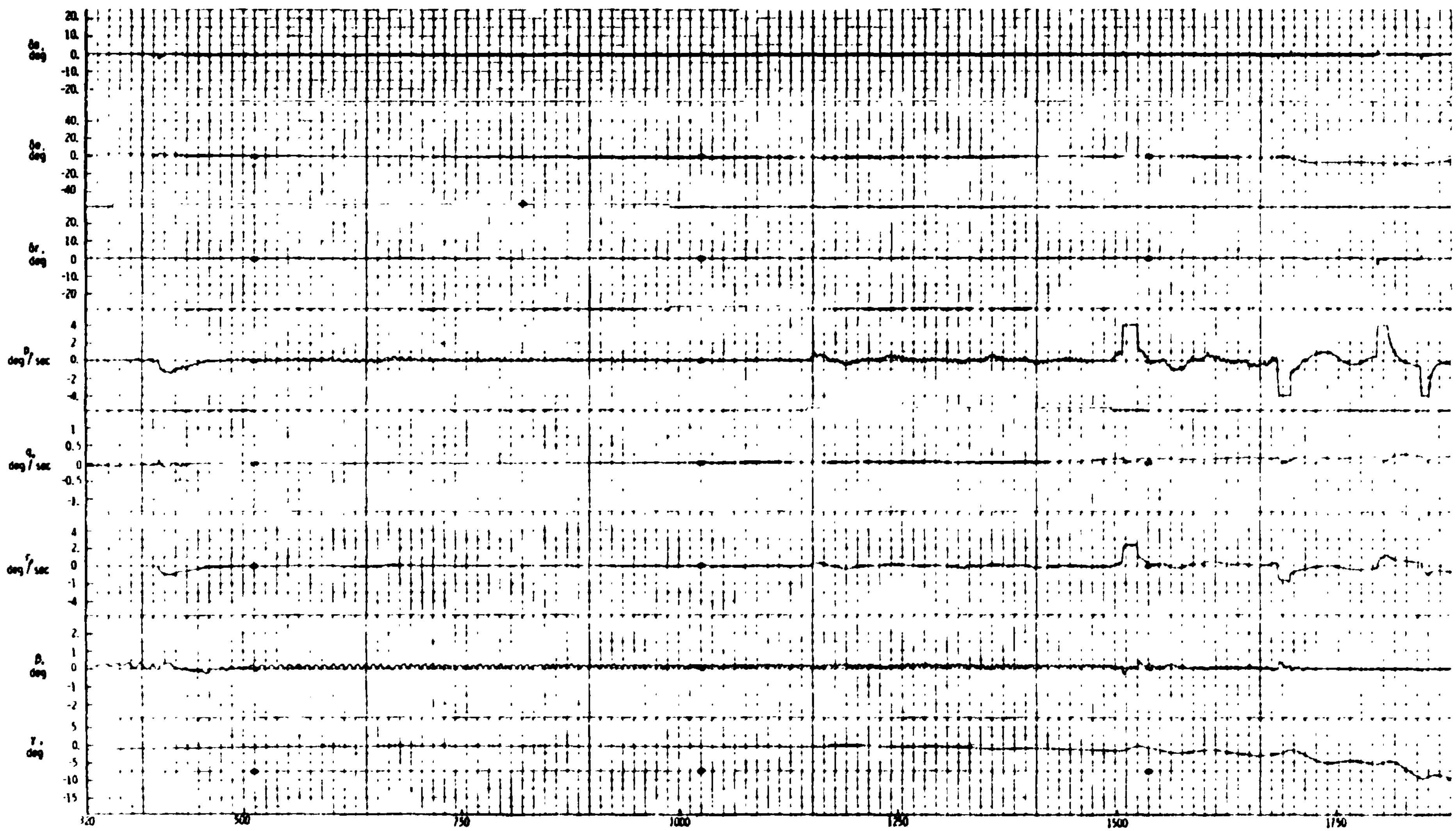

Time, sec

Figure 10. Concluded

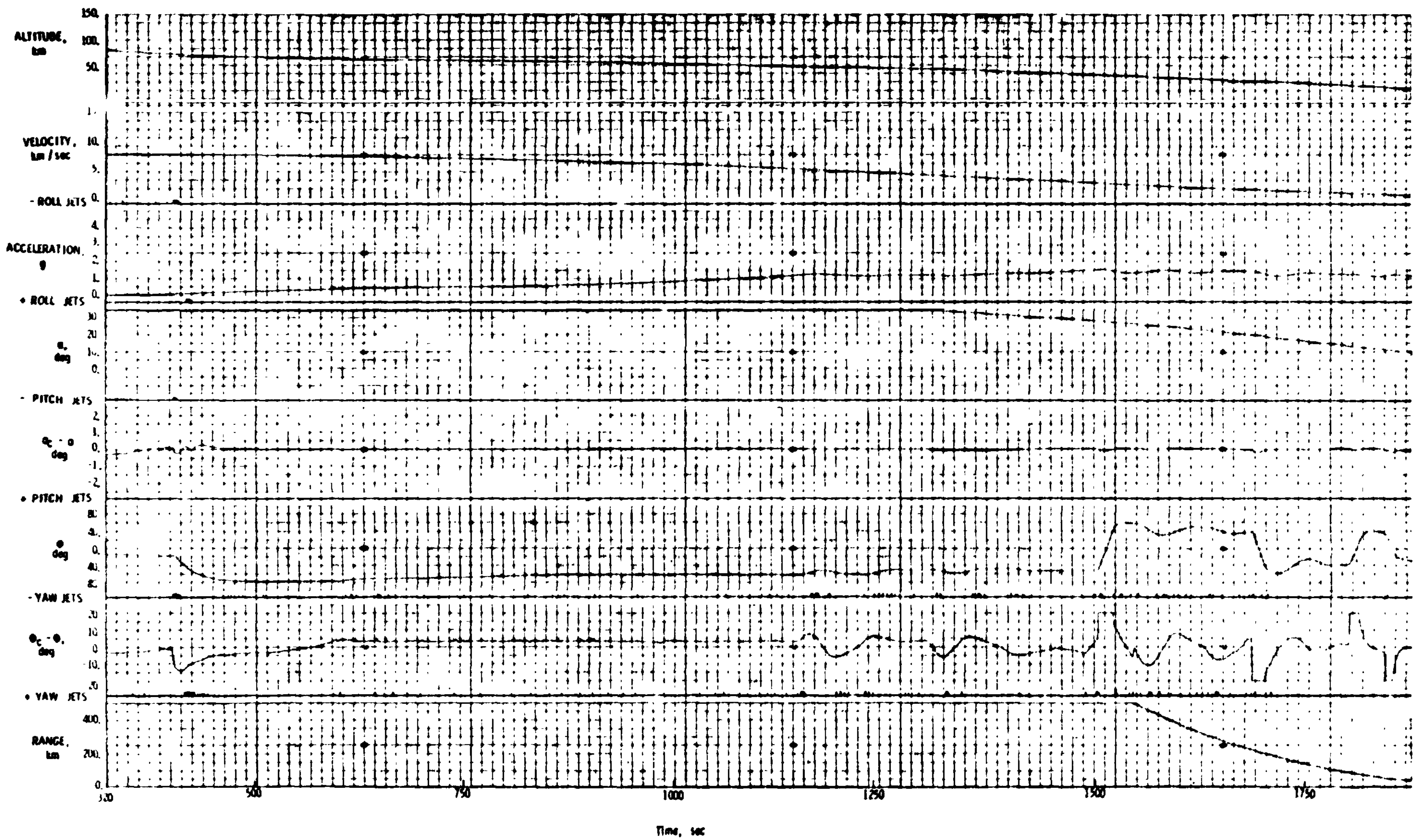

Figure 11. REVISED GUIDANCE - HYSTERESIS FACTORS C1 = 0.5, C2 = 0

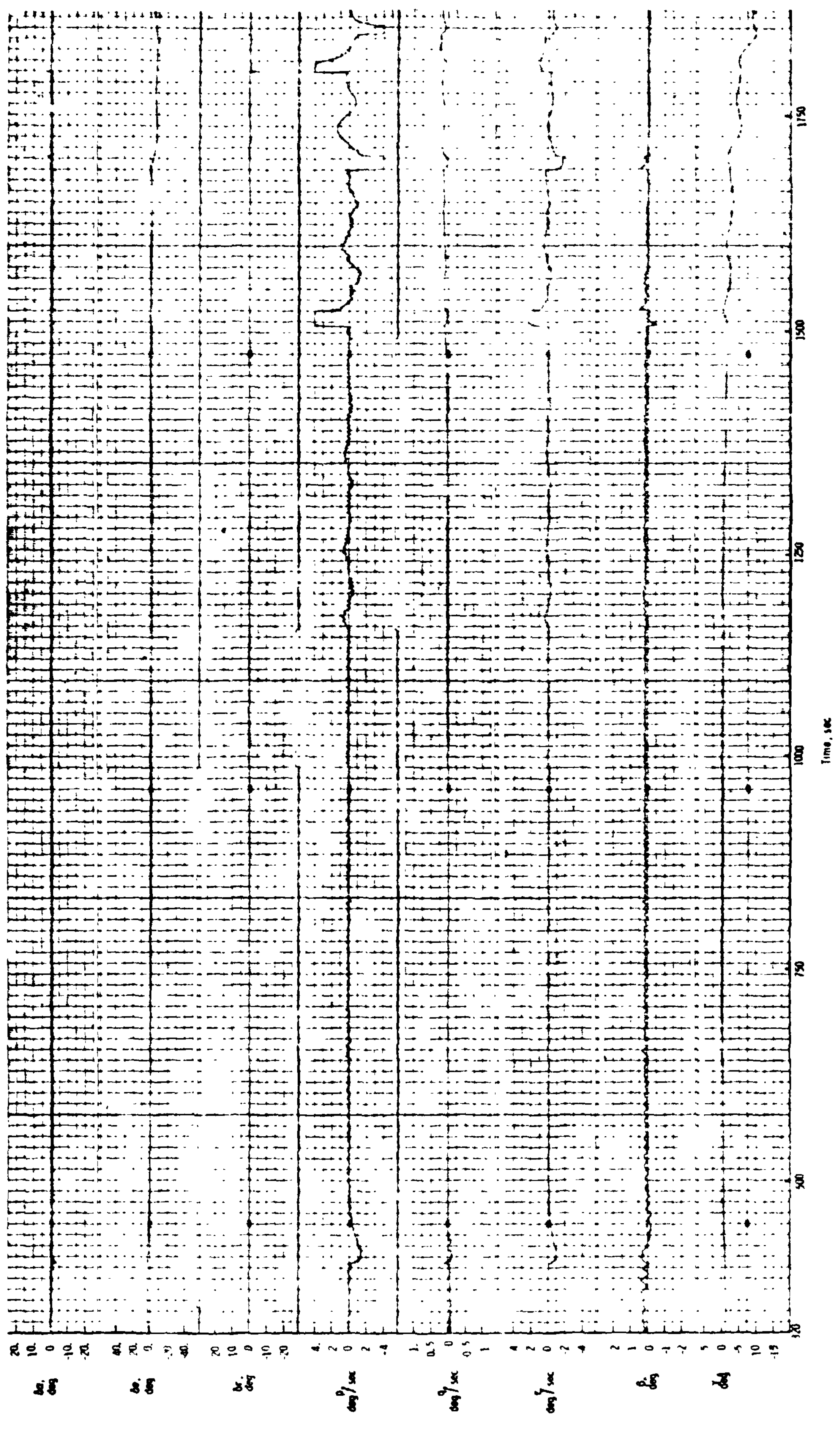

Figure 11. Concluded

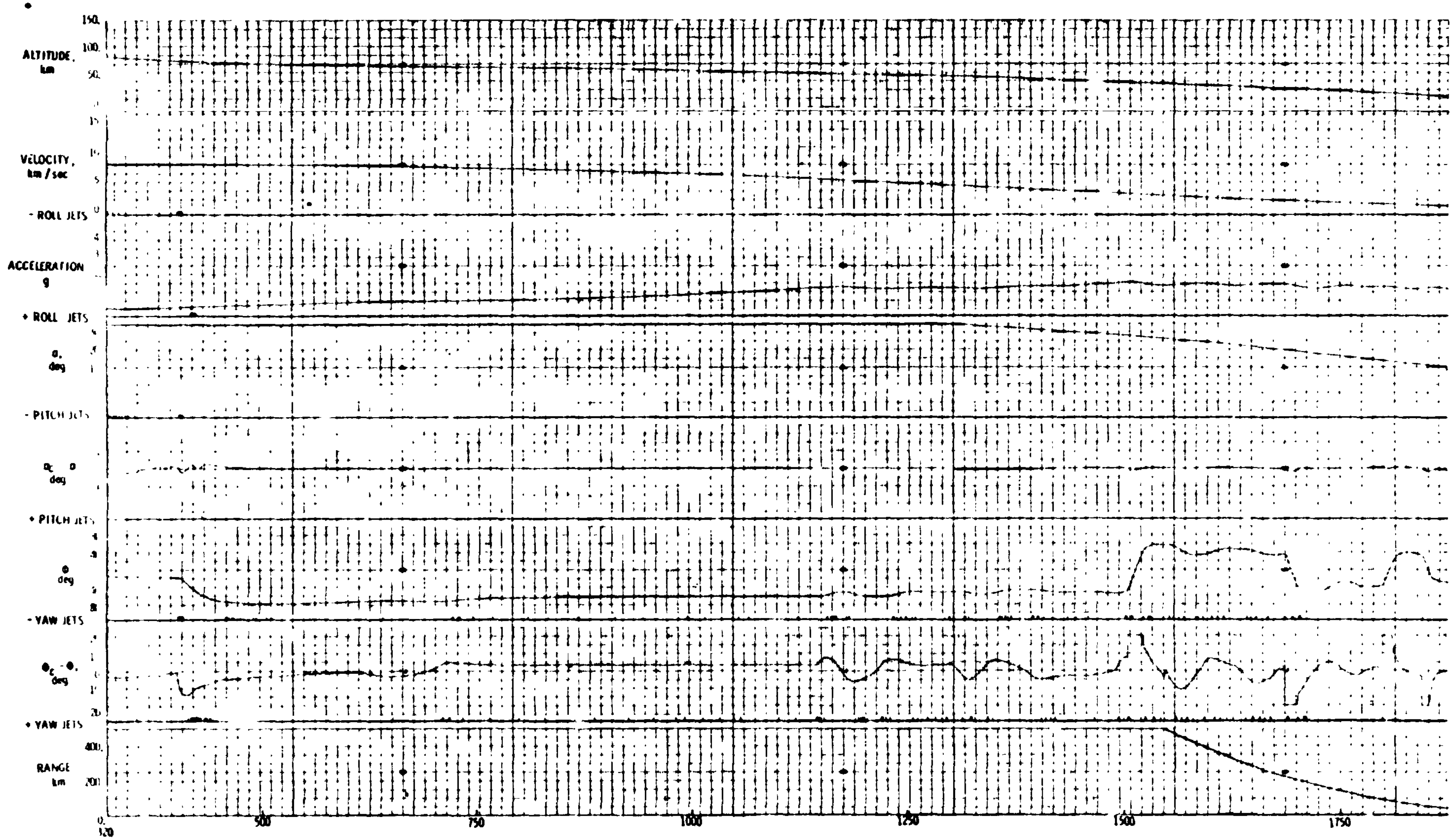

Figure 17. REVISED GUIDANCE - HYSTERESIS FACTORS $C1 = 1.0$, $C2 = -2$

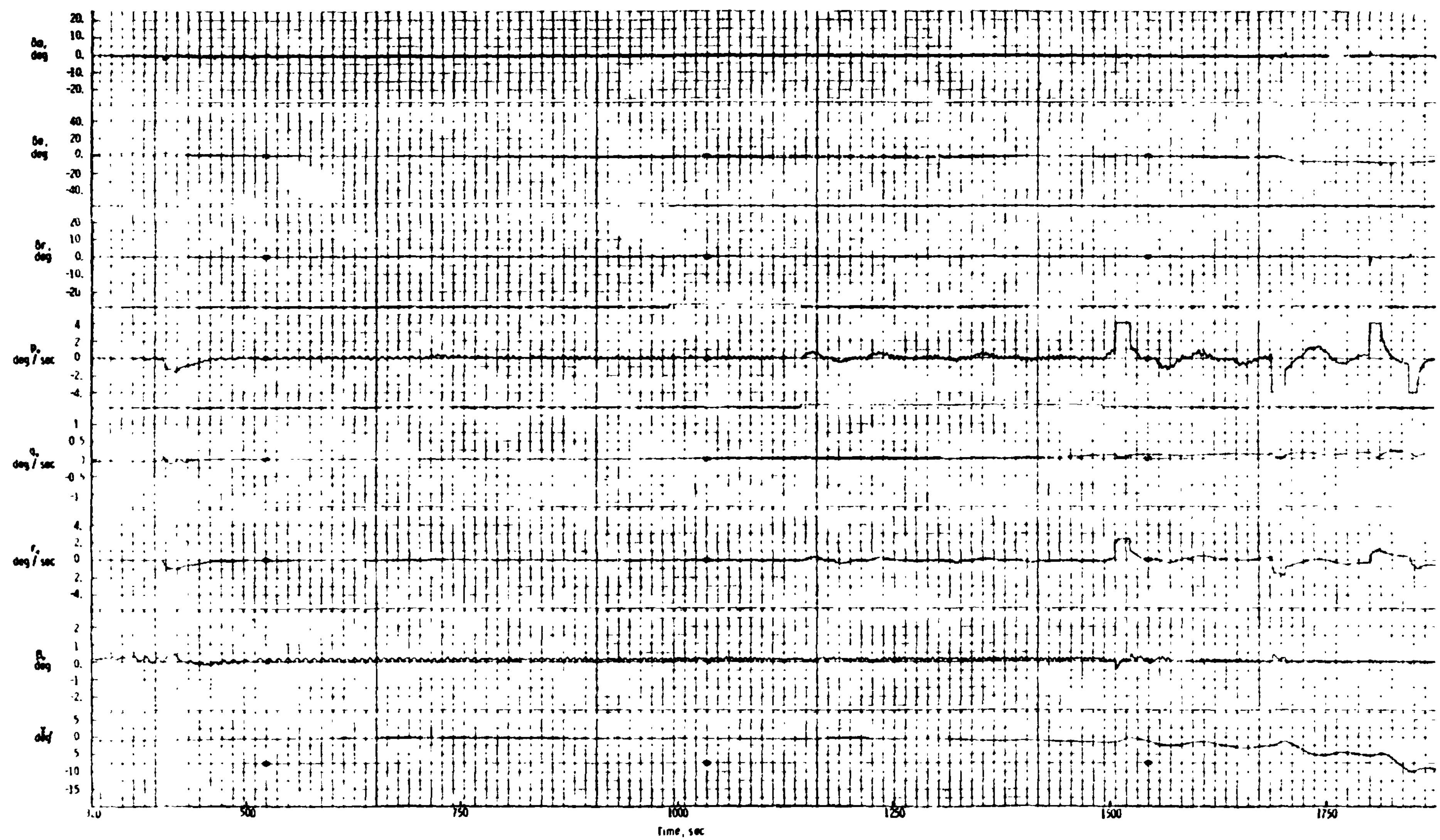

Figure 12 Concluded

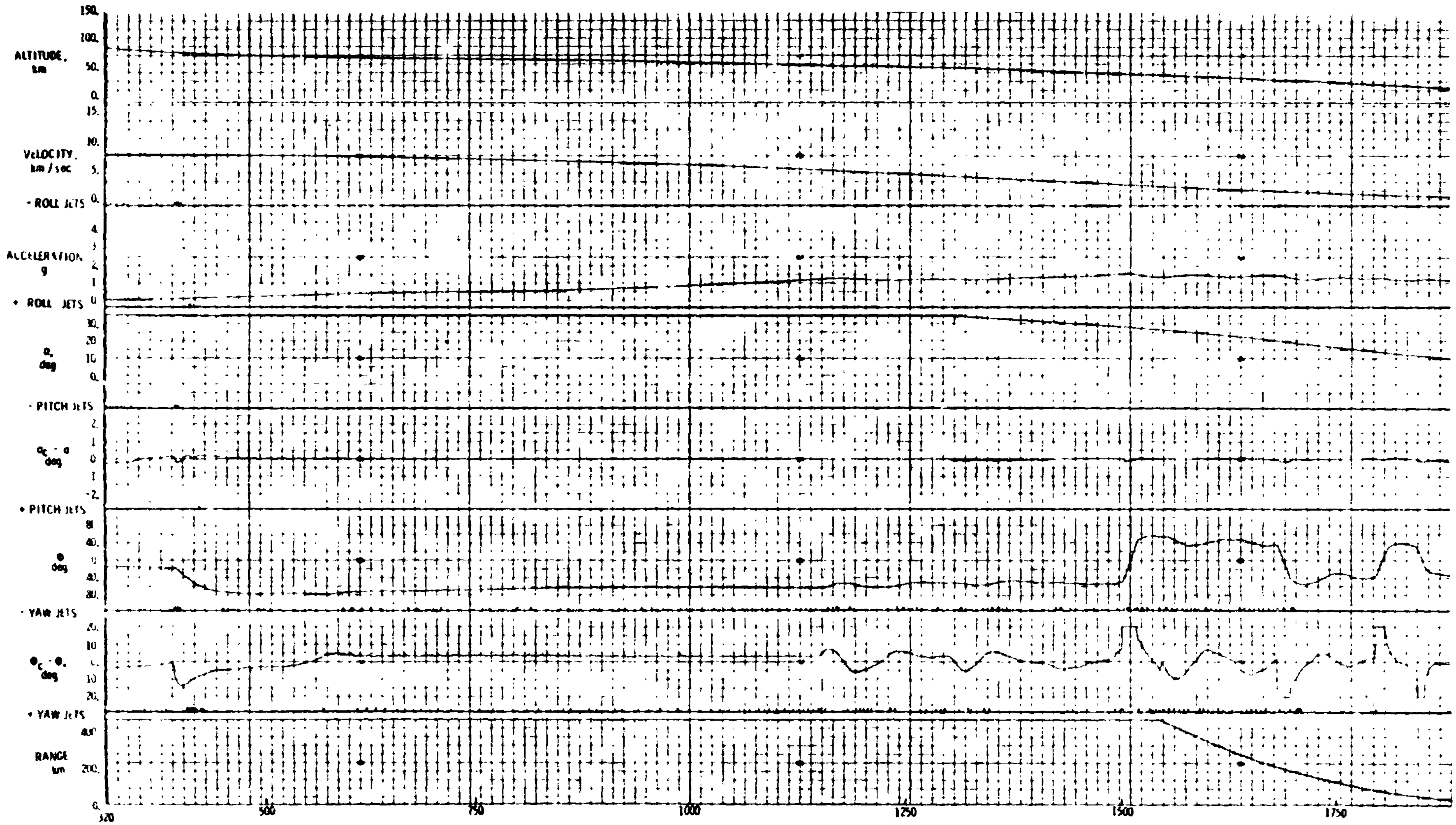

Figure 13. REVISED GUIDANCE - HYSTERESIS FACTORS C1 = 1.0, C2 = -5

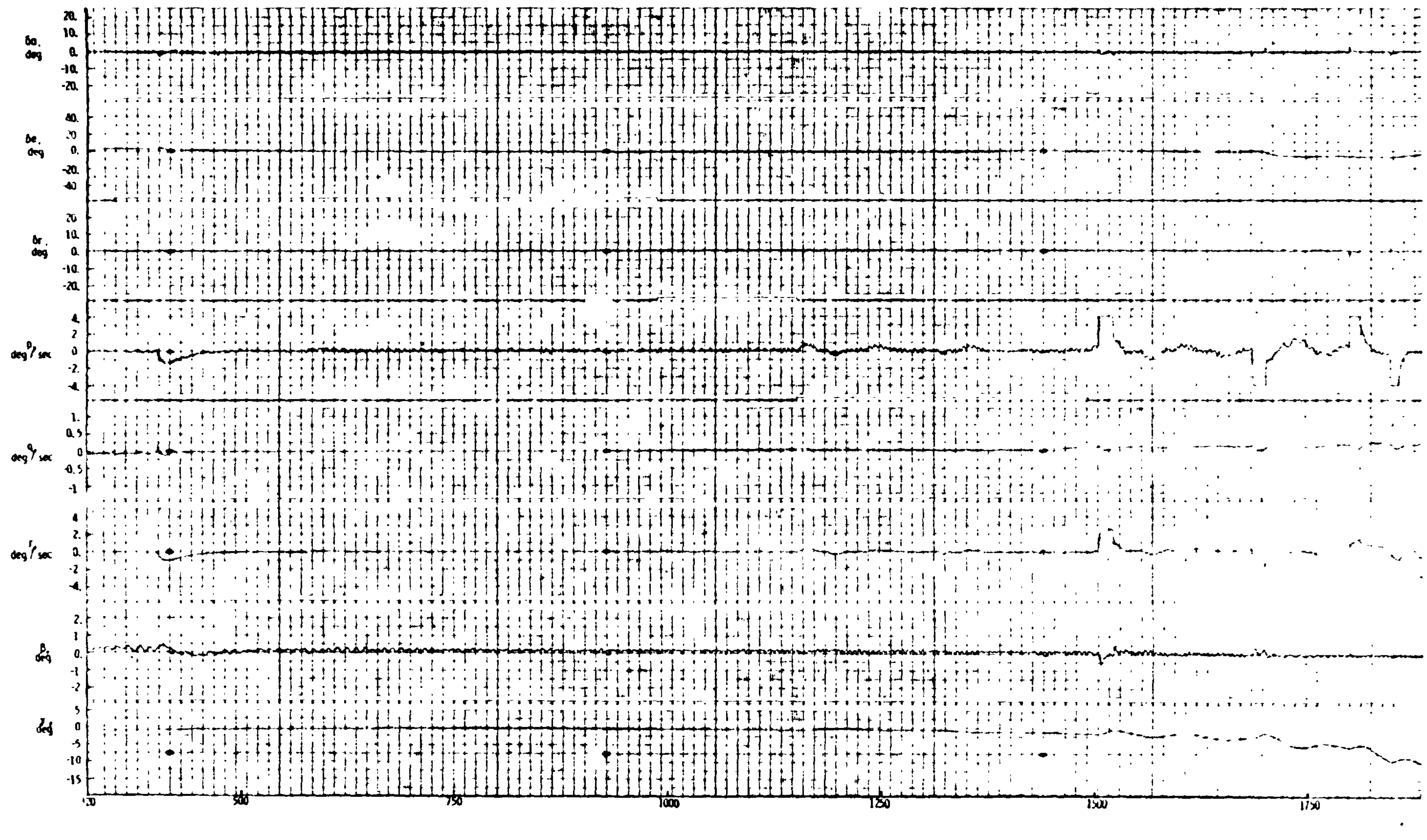

Figure 13. Concluded

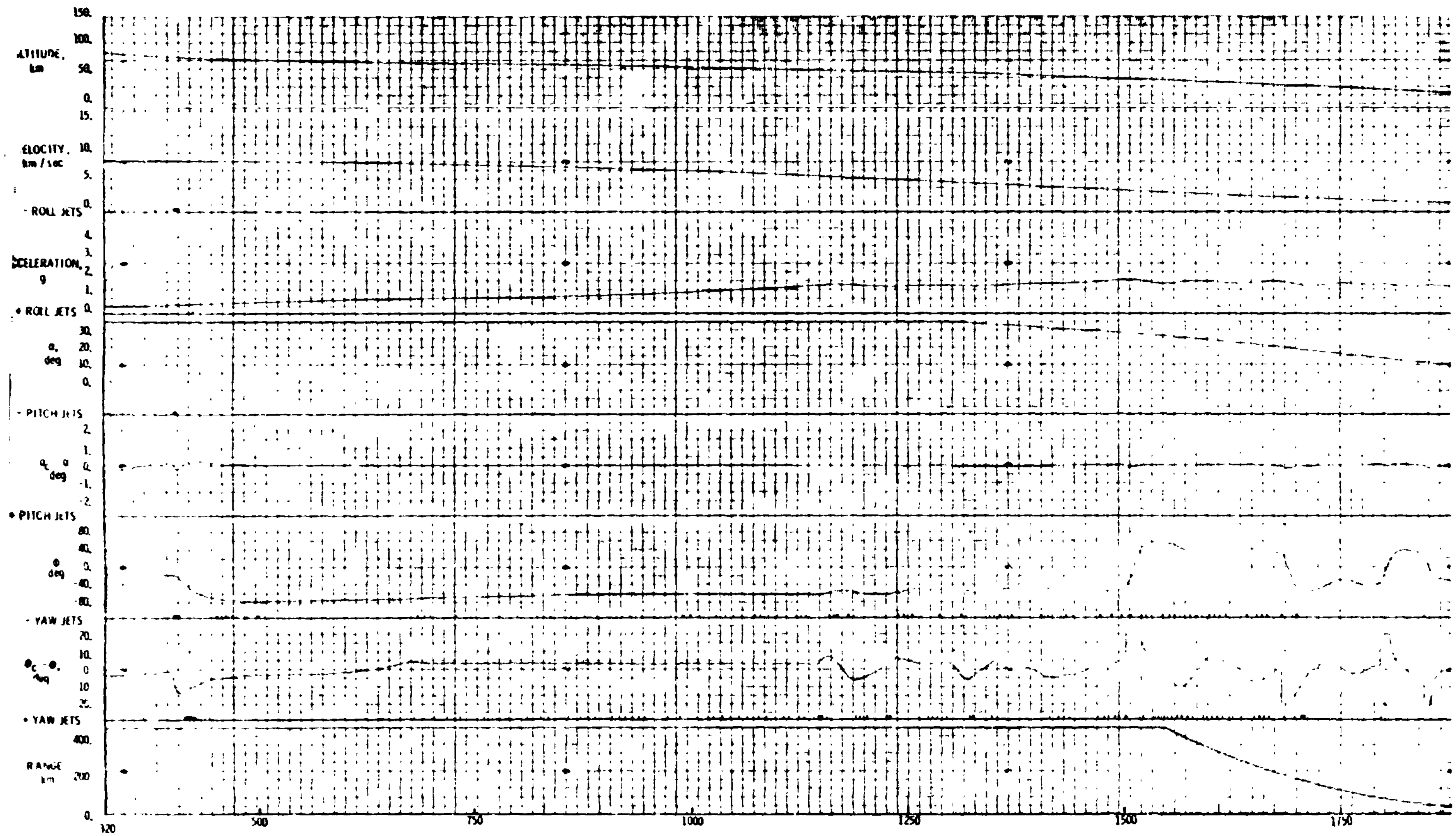

Figure 14. REVISED GUIDANCE - HYSTERESIS FACTORS C1 = 0.5, C2 = 5

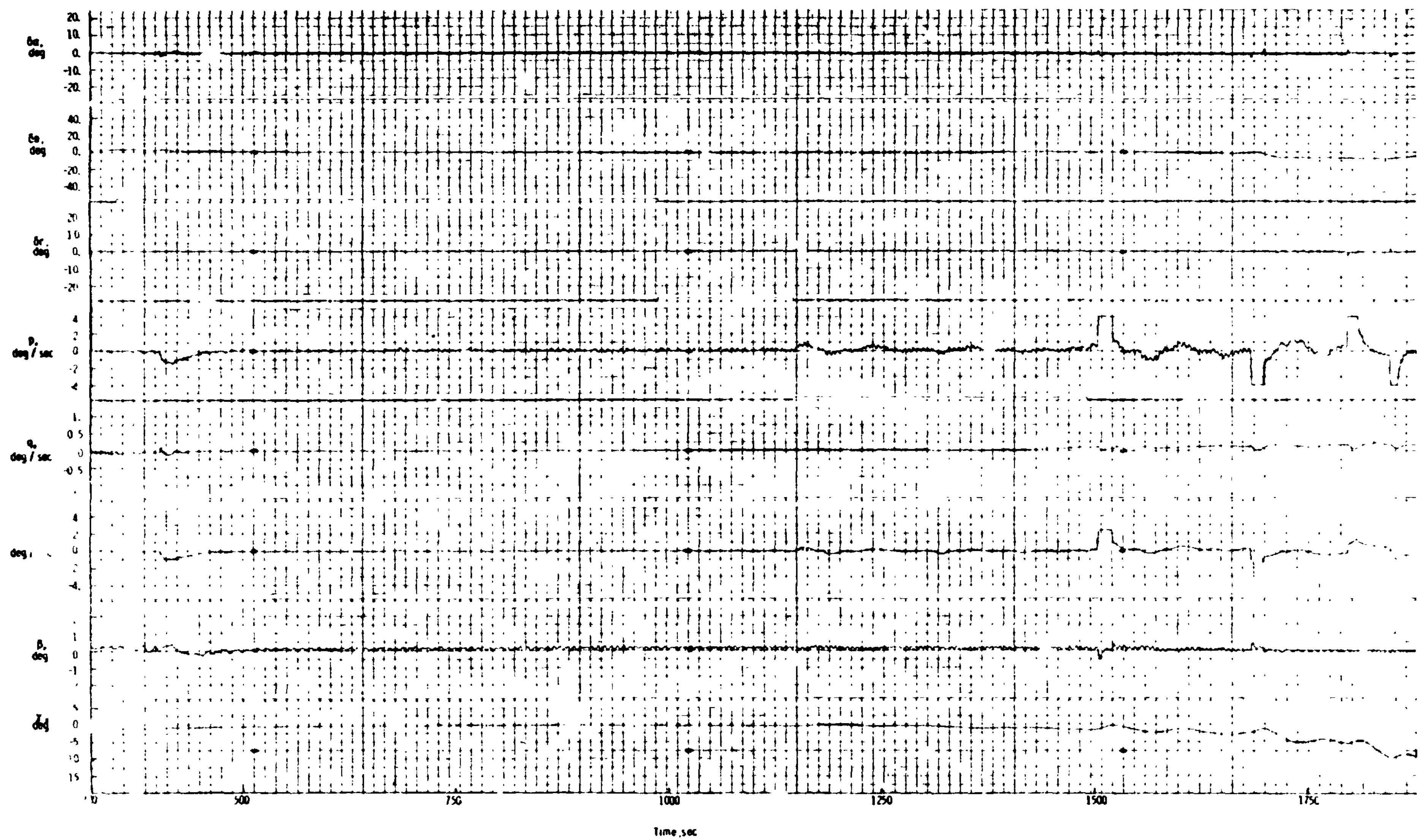

Figure 14 Concluded

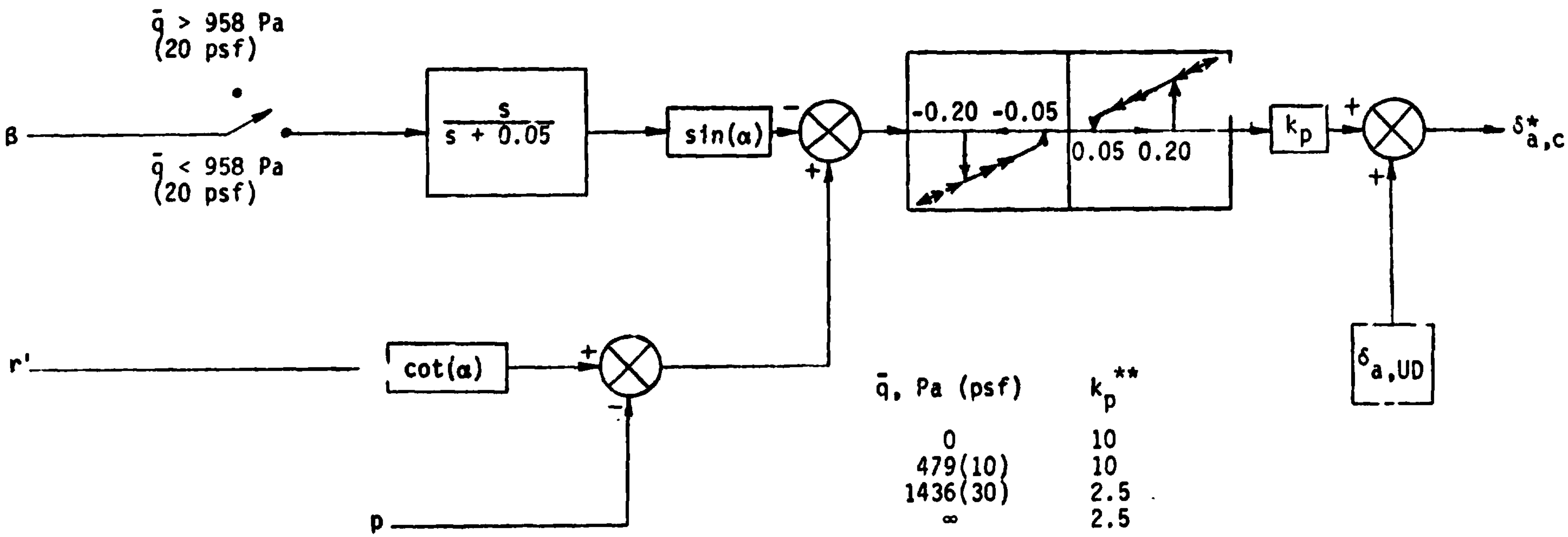

$\bar{q}$, Pa (psf)	k_p**
0	10
479(10)	10
1436(30)	2.5
∞	2.5

*For $\bar{q}$ < 92 Pa (2 psf), $\delta_{a,c} = 0$.

**k_p linearly varied between indicated points.

Figure 15. Aileron Command Block Diagram for $\alpha > 18°$ or $M > 5$.

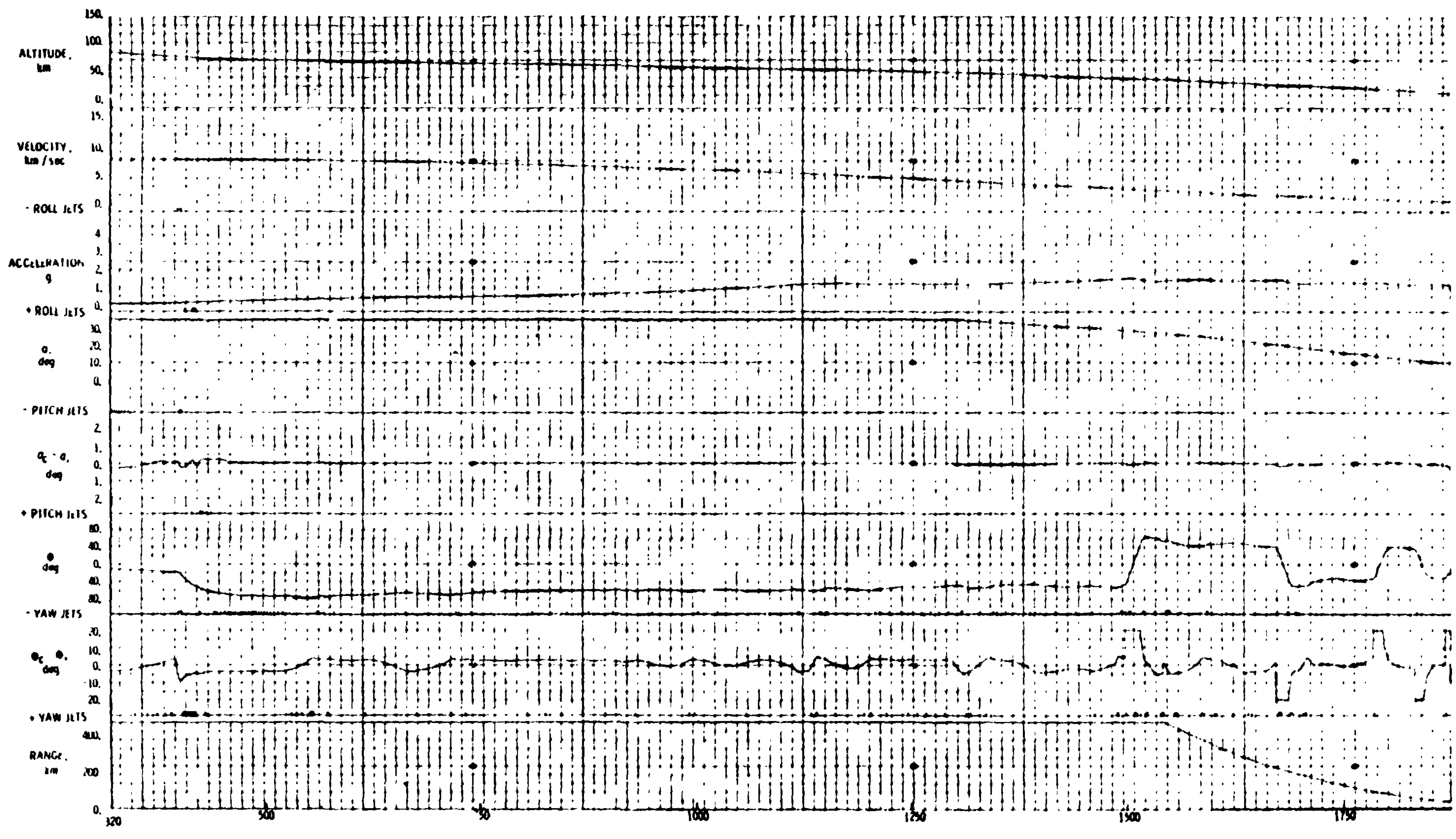

Figure 16. NOMINAL GUIDANCE NO DEADBAND IN AILERON CONTROL - NO HYSTERESIS

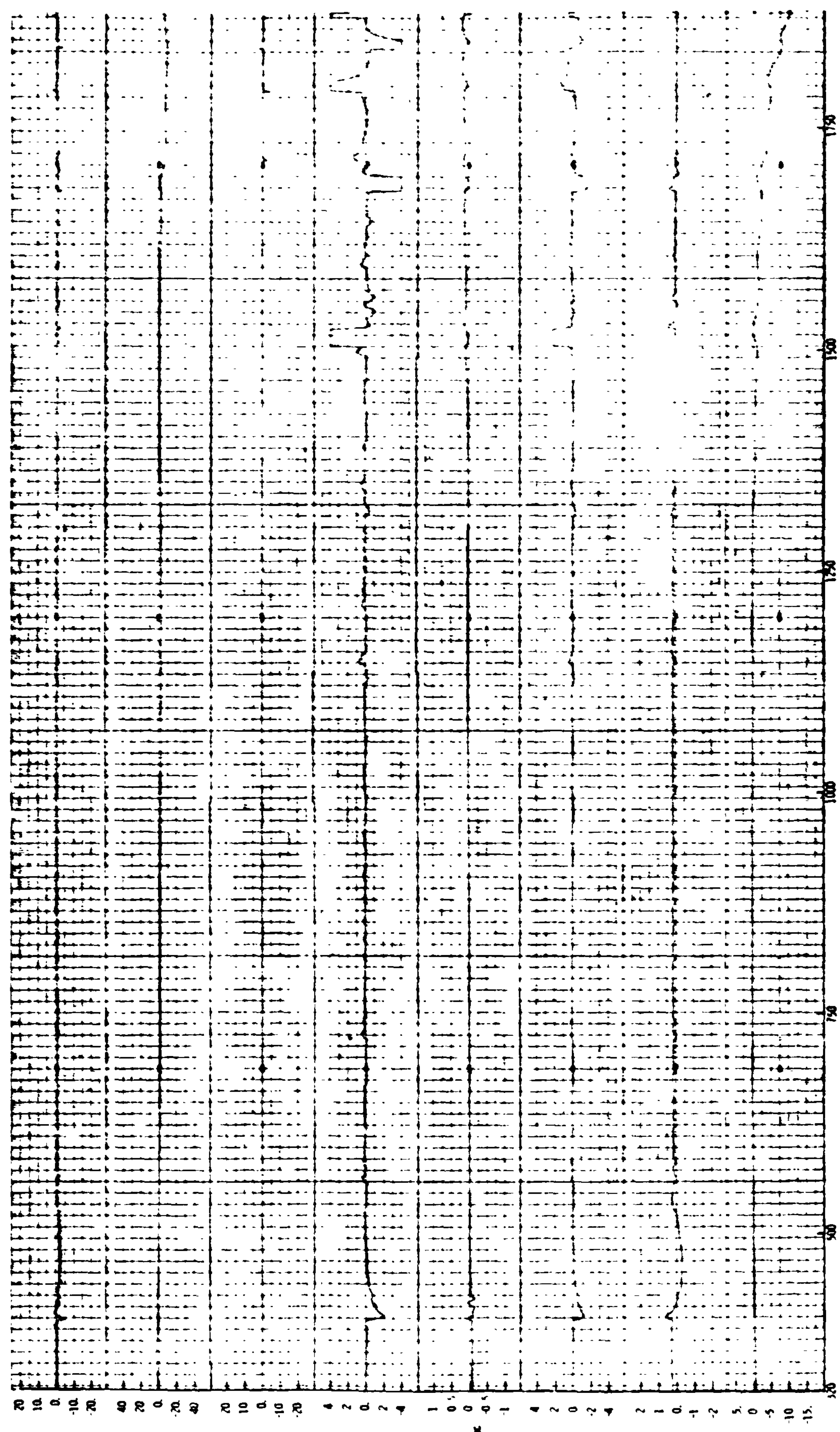

Figure 14. Concluded

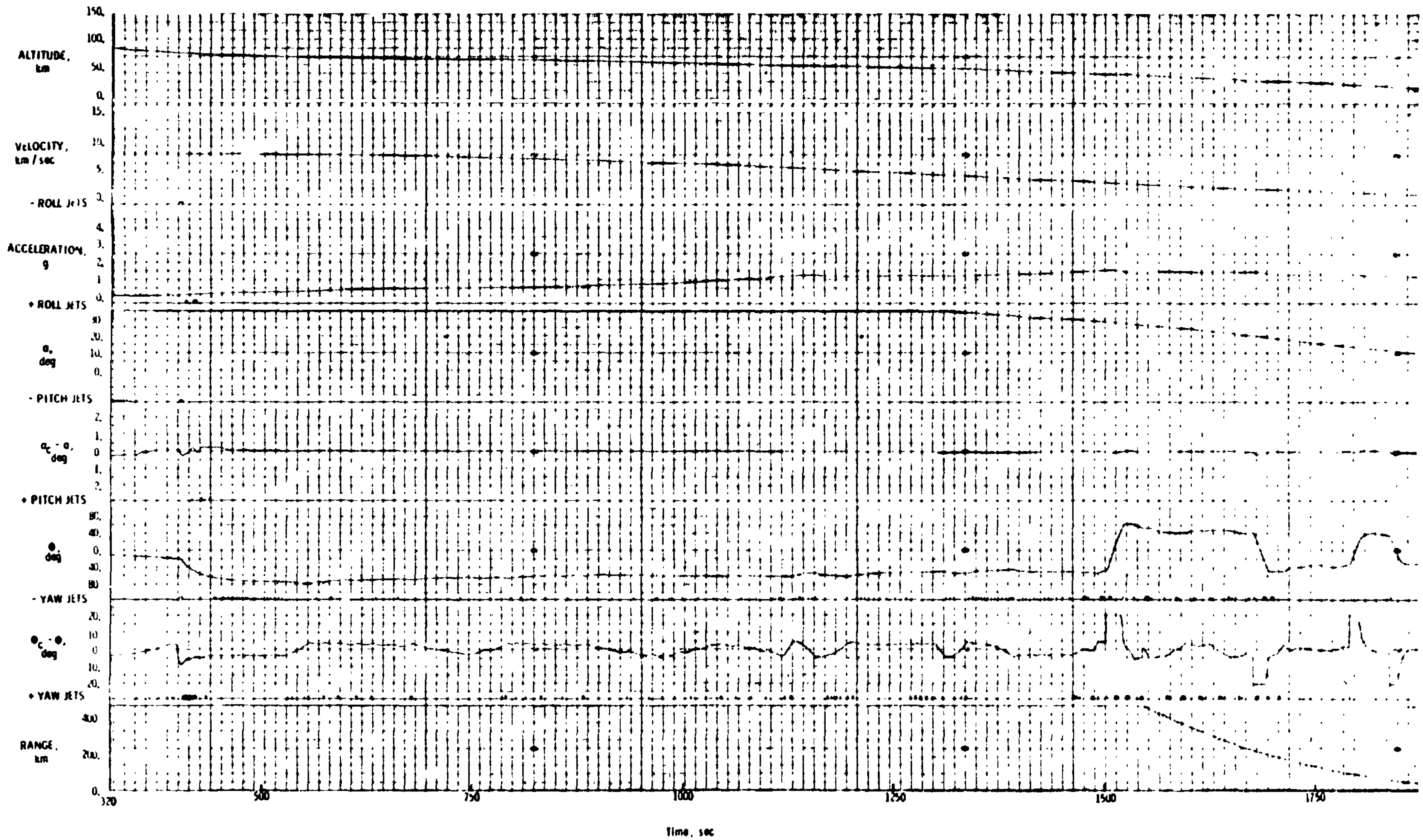

Figure 17. NOMINAL GUIDANCE - NO DEADBAND IN AILERON CONTROL - HYSTERESIS FACTORS C1 = 0.5, C2 = -5

Figure 17. Concluded

XII. APPENDIX A

Analytic Drag Control Entry Guidance System

The baseline guidance scheme controls the entry by roll modulation while flying a preselected angle-of-attack profile. Downrange is controlled by the magnitude of the roll angle and crossrange is controlled by multiple bank reversals. The guidance system outputs to the control system are commanded roll angle and commanded angle of attack.

The Analytic Drag Control Entry Guidance System (ADC, ref. 4) was developed by the NASA Johnson Space Center to approximate an optimum entry profile determined previously. This profile is achieved by dividing the entry into five major phases as illustrated in figure A-1:

1. Constant attitude phase
2. Constant heat rate phase
3. Equilibrium glide phase
4. Constant drag phase
5. Transition phase

The space shuttle orbiter is commanded to fly a constant attitude trajectory until a specified total acceleration is attained. At this point, a constant stagnation heat rate trajectory is flown through pullout to a relative velocity of 6248.4 m/sec (20 500 fps) or until the reference drag level becomes larger than that required to reach the target. If the latter condition is reached, the guidance scheme jumps to the constant drag phase. If this condition is not met, an equilibrium glide profile is flown until either it intersects the constant drag profile required to reach the target and jump to the constant drag phase, or the velocity drops off to 2743.2 m/sec (9000 fps). Whenever the velocity drops to 2743.2 m/sec (9000 fps), the transition phase is entered during which the commanded angle of attack is decreased to the value required at the Terminal Area Energy Management (TAEM) point, which occurs at a velocity of 457.2 m/sec (1500 fps) and an altitude of approximately 21 km (70 000 ft).

Table A-I shows the input constants that were used, and figure A-2 shows the block diagram of the guidance laws of reference 2 as modified for the Automatic Reentry Flight Dynamics Simulator.

SYMBOLS

PARAMETER	UNIT	DEFINITION
AK	sec^{-1}	dD/dV for constant heat rate phase, used to define C 3
ALDREF	n.d.	$(L/D)_{ref}$, used in controller
ALFM	m/sec^2	reference equilibrium glide drag
ALMN1	rad	minimum roll command outside of lateral deadband (YB)
ALMN2	rad	minimum roll command inside of lateral deadband (YB)
ALPCMD	deg	α_c, angle of attack command
ARC	m	distance from intersection with alinement circle to target
ARG	rad	$(L/D)_V/(L/D)$, used in roll command equations

ATK	m	radius of earth
BA	rad	equilibrium glide roll angle used in iteration loop
BAD	deg	final equilibrium glide roll angle
BA1	deg	first iteration equilibrium glide roll angle
BA2	deg	second iteration equilibrium glide roll angle
CAGI	sec^2/m^2	temporary calculation used in transition phase to calculate ALDREF and RDTREF
CIGAR	n.d.	transformation matrix from Earth Centered Inertial (ECI) axes to geocentric axes
CØSBADD	n.d.	temporary calculation in equilibrium glide ranging phase used to calculate DREFP
CTH	rad	great circle range from orbiter to target
C4	m/sec	parameter used to calculate RDTREF
C5	n.d.	parameter used to calculate RDTREF
C11	m^{-1}	parameter used to calculate RER1 and RDTREF
C16	sec^2/m	parameter used to calculate LØD1
C17	sec/m	parameter used to calculate LØD1
C21	m/sec^2	parameter used to calculate DREFP, RDTREF, SQ and TT11
C22	sec^{-1}	parameter used to calculate DREFP, E1, E2, RDTREF, SQ, TT11, and TT22
C23	m^{-1}	parameter used to calculate C22, DREFP, E1, E2, SQ, TT11, and TT22
D	N	total drag force
DBAR	m	distance from runway to alinement circle
DBB	deg	increment in roll angle in equilibrium glide phase

DELAZ	rad	azimuth error
DF	m/sec^2	final drag level in transition phase
DLIM	m/sec^2	control system limit drag level in transition phase
DRAG	m/sec^2	current drag acceleration level
DREFP	m/sec^2	drag reference used in controller
DT	m	planar range to target
DTH	rad	angle between alinement circle center and tangency point
DTR	rad/deg	$\pi/180$
DVHEAD	rad	azimuth between runway and heading to tangency point of alinement circle
D23	m/sec^2	parameter used to calculate AK
EEF	m^2/sec^2	current energy level
EEF4	m^2/sec^2	reference energy level used in transition phase
E1	n.d.	parameter used to calculate TT22
E2	n.d.	parameter used to calculate TT22
GAMMA	rad	flight path angle
GCLAT	rad	orbiter geocentric latitude
GCLATT	rad	target geocentric latitude
GS	m/sec^2	acceleration of gravity at sea level
GSTART	n.d.	acceleration in "g's" required to initiate constant heat rate phase
HA	m	current altitude
HADØT	m/sec	dHA/dt
HDSER	m^3/sec	parameter in oblate earth correction term to RDTREF
HS	m	altitude scale height

IDFG2	n.d.	switching flag in constant drag phase
IDFG3	n.d.	switching flag in transition phase
IFT	n.d.	initialization flag in equilibrium glide phase
ISLECT	n.d.	phase selector
ISTART	n.d.	initialization flag
ISTP	n.d.	iteration flag in equilibrium glide phase
ISTRT	n.d.	flag indicating acceleration level equal to GSTART has been reached
ITR	n.d.	iteration flag in transition phase
L/D	n.d.	lift to drag ratio
$(L/D)_V$	n.d.	lift to drag ratio in vertical plane
LMN	n.d.	minimum value of LØD1
LØD1	n.d.	desired (L/D_V)
PSIE	rad	current heading of orbiter
PSIET	rad	current heading to target
RAZ	rad	runway azimuth
RCG	m	predicated range in constant drag phase
RDC	n.d.	parameter used in RDTREF calculation
RDTØLD	m/sec	final RDTREF in equilibrium glide phase
RDTØL2	m/sec	final RDTREF in constant drag phase
RDTREF	m/sec	altitude rate reference
REC	n.d.	vector defining runway coordinate system
REC1	n.d.	$[REC]^{-1}$
REH	m	distance from center of earth to vehicle
REQ	m	predicted equilibrium glide phase range
RER1	m	parameter in range prediction for transition phase

RFF	m	predicted range in constant heat rate phase
RG	m	vector from orbiter to runway center
RGP	m	vector from orbiter to alinement circle center
RK2RØL	n.d.	roll direction (+ right, - left)
RLØN	rad	orbiter's longitude
RLONT	rad	target longitude
ROLLC	rad	ϕ_c, roll angle command
RPT	m	desired range in transition phase
RPT1	m	range bias below velocity of 456.2 m/sec
RTE	m	radius of earth at runway
RTURN	m	radius of alinement circle
R11	m	first iteration of range prediction in equilibrium glide and transition phases
R12	m	second iteration of range prediction in equilibrium glide and transition phases
SQ	sec^{-2}	parameter used in constant heat rate range prediction
SQQ	sec^{-1}	parameter used in constant heat rate range prediction
TA	m	vector from alinement circle tangency point to vehicle
TAP	m	vector TA in geocentric coordinates
TARE	m	target vector from alinement circle center to runway
TDREF	m/sec^2	parameter used in DREFP calculation in equilibrium glide phase
TEMP	m	temporary calculation in equilibrium glide phase
TRANGE	m	great circle range from orbiter to target

TT11	m	parameter used in range prediction in constant heat rate phase
TT22	m	parameter used in range prediction in constant heat rate phase
T1	m/sec^2	parameter used in calculation of ALDREF
T2	m/sec^2	constant drag level required to reach the target
U	rad	| DVHEAD |
UTARE	n.d.	TARE unit vector
UXYZE	n.d.	RG unit vector
V	m/sec	earth relative velocity
VBB	m/sec	intersection velocity between constant heat rate phase and equilibrium glide phase
VCG	m/sec	predicted intersection velocity between constant drag phase and equilibrium glide phase
VINERT	m/sec	inertial velocity
VØLD	m/sec	final velocity in equilibrium glide phase
VØLD2	m/sec	final velocity in constant drag phase
VQ	m	predicted final velocity for constant drag phase
VSAT	m/sec	reference circular orbit velocity
VSATS	m^2/sec^2	$(VSAT)^2$
V1ØLD	m/sec	value of VØLD-152.4
V2ØLD	m/sec	value of VØLD2-152.4
XLFAC	m/sec^2	total acceleration
XLØD	n.d.	L/D
XYZE	m	geocentric position vector
YB	rad	lateral deadband (amount of overshoot that guidance system will allow before commanding roll reversal)

TABLE A-I.- ADC GUIDANCE INPUT CONSTANTS

PARAMETER	VALUE	UNIT
ALFM	7.62	m/sec^2
ALMN1	0.7986355	n.d.
ALMN2	0.9659258262	n.d.
ATK	6.36670702×10^6	m
DBAR	14360.4	m
DF	5.819	m/sec^2
EEF4	1.8580608×10^5	m^2/sec^2
GCLATT	34.55577617	deg
GS	9.815	m/sec^2
GSTART	0.05	n.d.
RAZ	-0.7679448709	rad
RLØNT	-120.5338	deg
RPT	4.218856×10^5	m
RPT1	23150	m
RTE	6.373298953×10^6	m
RTURN	4632.96	m
VSAT	7853.54	m/sec
VQ	2133.6	m/sec

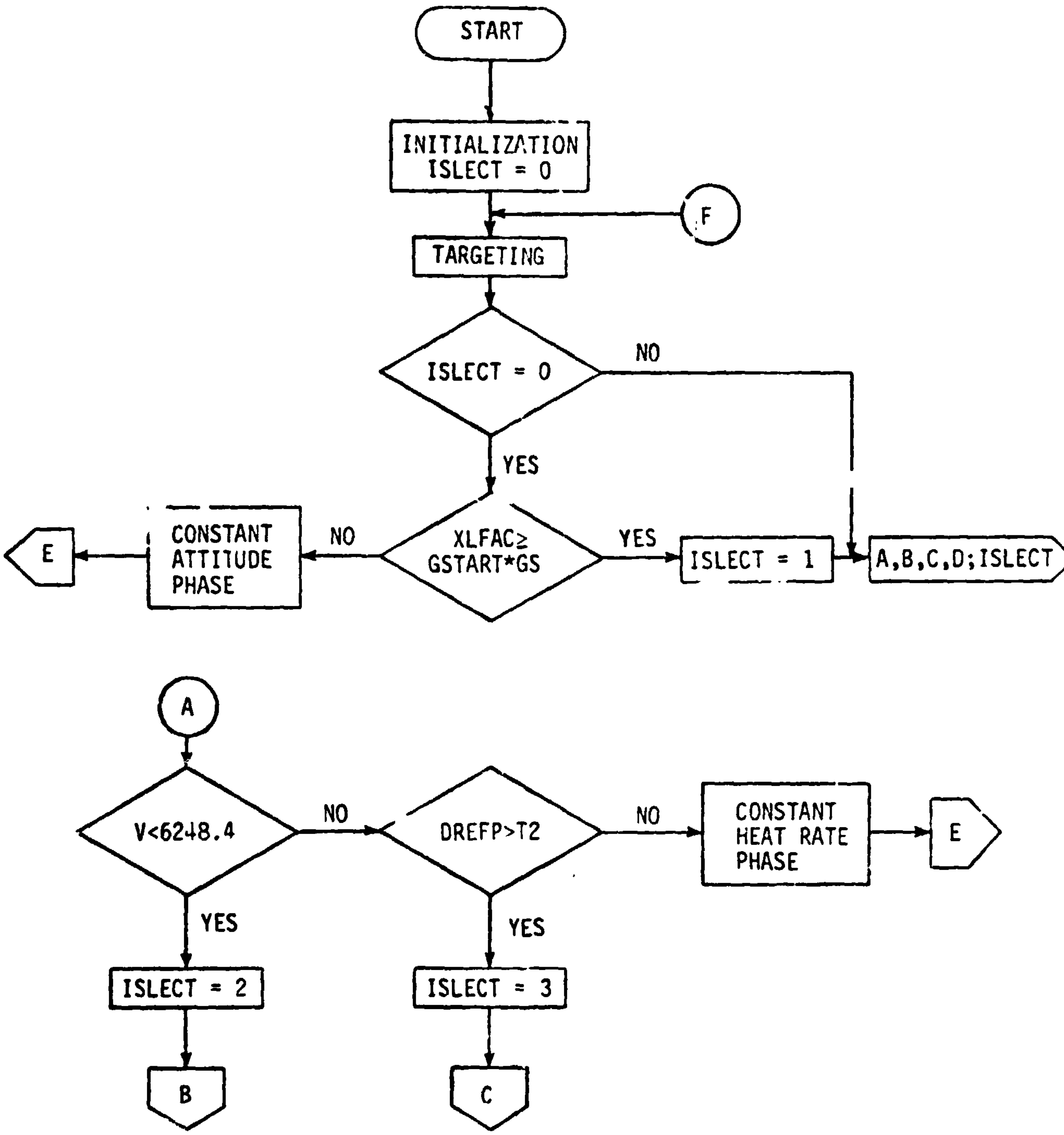

Figure A-1.- Analytic Drag Control Entry Guidance System flow diagram.

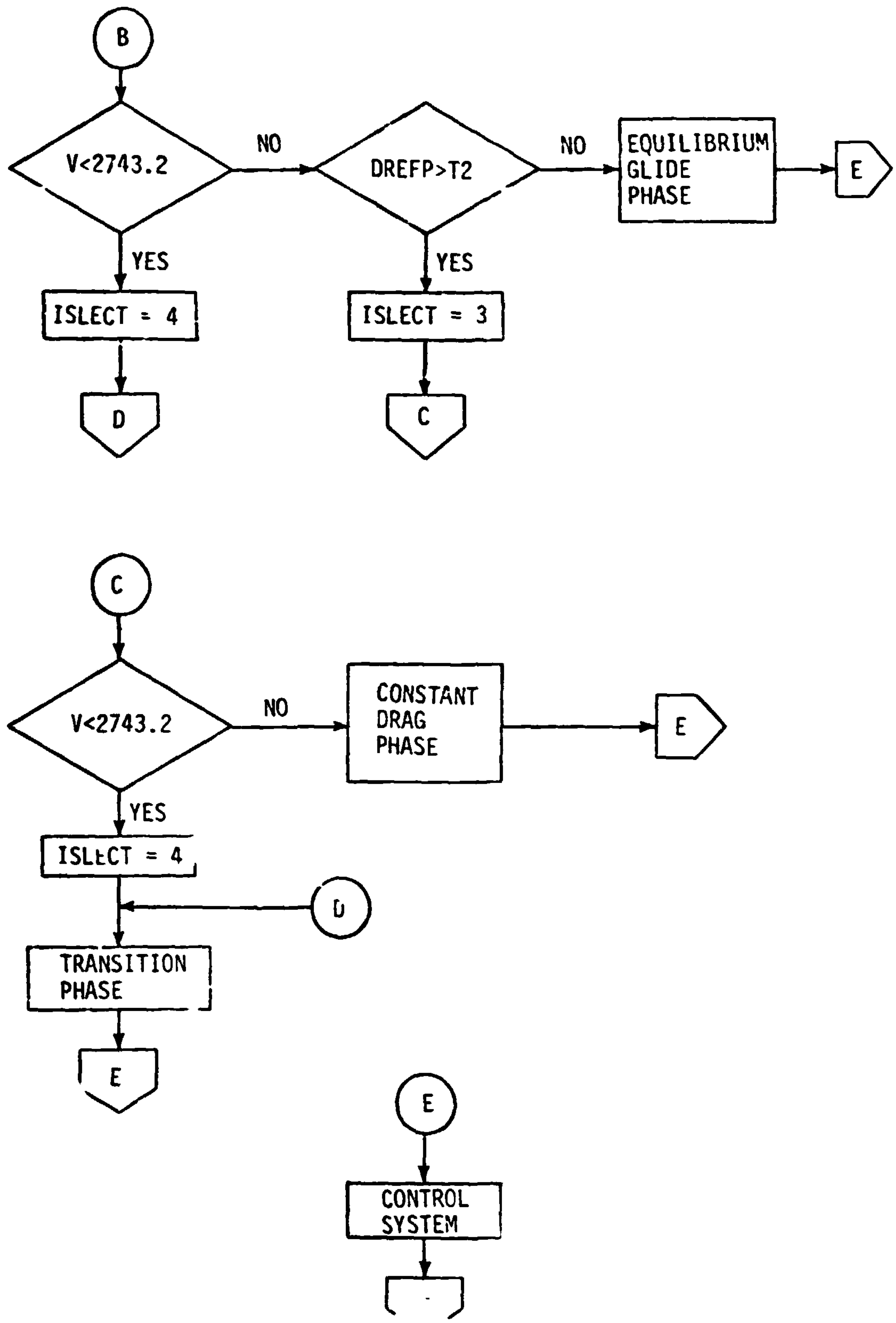

Figure A-1.- Concluded.

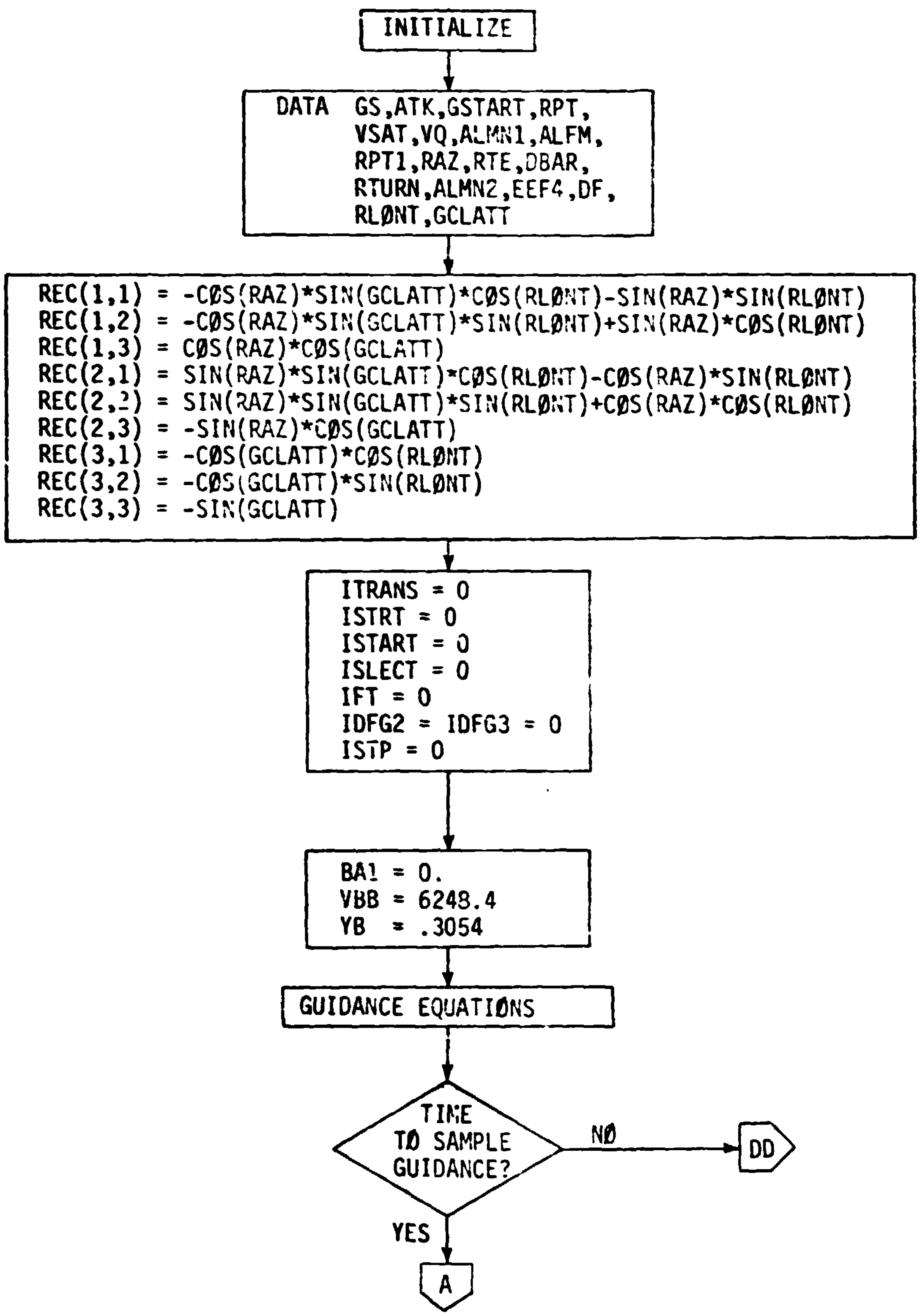

Figure A-2.- Analytic Drag Control Entry Guidance System block diagram.

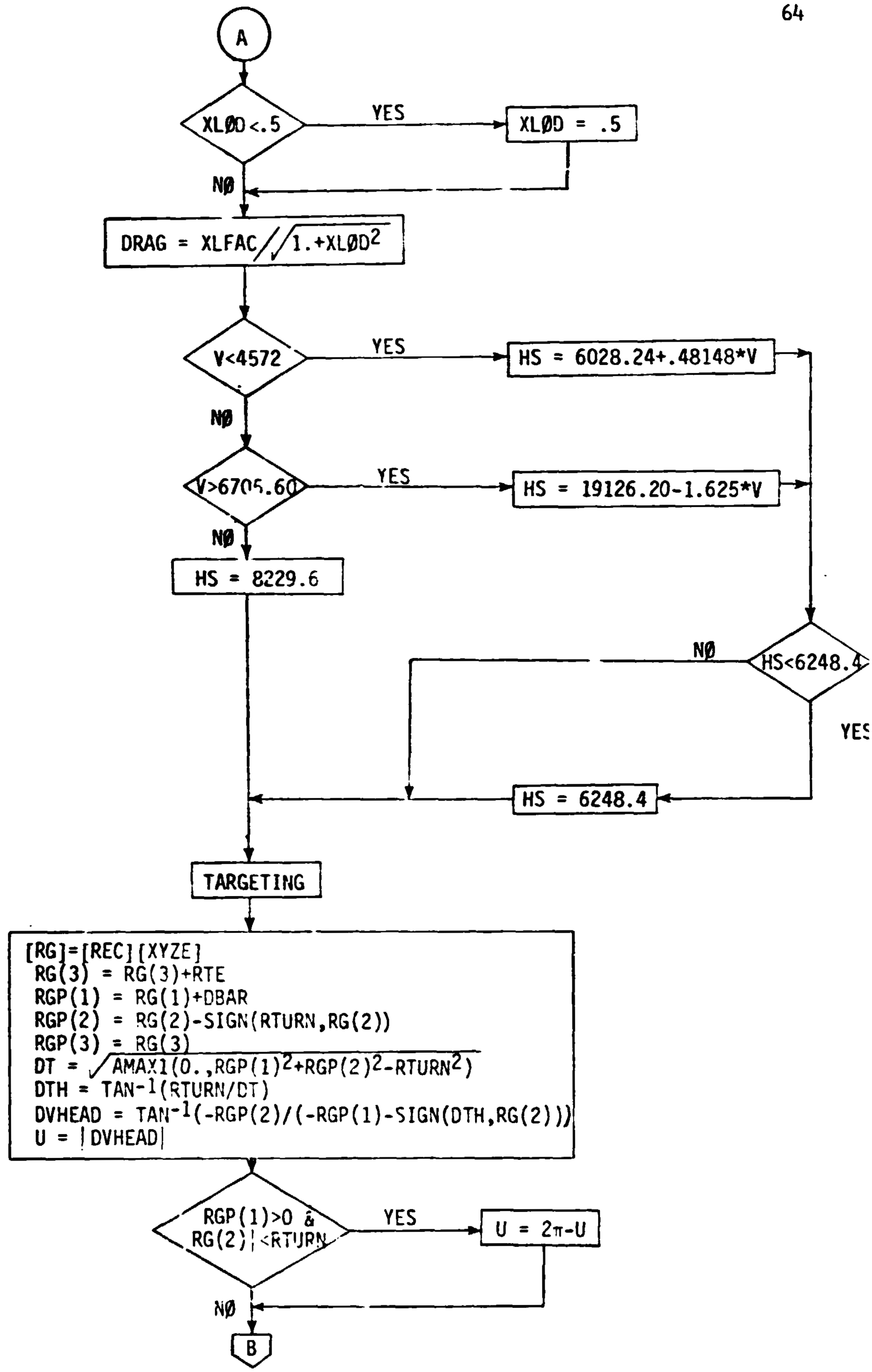

Figure A-2.- Continued.

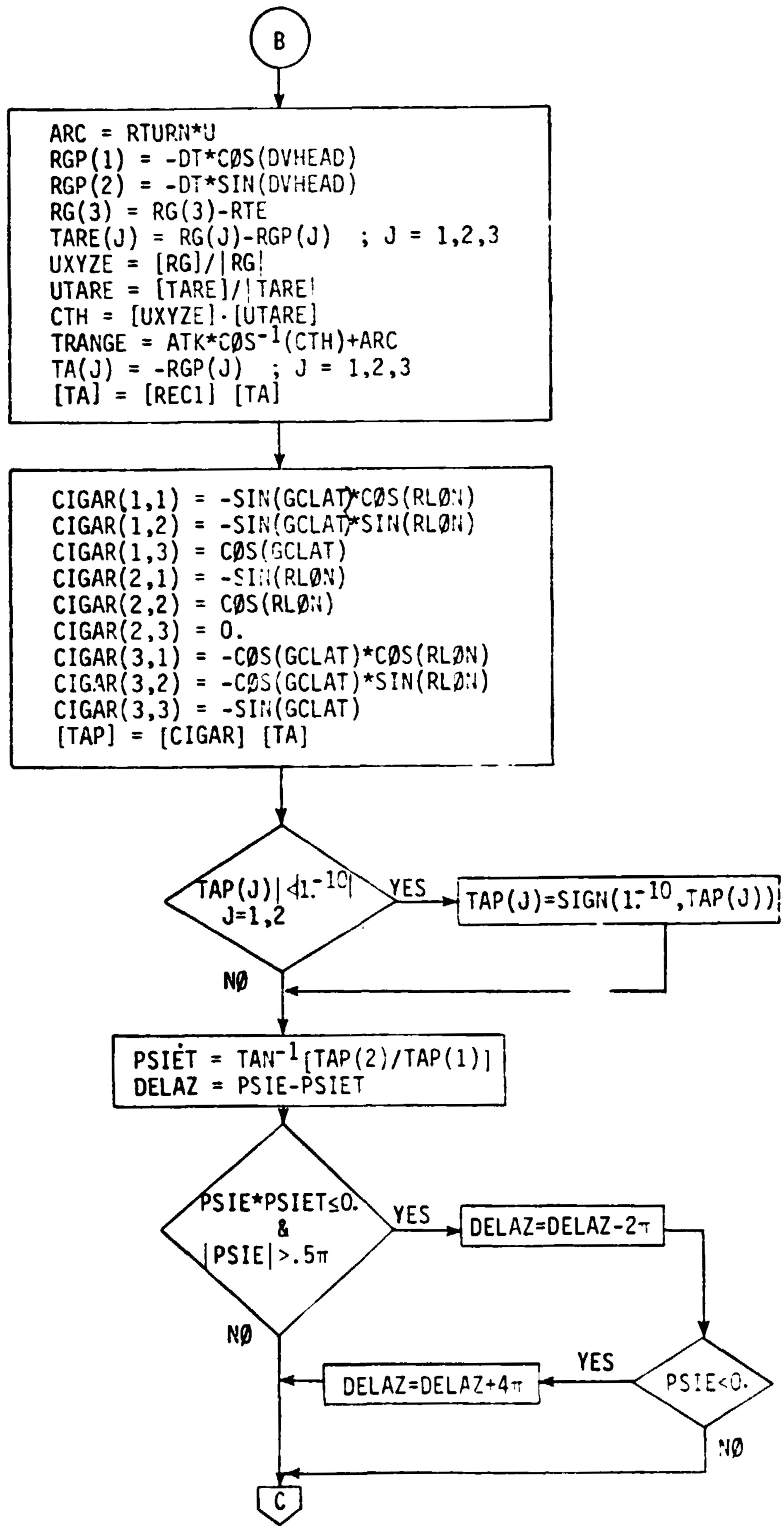

Figure A-2.- Continued.

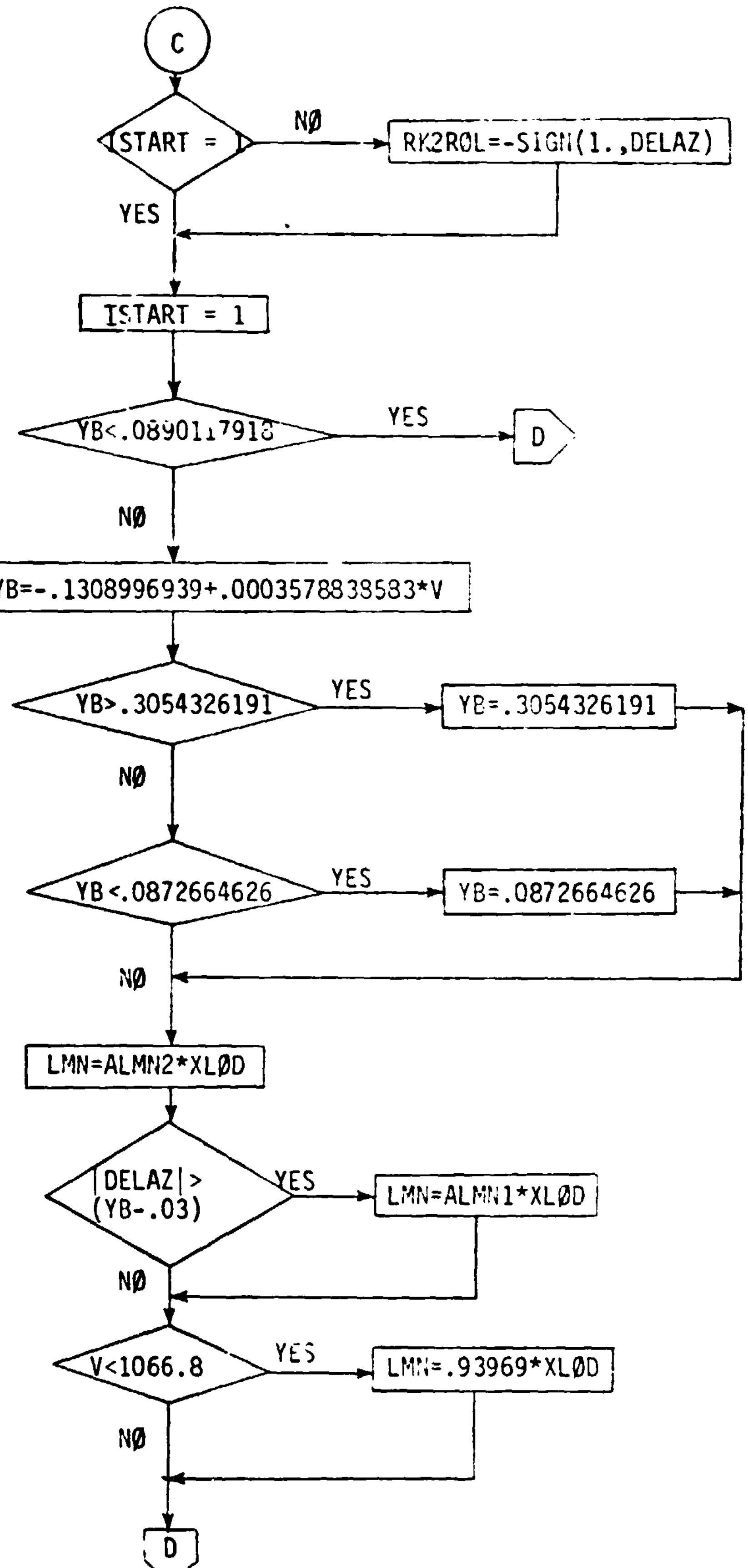

Figure A-2.- Continued.

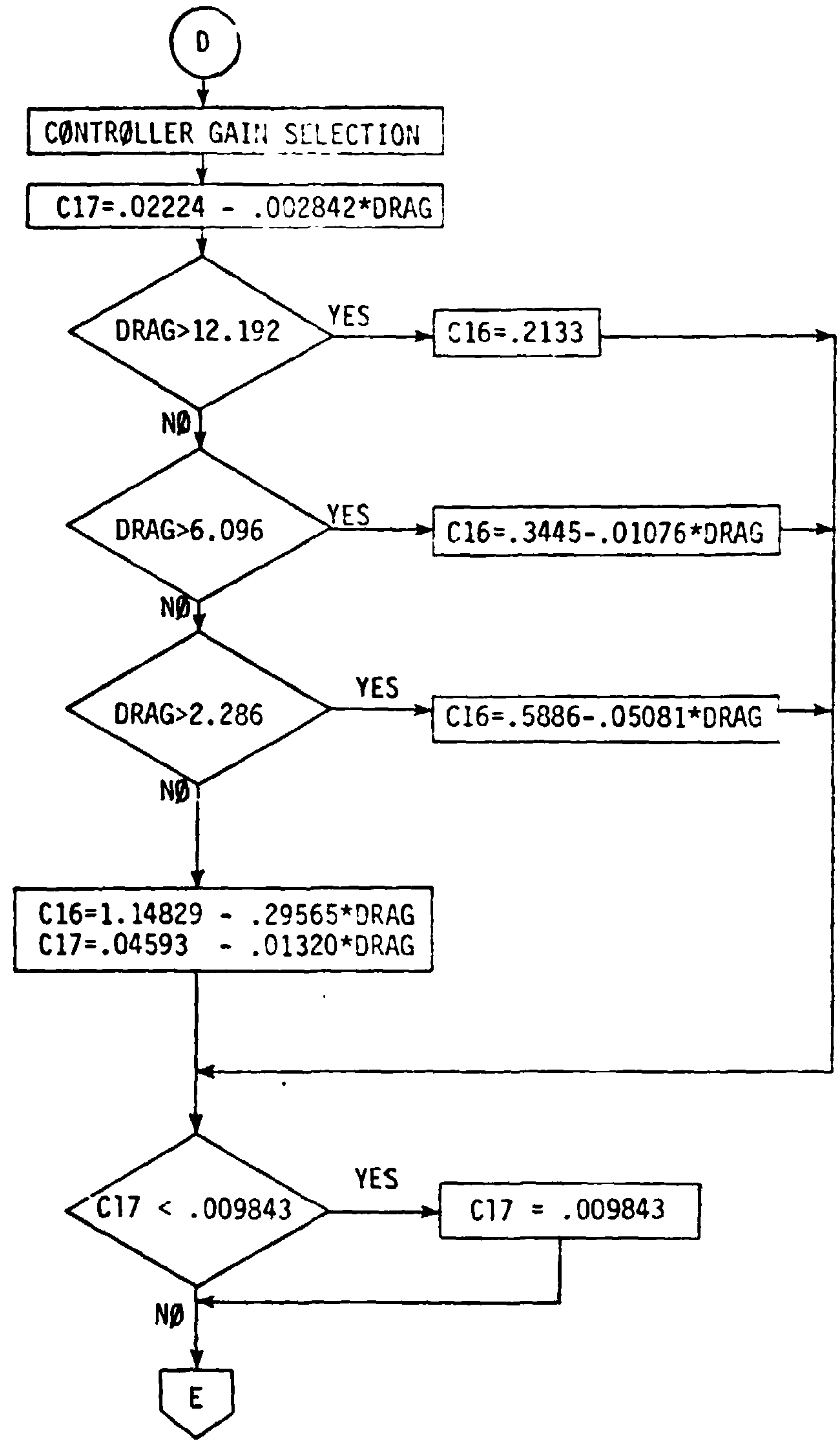

Figure A-2.- Continued.

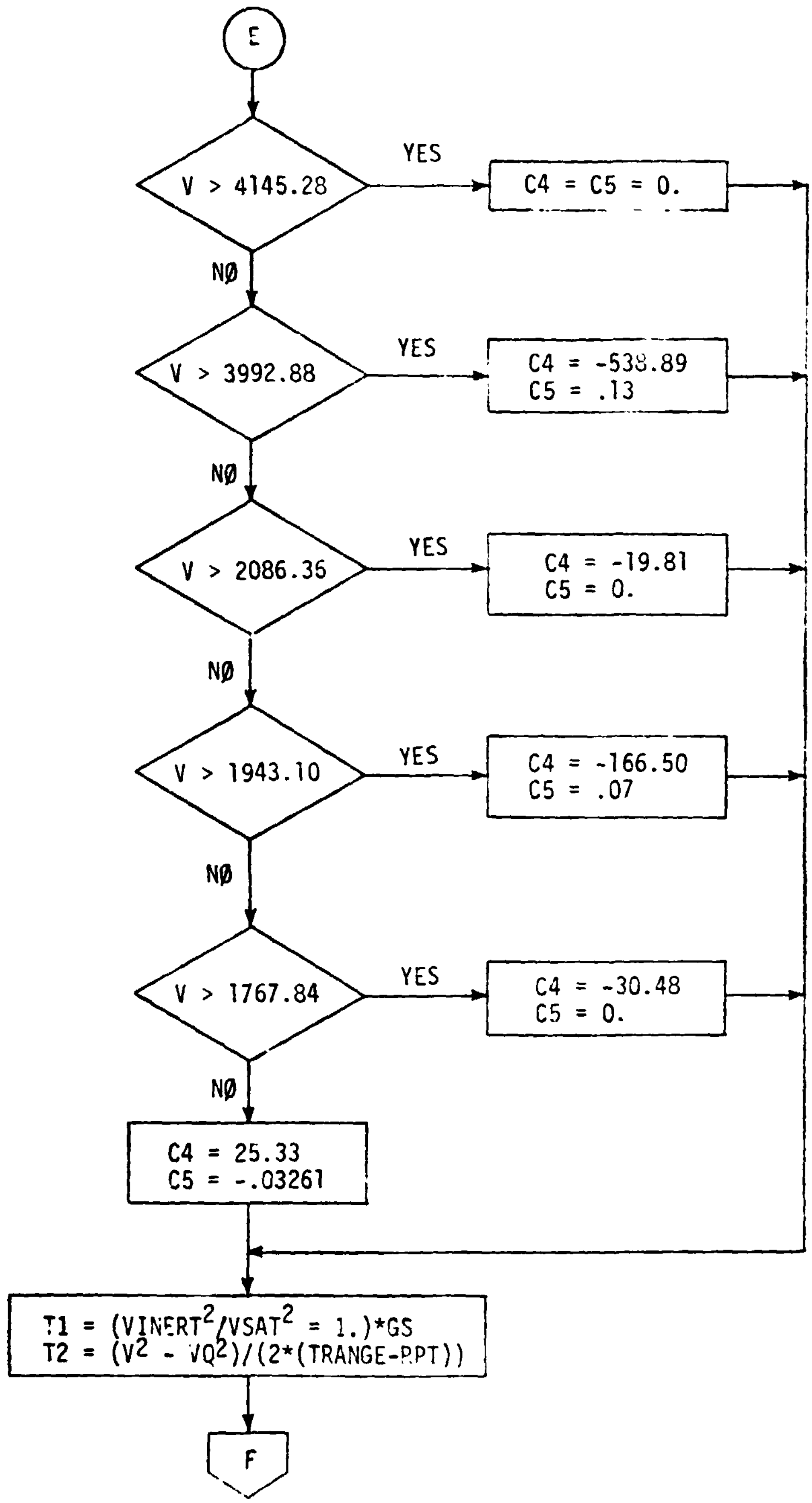

Figure A-2.- Continued.

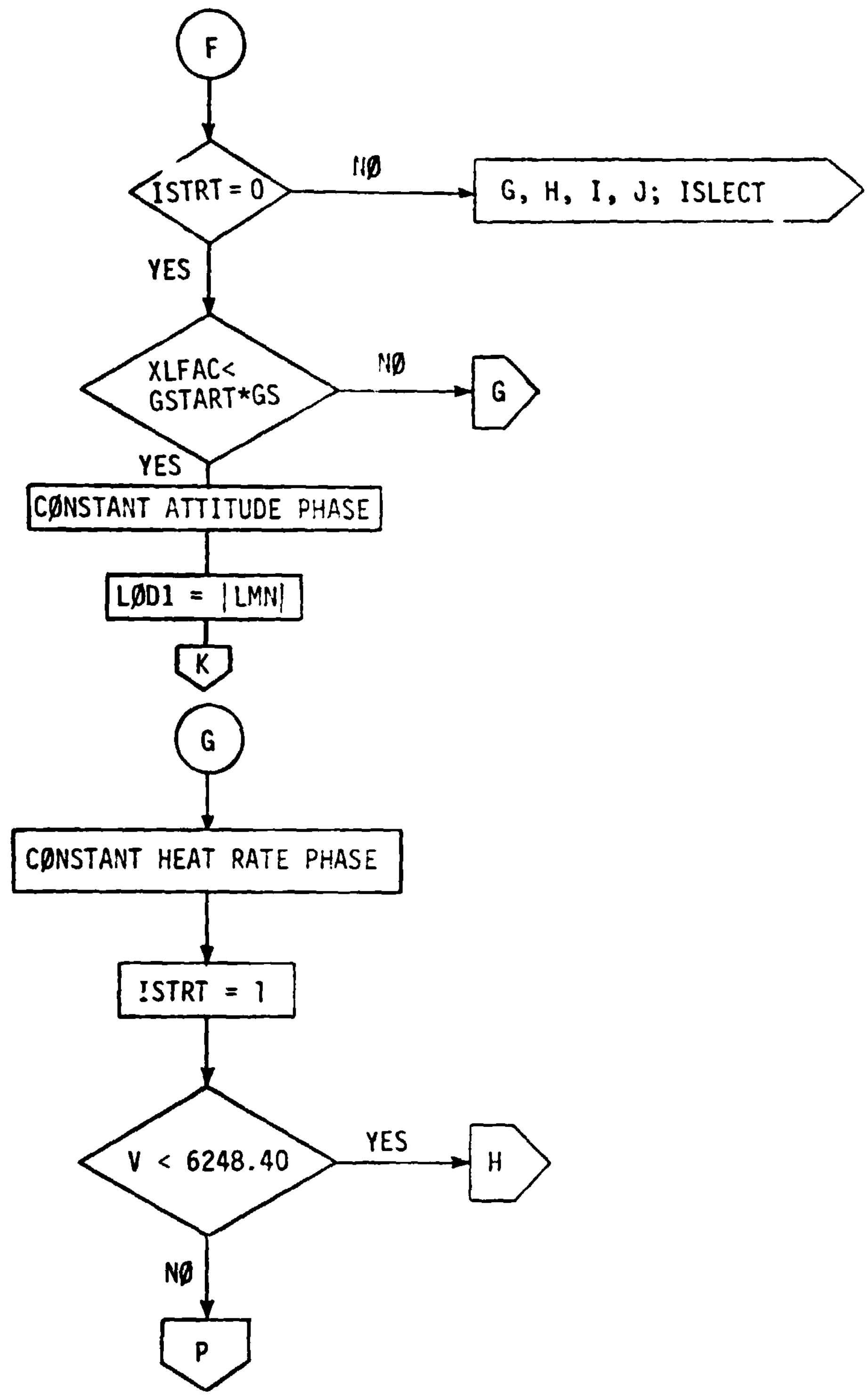

Figure A-2.- Continued.

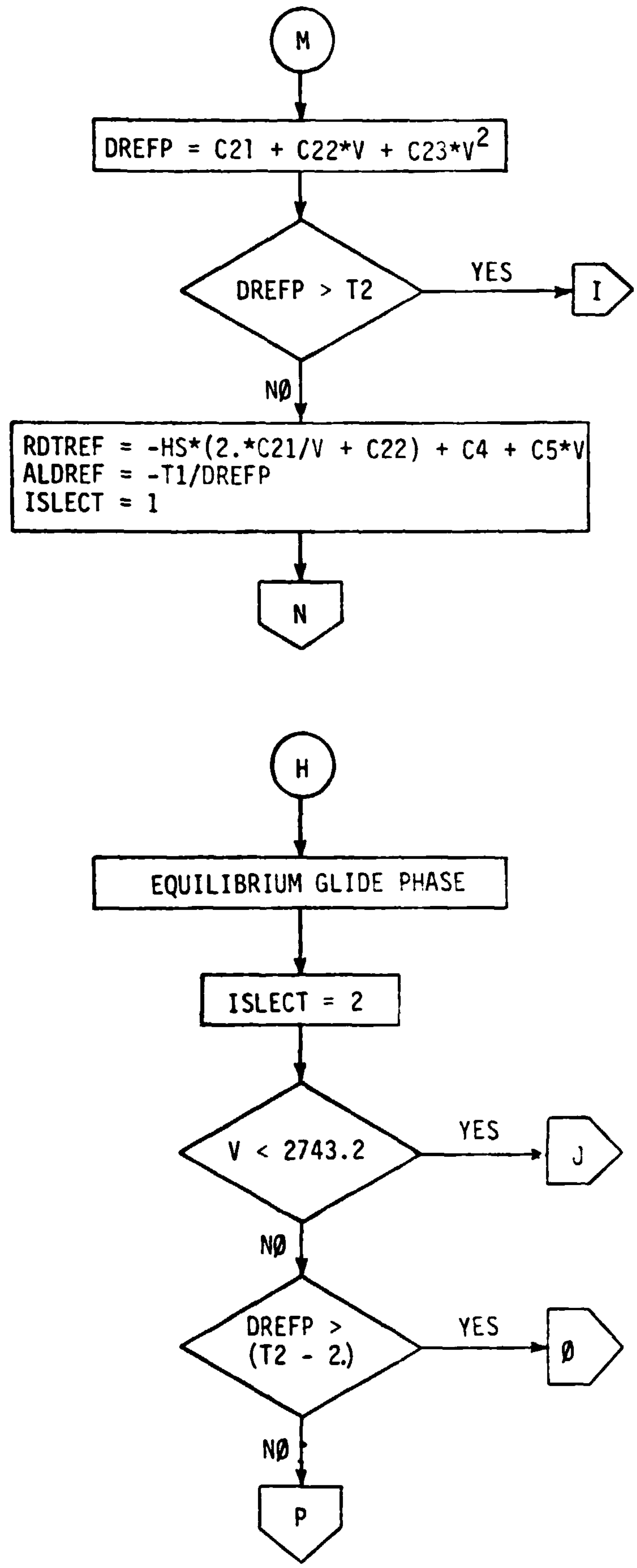

Figure A-2.– Continued.

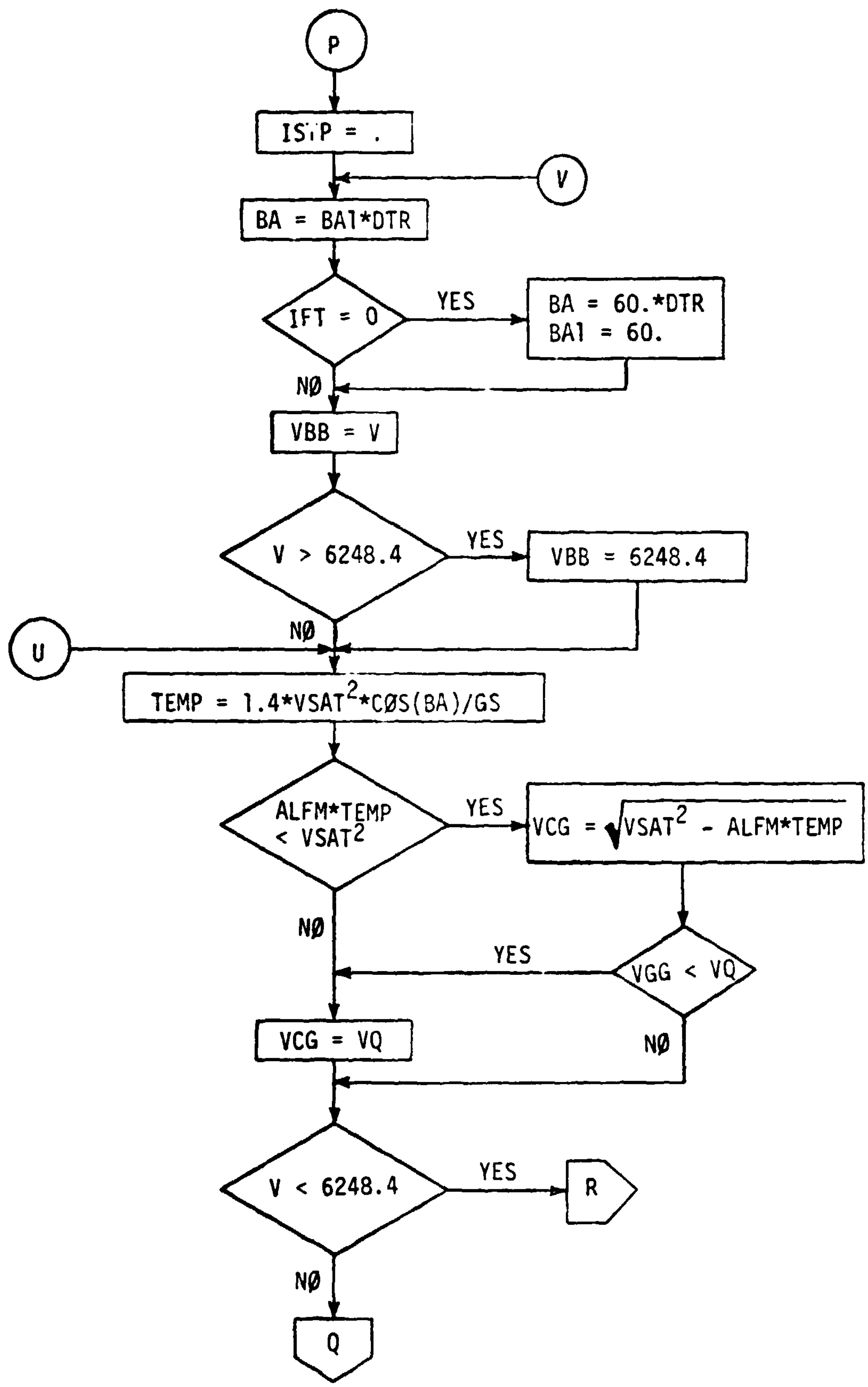

Figur. A-2.- Continued.

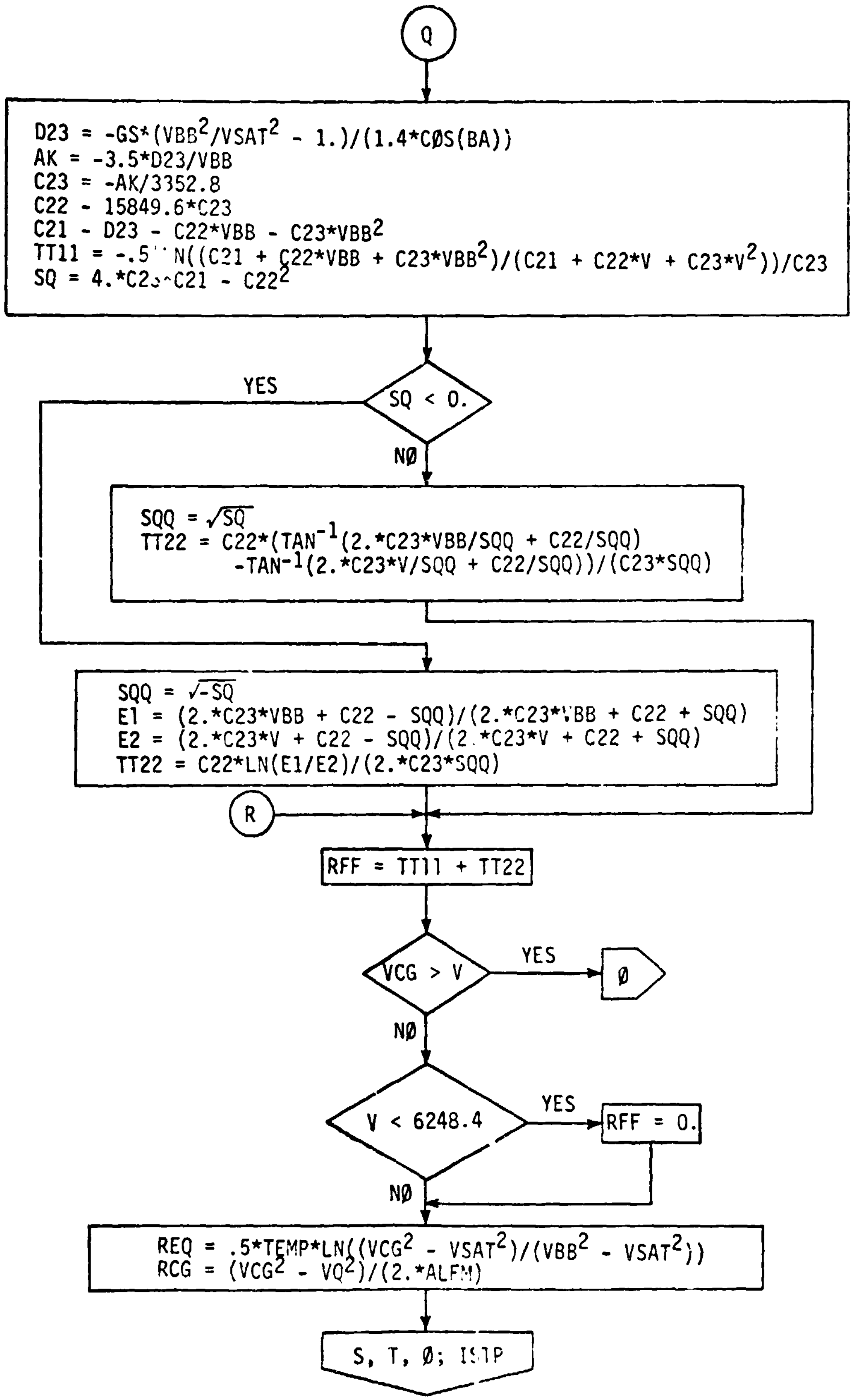

Figure A-2.- Continued.

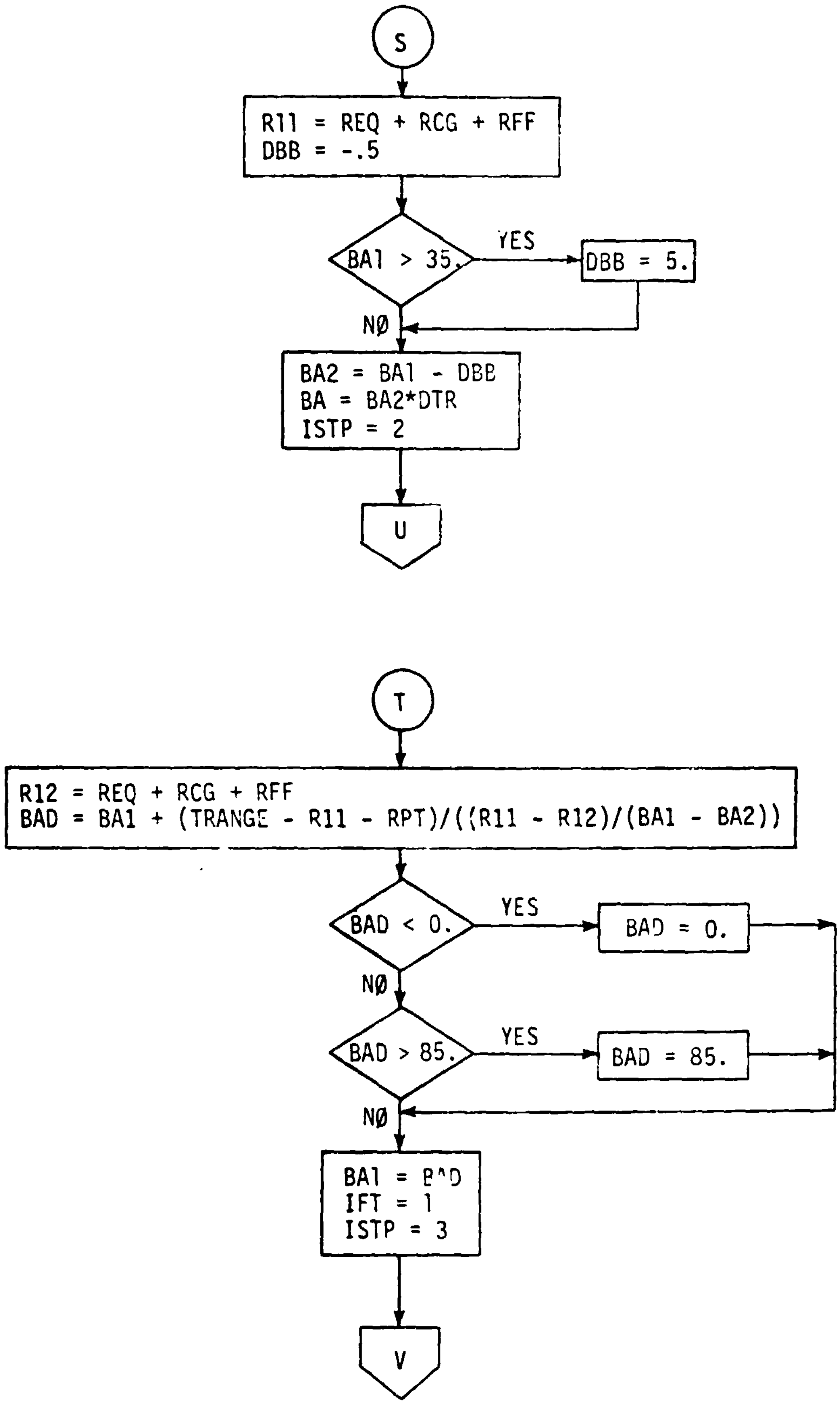

Figure A-2.– Continued.

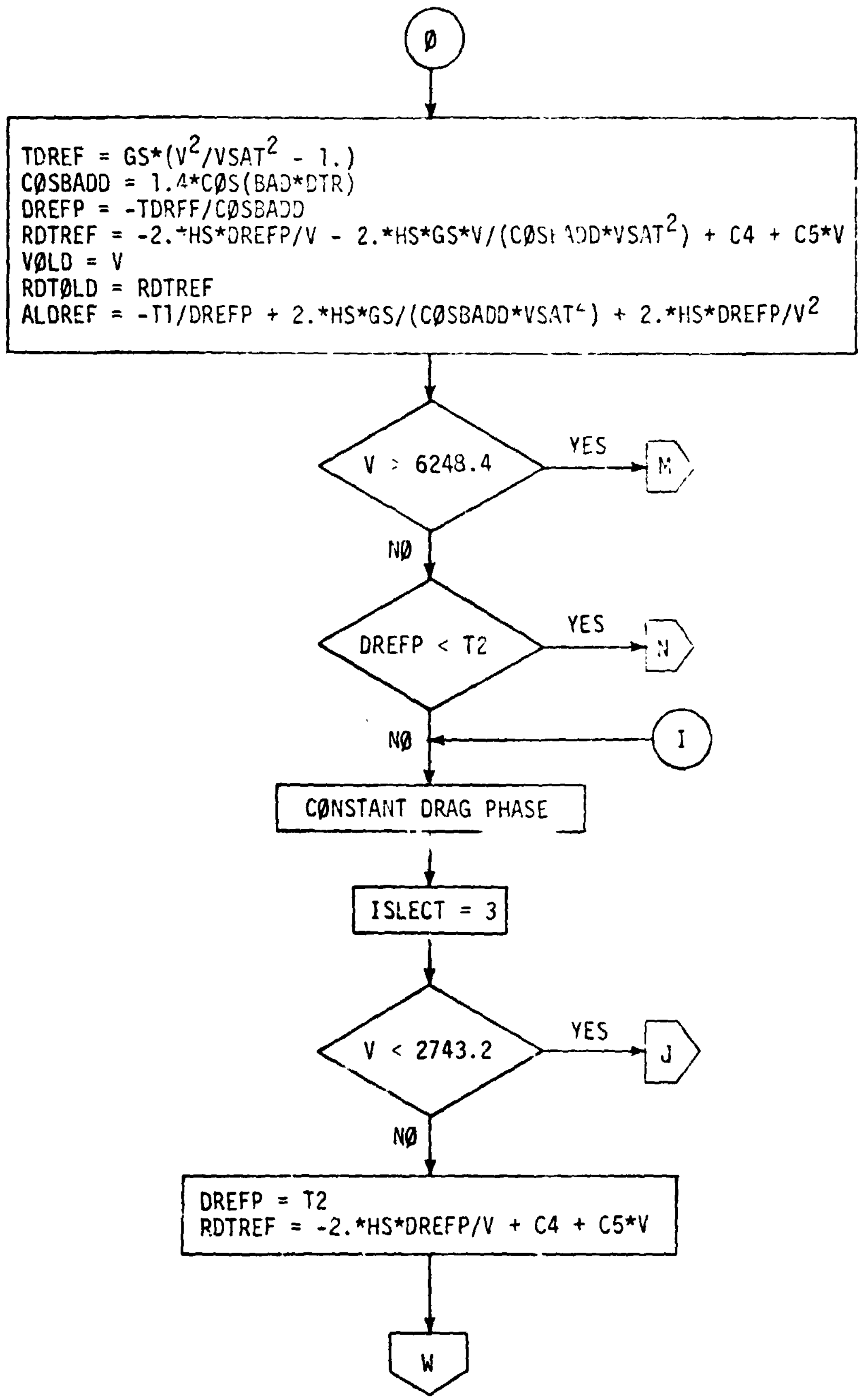

Figure A-2.– Continued.

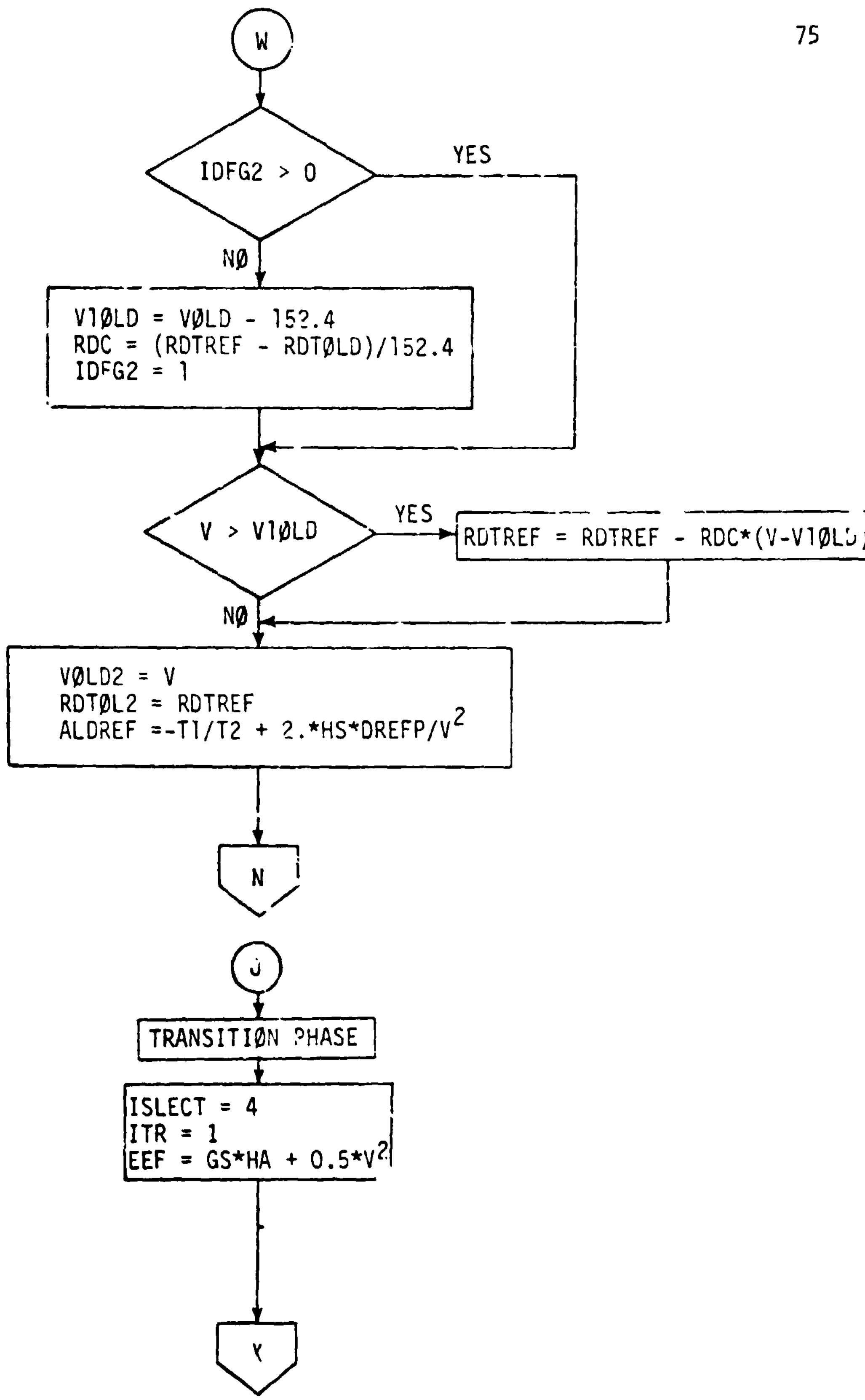

Figure A-2.- Continued.

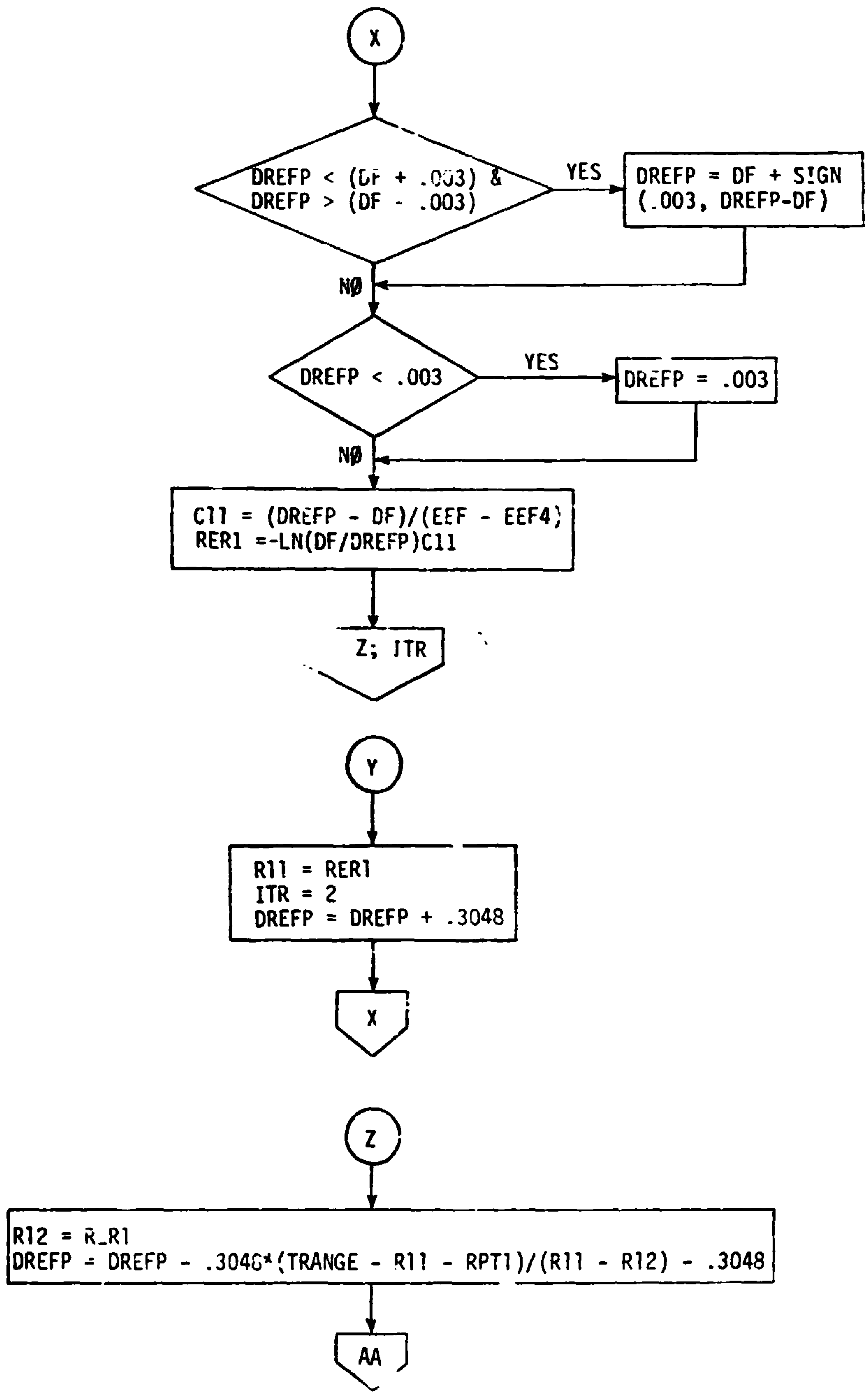

Figure A-2.- Continued.

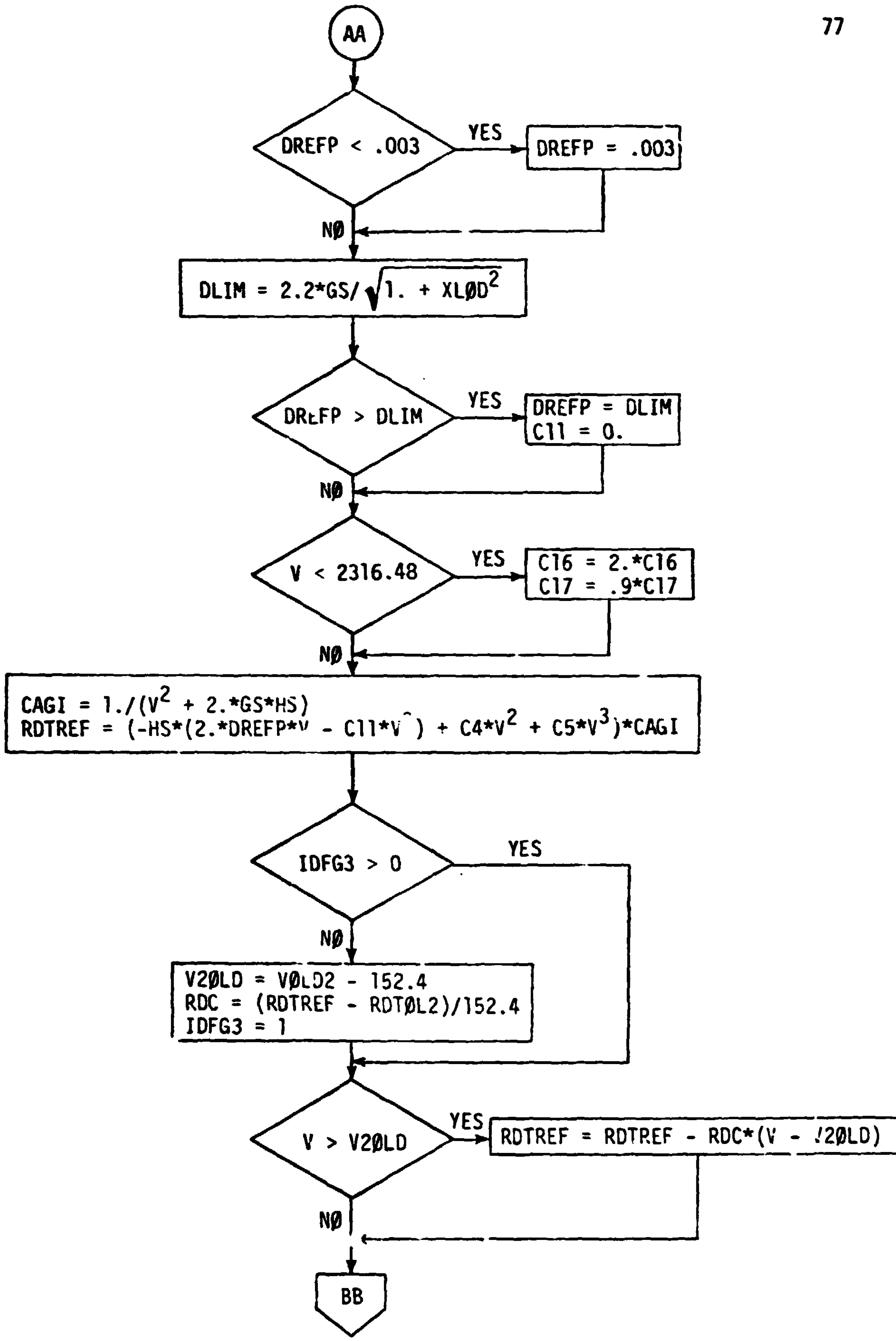

Figure A-2.- Continued.

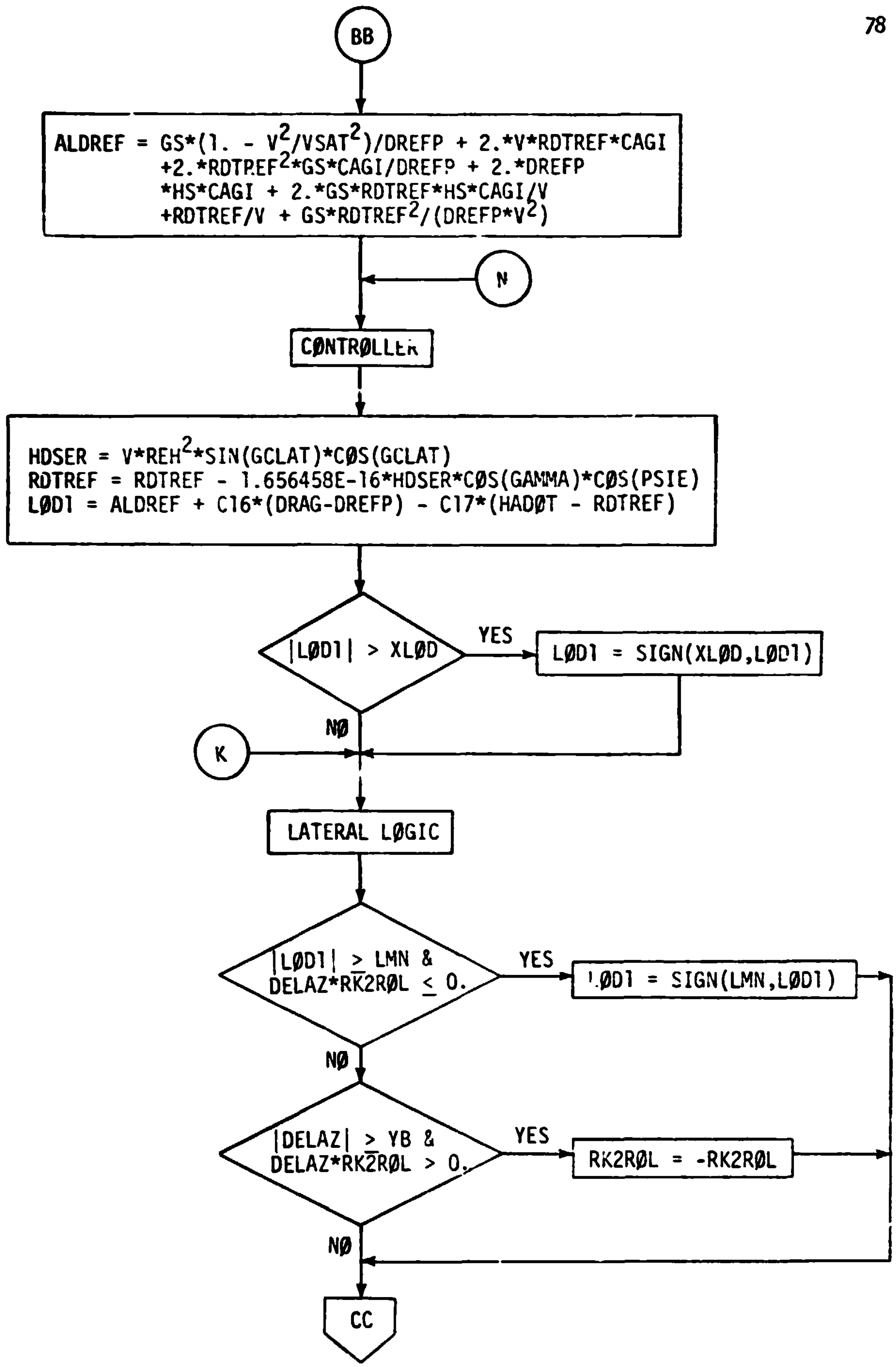

Figure A-2.- Continued.

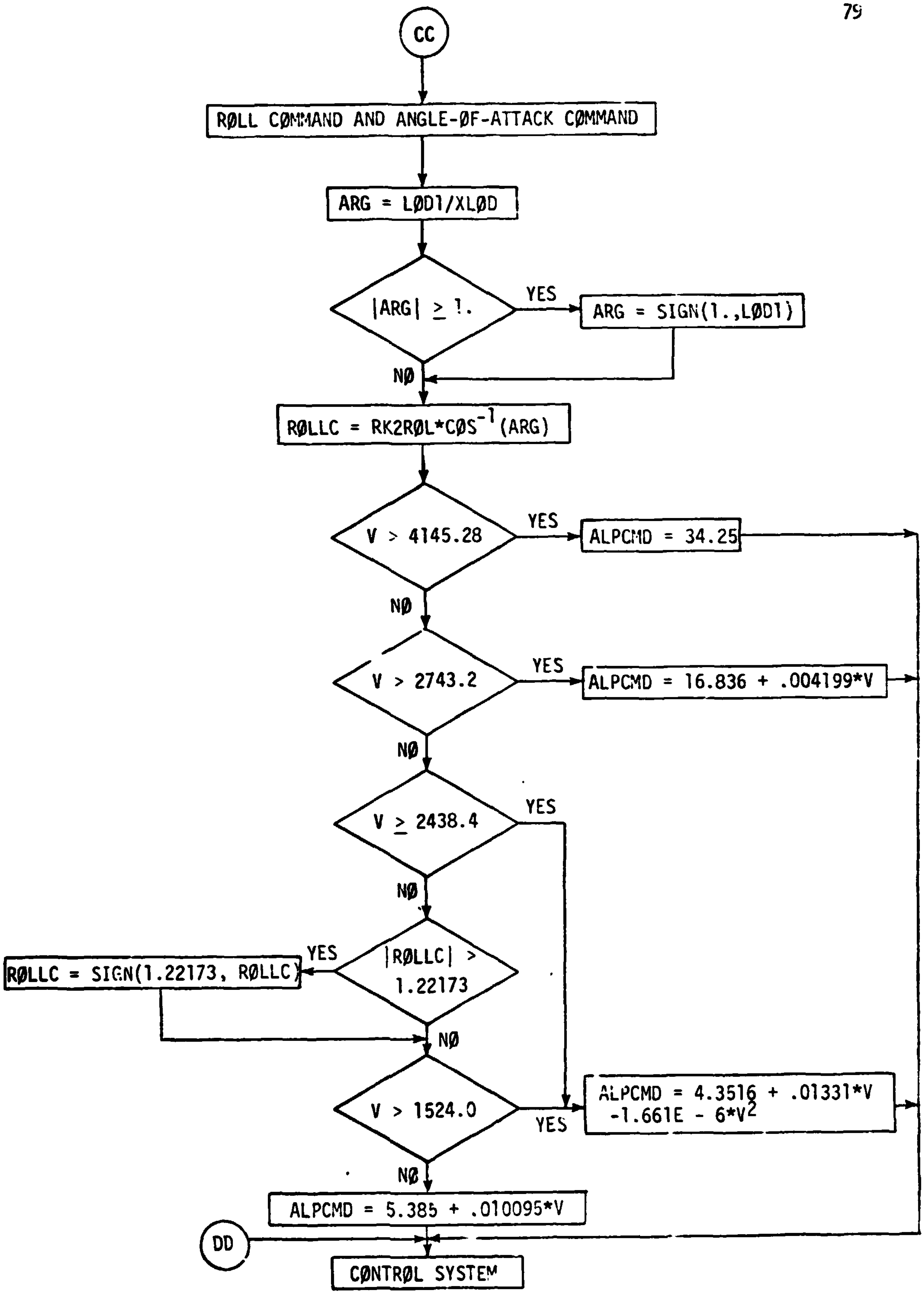

Figure A-2.- Concluded.

XIII. APPENDIX B

Digital Autopilot

The Digital Autopilot (DAP) is designed to automatically fly the space shuttle orbiter from deorbit to the Terminal Area Energy Management (TAEM) interface which occurs at an altitude of approximately 21.3 km (70 000 ft) with a velocity of 457.2 m/sec (1500 ft/sec). The DAP directs both the reaction control system (RCS), and the aerodynamic control surfaces.

The speed brake (δ_{SB}) and body flap (δ_{BF}) deflection schedules are shown in figure B-1, where δ_{SB} is determined from a preset velocity schedule and δ_{BF} is dependent on the center-of-gravity location. Figures B-2 through B-11 are block diagrams of the various elements of the DAP. Two types of signal limiting filters are used in this autopilot. The first type is illustrated below:

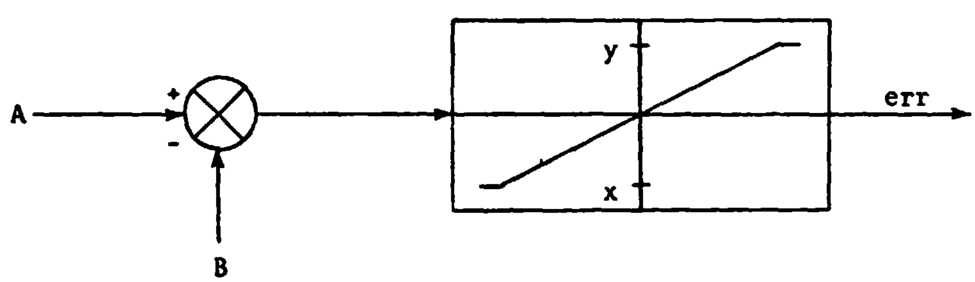

This filter limits the value of the quantity (A-B) to be between x and y. The second type, called a "hysteresis filter," can appear in one of two ways:

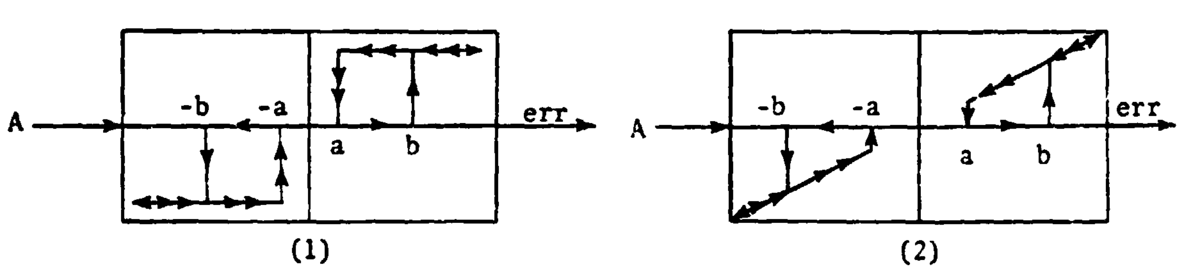

As A increases from zero, "err" remains zero until point "b" is reached. At this time, "err" becomes the value indicated (either a constant value if filter is type 1 or equal to A if filter is type 2), and continues as A increases. As A starts to decrease, it remains the value indicated until point "a" is reached, where "err" becomes zero again. A similar situation would exist for an A decreasing from zero.

The elevons are used for both elevator (δ_e) and aileron (δ_a) functions. The elevator command block diagram is shown in figure B-2. The aileron functions in one of two ways depending on the flight regime: for $\alpha < 18^\circ$ and $M < 5$, the aileron is used for roll attitude (ϕ) control, figure B-3(a); when these conditions are not present, the ailerons are used for turn coordination, figure B-3(b). If the orbiter has a lateral center-of-gravity offset, the number of positive yaw (roll) thruster firings will not equal the number of negative yaw (roll) thruster firings due to the induced sideslip. By counting the number of positive and negative yaw and roll thruster firings, it is possible to establish the "steady state" aileron deflection required to offset this induced sideslip. This is the role of the "up-down counter" shown in figure B-4. The number in parentheses in the block diagrams are the expressed values in English units. Figure B-5 shows that the commanded left and right elevon deflections are functions of δ_e, $\delta_{a,c}$, and $\delta_{e,c}$. The rudder (δ_r), figure B-6, is used for turn coordination when the aileron is used for roll control. If the ailerons are being used for turn coordination, the rudder is inoperative.

The pitch RCS, figure B-7, is operative for $\bar{q}$ less than 958 Pa (20 psf). In this regime it is used, along with the elevator, for longitudinal control.

The roll RCS, figure B-8, is operative for $\bar{q}$ less than 479 Pa (10 psf) and is used, along with the ailerons, for turn coordination.

The yaw RCS, figure B-9, is operative throughout the entry until TAEM and serves one of two purposes depending on the flight conditions. If the ailerons are used for attitude control, the yaw RCS, figure B-9(a), aids the rudder in maintaining turn coordination. If the conditions are such that the ailerons are used for turn coordination, the yaw RCS, figure B-9(b), is used for roll attitude (ϕ) control.

To integrate the linear first order differential equation in the control system, a convolution technique is used. This is a one-pass scheme that has demonstrated a high degree of accuracy in other real-time simulations, including piloted simulations. To illustrate, refer to figure B-10, which shows a typical first order system, $\dot{x}(t) + W\,x(t) = U(t)$ where $U(t)$ is the forcing function. The solution is

$$x(t) = e^{-Wt}\,x(0) + \int_0^t e^{-W(t-\tau)}\,U(\tau)\,d\tau$$

The convolution technique is a numerical method based on a Taylor series approximation (first two terms) of the forcing function, U, and results in the following difference equation:

$$x(t_k+h) = P(h)\, x(t_k) + Q(h)\, \bar{U}(t_k)$$

where $P(h) = e^{-Wh}$

$$Q(h) = [q_1(h), q_2(h)]$$

$$\bar{U}(t_k) = \begin{bmatrix} U(t_k) \\ \dot{U}(t_k) \end{bmatrix}$$

$$q_1(h) = \int_0^h e^{-W(h-\tau)}\, d\tau = (1 - e^{-Wh})/W = (1 - P)/W$$

$$q_2(h) = \int_0^h \tau e^{-W(h-\tau)}\, d\tau = (-1 - e^{-Wh} + Wh)/W^2 = (h - q_1)/W$$

The control actuators, figure B-11, are handled the same way, except that provisions are made for both position and rate limits.

The RCS model uses the following equations to account for aerodynamic interference:

$$L_{RCS} = L_{RJ}\ [(RJP - RJN)\, K_L + (YJP - YJN)\, C_{LN}]$$

$$M_{RCS} = M_{PJ}\ [(PJP)\, K_{MU} - (PJN)\, K_{MD} + (YJP + YJN)\, C_{MN} + (RJP + RJN)\, C_{ML}]$$

$$N_{RCS} = M_{YJ}\ [(YJP - YJN)\, K_N + (RJP - RJN)\, C_{NL}]$$

The values for the coefficients are shown in Table B-I.

SYMBOLS

Parameter	Unit	Definition
a_y	m/sec^2	side acceleration at center of gravity
c_e	m	elevon reference chord
c_r	m	rudder reference chord
C_{he}	n.d.	elevon hinge moment coefficient
C_{h_β}	n.d.	∂(rudder hinge moment)/$\partial\beta$
$C_{h_{\delta_r}}$	n.d.	∂(rudder hinge moment)/$\partial\delta r$
C_{LN}	n.d.	rolling moment coefficient due to yaw RCS
C_{ML}	n.d.	pitching moment coefficient due to roll RCS
C_{MN}	n.d.	pitching moment coefficient due to yaw RCS
C_{NL}	n.d.	yawing moment coefficient due to roll RCS
DEMX	deg/sec	maximum elevon rate
DRMX	deg/sec	maximum rudder rate
E_P	n.d.	pitch RCS error signal
E_R	n.d.	roll RCS error signal
E_Y	n.d.	yaw RCS error signal
$f(\delta e)$	deg	function of δe used to limit $\delta_{a,c}$
g	m/sec^2	acceleration due to gravity
h	sec	integration step size
H_{m_e}	N·m	elevon hinge moment
H_{m_r}	N·m	rudder hinge moment
K_L	n.d.	rolling moment RCS amplification factor
K_{MD}	n.d.	pitching moment RCS amplification factor due to down firing jets
K_{MU}	n.d.	pitching moment RCS amplification factor due to up firing jets

K_p	n.d.	aileron gain
K_α	n.d.	elevator gain
K_{δ_r}	n.d.	rudder gain
L_{RCS}	N•m	rolling moment due to RCS
L_{RJ}	N•m	ideal rolling moment due to firing of 1 roll jet
M	n.d.	Mach number
M_{PJ}	N•m	ideal pitching moment due to firing of 1 pitch jet
M_{RCS}	N•m	pitching moment due to RCS
N_{RCS}	N•m	yawing moment due to RCS
N_{YJ}	N•m	ideal yawing moment due to firing of 1 yaw jet
p	deg/sec	roll rate
P	n.d.	convolution coefficient
PJN	n.d.	number of negative pitch jets firing
PJP	n.d.	number of positive pitch jets firing
q	deg/sec	pitch rate
$\bar{q}$	Pa	dynamic pressure
q_1	sec	convolution coefficient
q_2	sec^2	convolution coefficient
Q		vector of convolution coefficients
r	deg/sec	yaw rate
r'	deg/sec	$r-(180\ g \sin\phi \cos\theta)/\pi V_R$
RJN	n.d.	number of negative roll jets firing
RJP	n.d.	number of positive roll jets firing
s		Laplacian operator
S_e	m^2	elevon reference area
S_r	m^2	rudder reference area

t	sec	time
t_k	sec	time at the k^{th} sample
$U(t)$		convolution forcing function
$\overline{U}$		vector of forcing function terms
$\dot{U}(t)$		dU/dt
V	m/sec	atmospheric relative velocity
Vr	m/sec	earth relative velocity
W	sec^{-1}	filter root
$x(t)$		convolution state variable
$\dot{x}(t)$		dx/dt
y	m	lateral offset
YJN	n.d.	number of negative yaw jets firing
YJP	n.d.	number of positive yaw jets firing
α	deg	angle of attack
α_c	deg	commanded angle of attack from guidance system
β	deg	angle of sideslip
θ	deg	pitch angle
ϕ	deg	roll angle
ϕ_c	deg	commanded roll angle to control system
δ_a	deg	aileron deflection
$\delta_{a,c}$	deg	commanded aileron deflection
$\delta_{a,UD}$	deg	commanded aileron deflection from up-down counter
δ_{BF}	deg	body flap deflection
δ_e	deg	elevator deflection
$\delta_{e,c}$	deg	commanded elevator deflection
$\delta_{e\ell}$	deg	left elevon panel deflection
$\delta_{e\ell,c}$	deg	command left elevon panel deflection

$\dot{\delta}_{e,\ell m}$	deg	maximum change in elevon command allowed by rate limit
δ_{er}	deg	right elevon panel deflection
$\delta_{er,c}$	deg	commanded right elevon panel deflection
$\delta_{e,t}$	deg	initial elevator setting
δ_r	deg	rudder deflection
$\delta_{r,c}$	deg	commanded rudder deflection
$\delta_{r,\ell m}$	deg	maximum change in rudder command allowed by rate limit
δ_{SB}	deg	speed brake deflection
τ	sec	variable of integration

TABLE B-I.- INTERFFRENCE RCS VALUES

Jet Moment	Value
L_{RJ}	11185.5
M_{PJ}	38325.6
N_{YJ}	38878.8

$\bar{q}$ (Pa)	K_L	K_{MU}	K_{MD}	K_N	C_{LN}	C_{MN}	C_{ML}	C_{NL}
0	.746	1.0	.740	1.02	-.624	0	.130	-.141
119.7	.688	1.0	.678	1.02	-.9[illegible]3	.038	.161	-.115
239.4	.630	1.0	.616	1.02	-1.069	.076	.192	-.111
478.8	.533	1.0	.541	1.02	-1.069	.114	.230	-.111
718.2	.475	1.0	.512	1.02	-1.069	.133	.244	-.111
957.6	.436	1.0	.493	1.02	-1.069	.152	.253	-.111

$\bar{q} > 957.6$ Pa

M	K_N	C_{LN}	C_{MN}
2	1.02	- .701	.076
5	1.02	- .934	.076
10	1.02	-1.166	.076
30	1.02	-1.069	.152

BODY FLAP, δ_{BF}, SCHEDULE

Forward c.g.	$\delta_{BF} = -11.7^{\circ}$
Aft c.g.	$\delta_{BF} = 16.3^{\circ}$

SPEED BRAKE, δ_{SB}, SCHEDULE

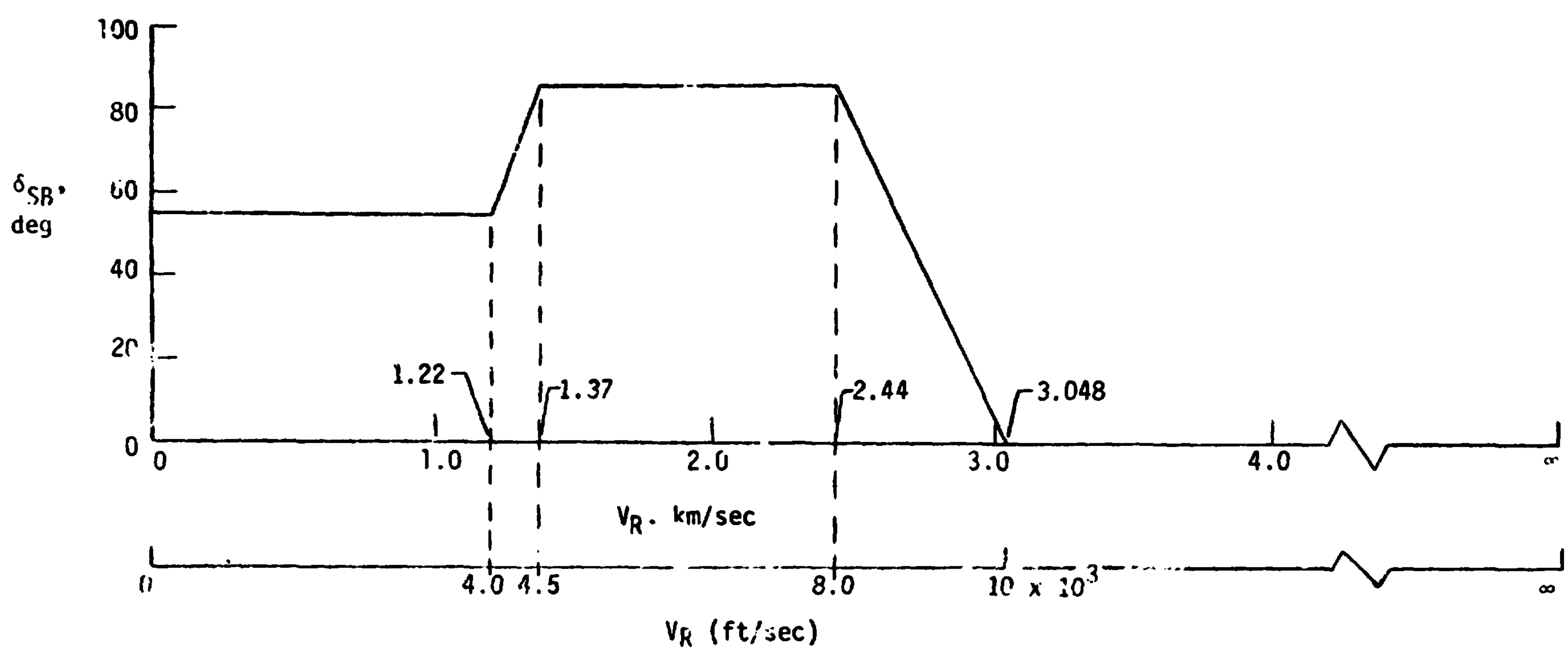

Figure B-1.- Booy flap and speed brake schedules.

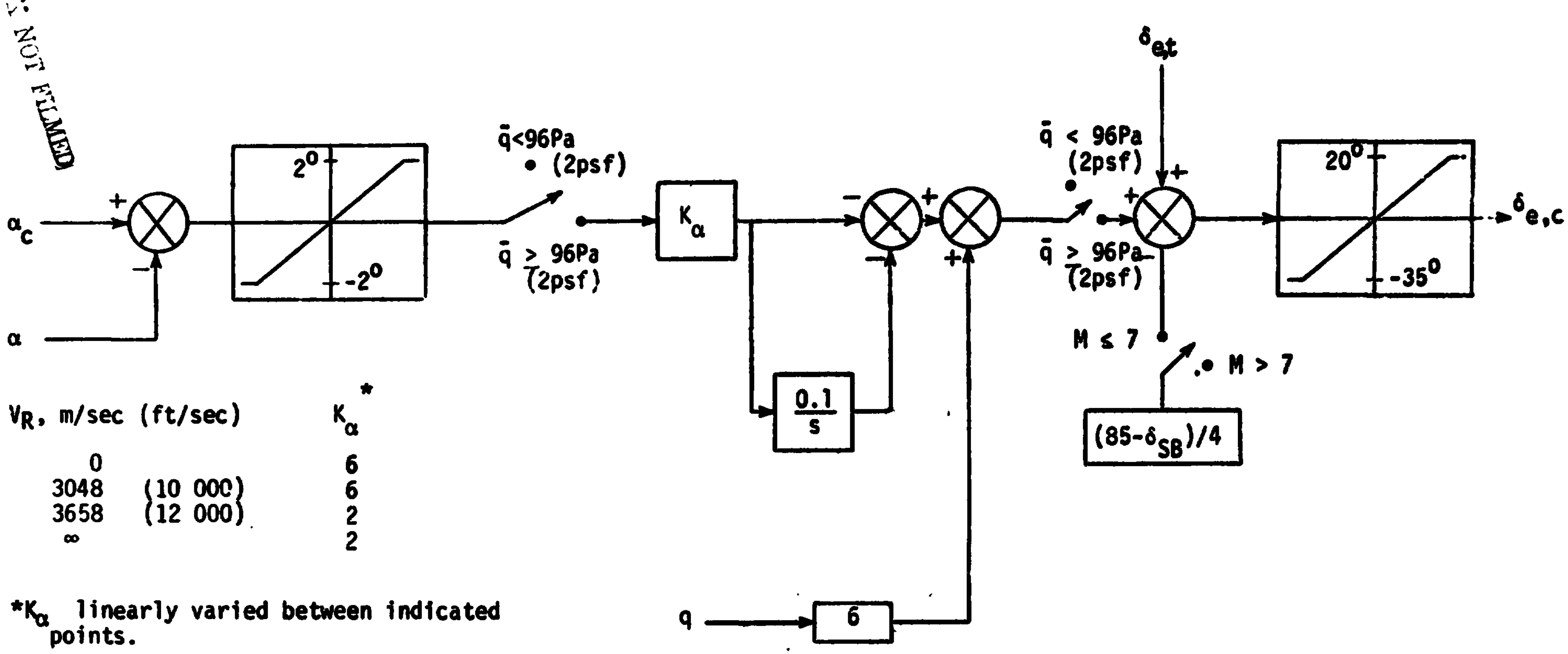

V_R, m/sec (ft/sec)		K_α*
0		6
3048	(10 000)	6
3658	(12 000)	2
∞		2

*K_α linearly varied between indicated points.

Figure B-2.- Elevator command block diagram.

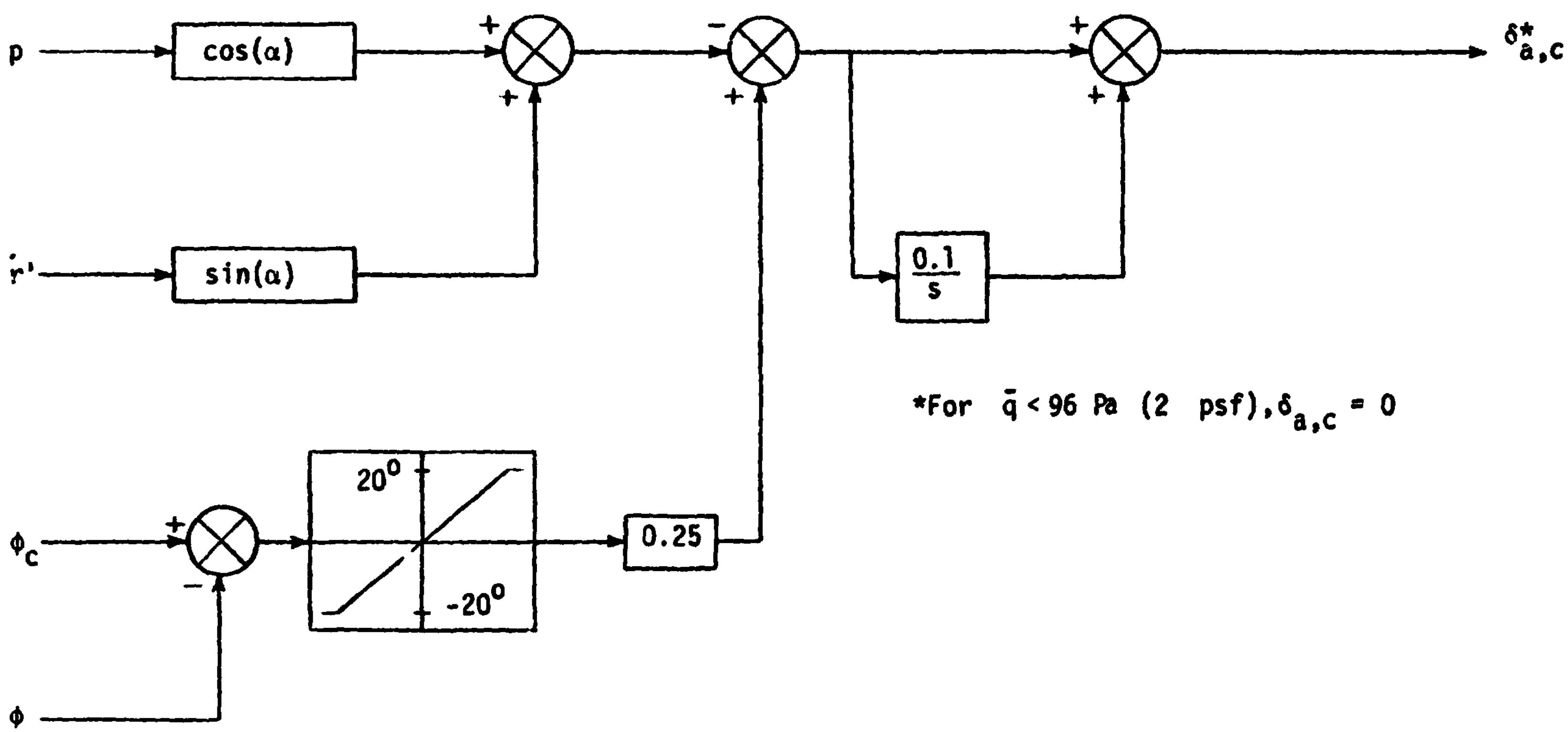

(a) $\alpha \leq 18°$ and $M \leq 5$.

Figure B-3.- Aileron command block diagram.

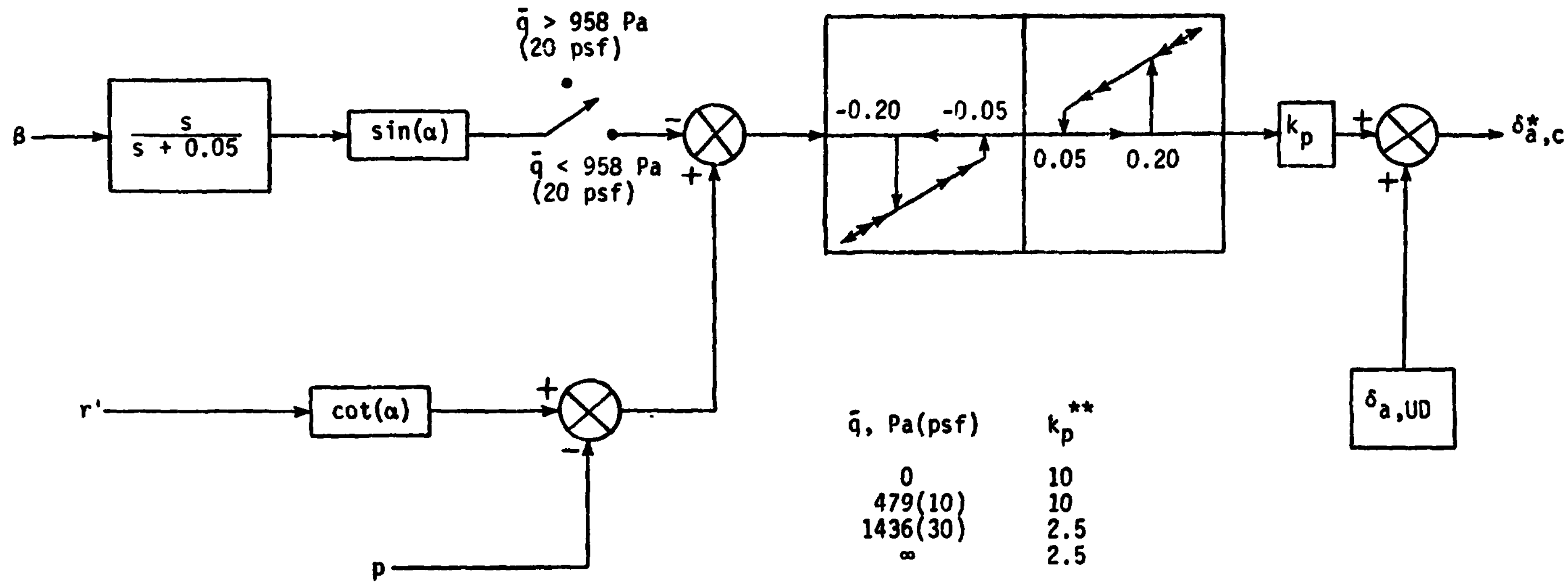

$\bar{q}$, Pa(psf)	k_p**
0	10
479(10)	10
1436(30)	2.5
∞	2.5

*For $\bar{q}$ < 96 Pa (2 psf), $\delta_{a,c} = 0$

**k_p linearly varied between indicated points.

b) $\alpha > 18°$ or $M > 5$.

Figure B-3.- Concluded.

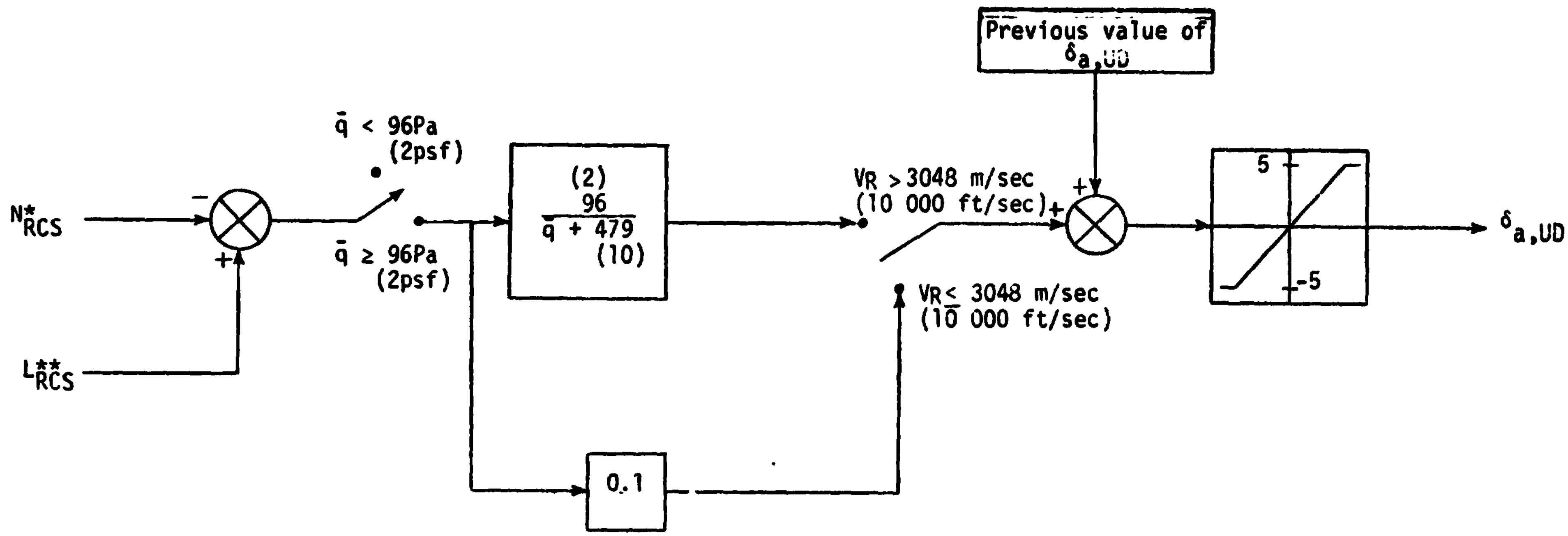

*Number of yaw jets that came on (+ for positive jet, - for negative jet).

**Number of roll jets that came on (+ for positive jet, - for negative jet).

Figure B-4.- Up-down counter block diagram.

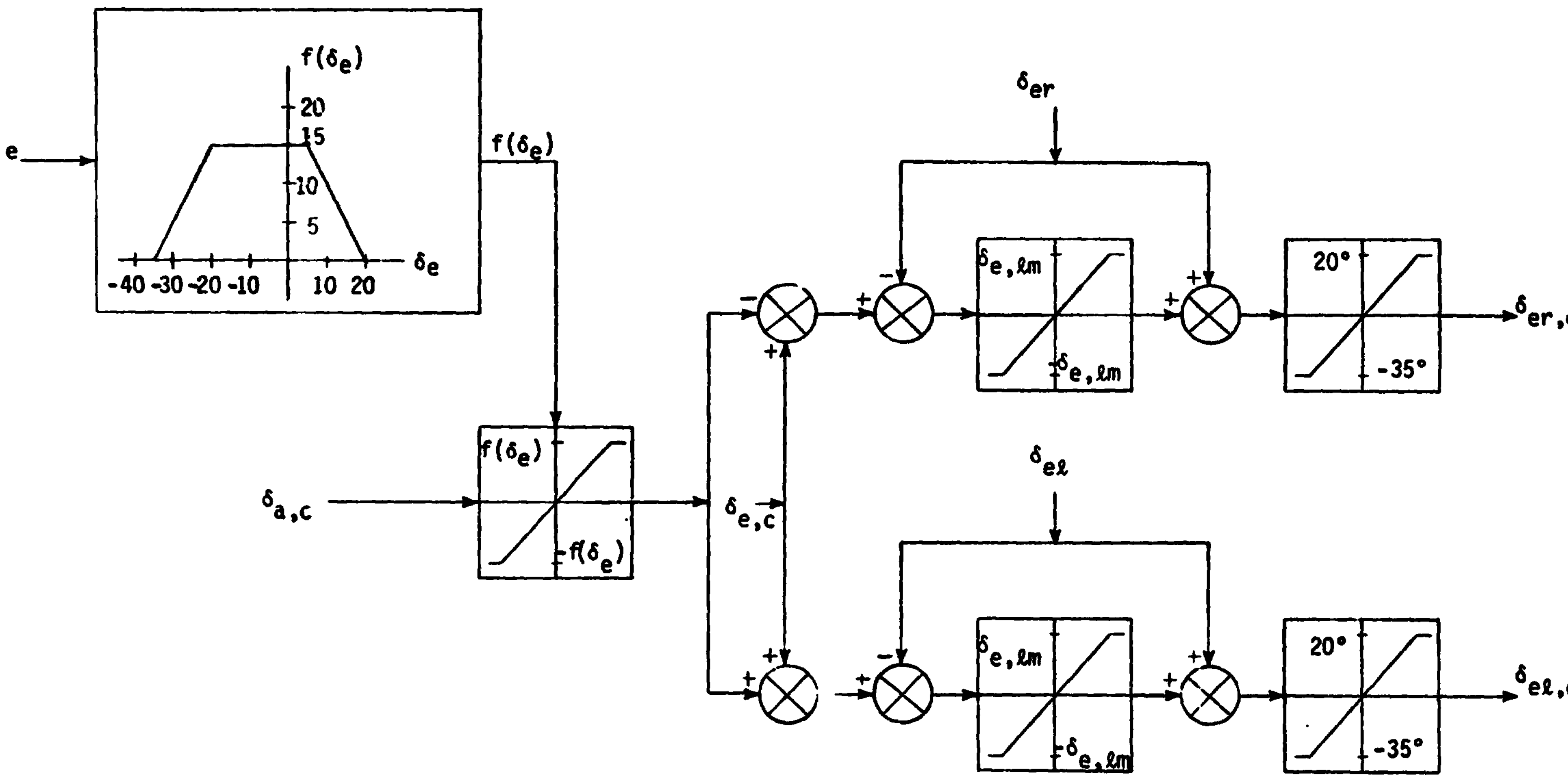

Figure B-5.- Right and left elevon panel commands.

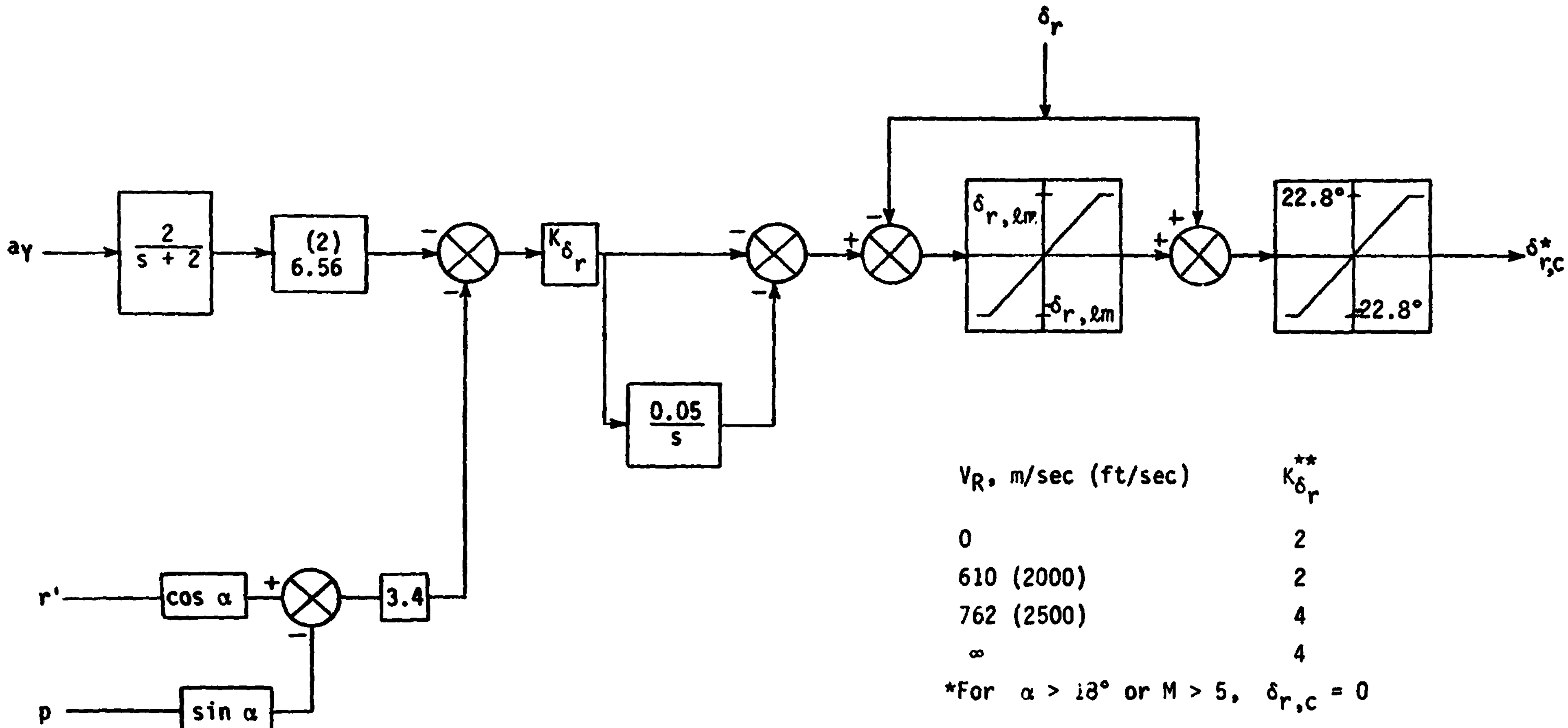

V_R, m/sec (ft/sec)	$K^{**}_{\delta_r}$
0	2
610 (2000)	2
762 (2500)	4
∞	4

*For $\alpha > 18°$ or $M > 5$, $\delta_{r,c} = 0$

**K_{δ_r} linearly varied between indicated points.

Figure B-6.- Rudder command block diagram.

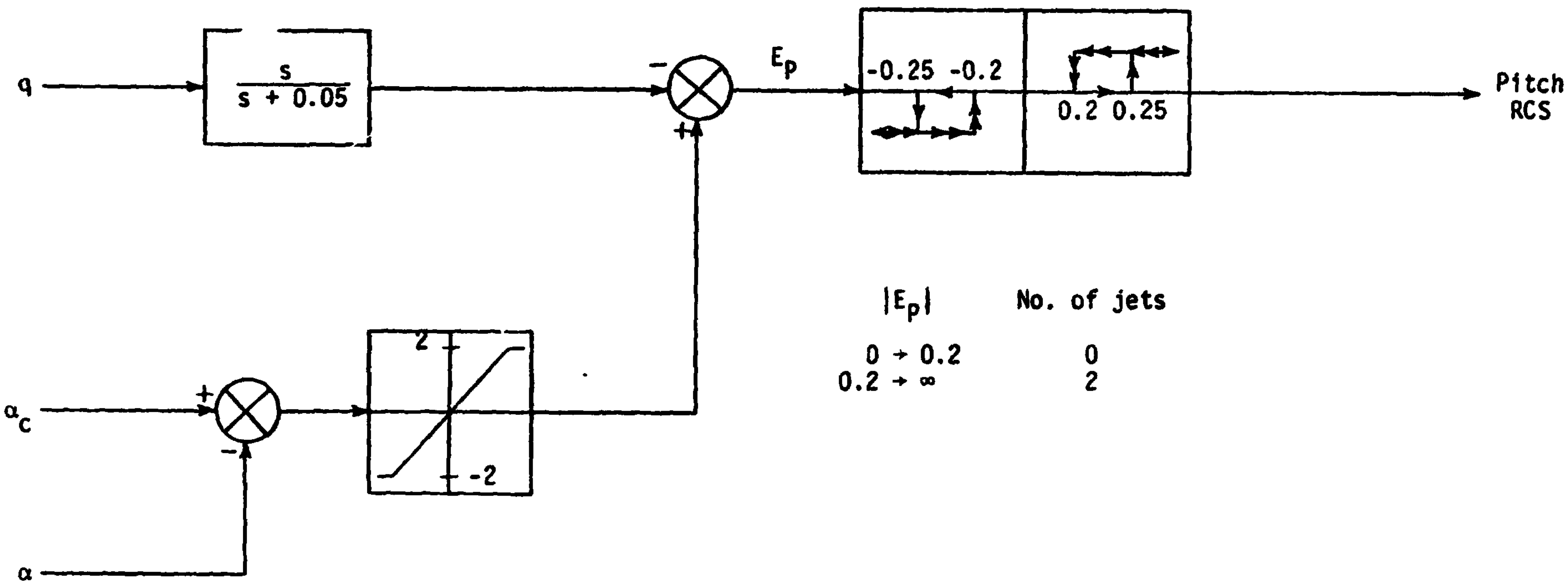

$\lvert E_p \rvert$	No. of jets
0 → 0.2	0
0.2 → ∞	2

Figure B-7.- Pitch RCS error signal block diagram.

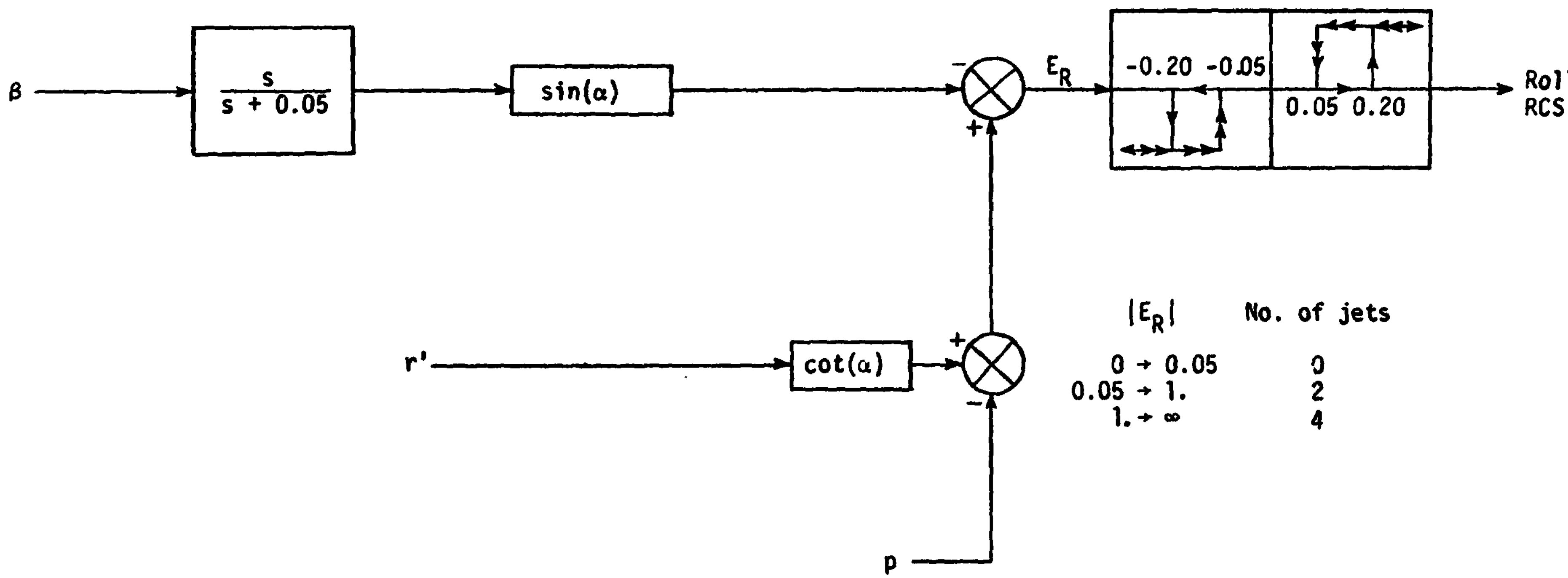

$\lvert E_R \rvert$	No. of jets
$0 \to 0.05$	0
$0.05 \to 1.$	2
$1. \to \infty$	4

Figure B-8.- Roll RCS error signal block diagram.

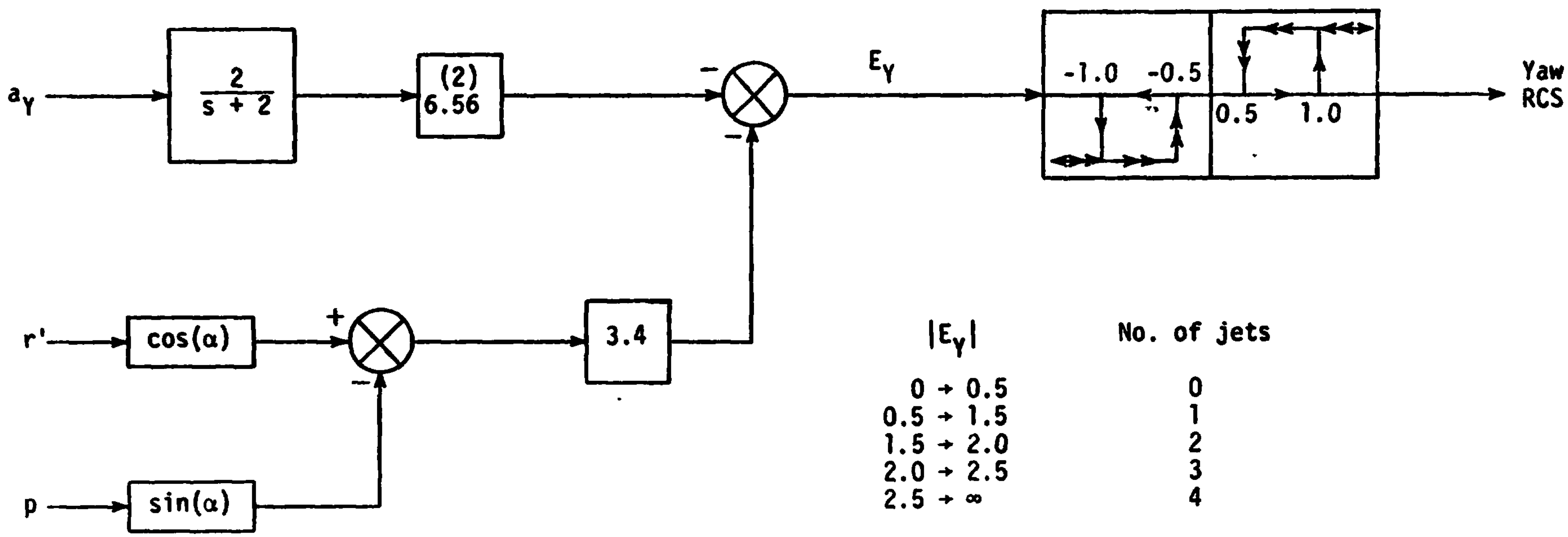

$\lvert E_Y \rvert$	No. of jets
0 → 0.5	0
0.5 → 1.5	1
1.5 → 2.0	2
2.0 → 2.5	3
2.5 → ∞	4

(a) $\alpha \leq 18°$ and $M \leq 5$.

Figure B-9.- Yaw RCS error signal block diagram.

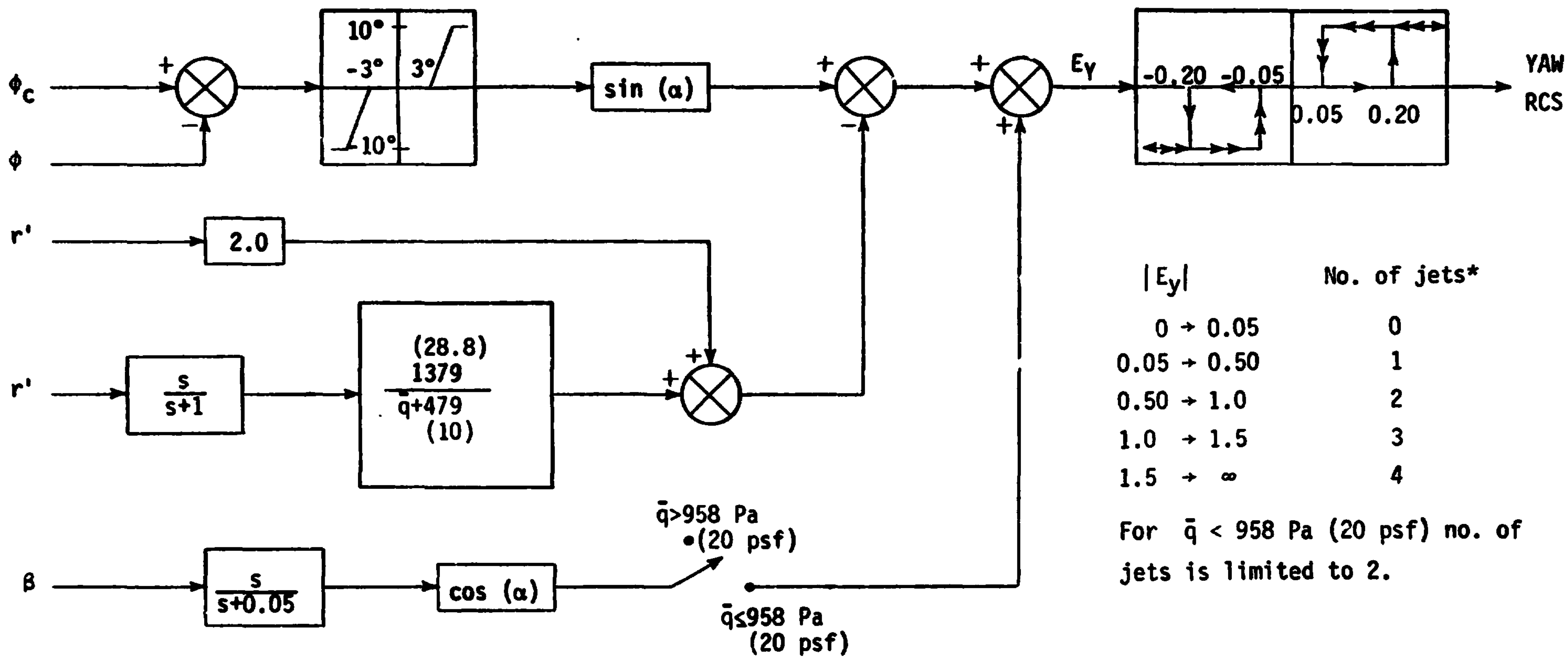

$\lvert E_y \rvert$	No. of jets*
0 → 0.05	0
0.05 → 0.50	1
0.50 → 1.0	2
1.0 → 1.5	3
1.5 → ∞	4

*For $\bar{q}$ < 958 Pa (20 psf) no. of jets is limited to 2.

b) α>18° or M>5

Figure B-9. Concluded.

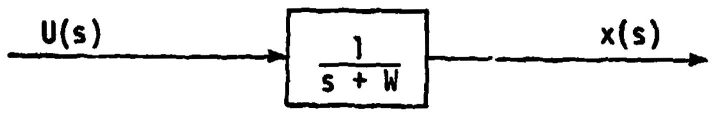

$$x(t_k + h) = P\, x(t_k) + q_1\, U(t_k) + q_2\, \dot{U}(t_k)$$

$$\dot{x}(t_k + h) = U(t_k + h) - W\, x(t_k + h)$$

where

$$P = e^{-Wh}$$

$$q_1 = (1 - P)/W$$

$$q_2 = (h - q_1)/W$$

Figure B-10.- First order system.

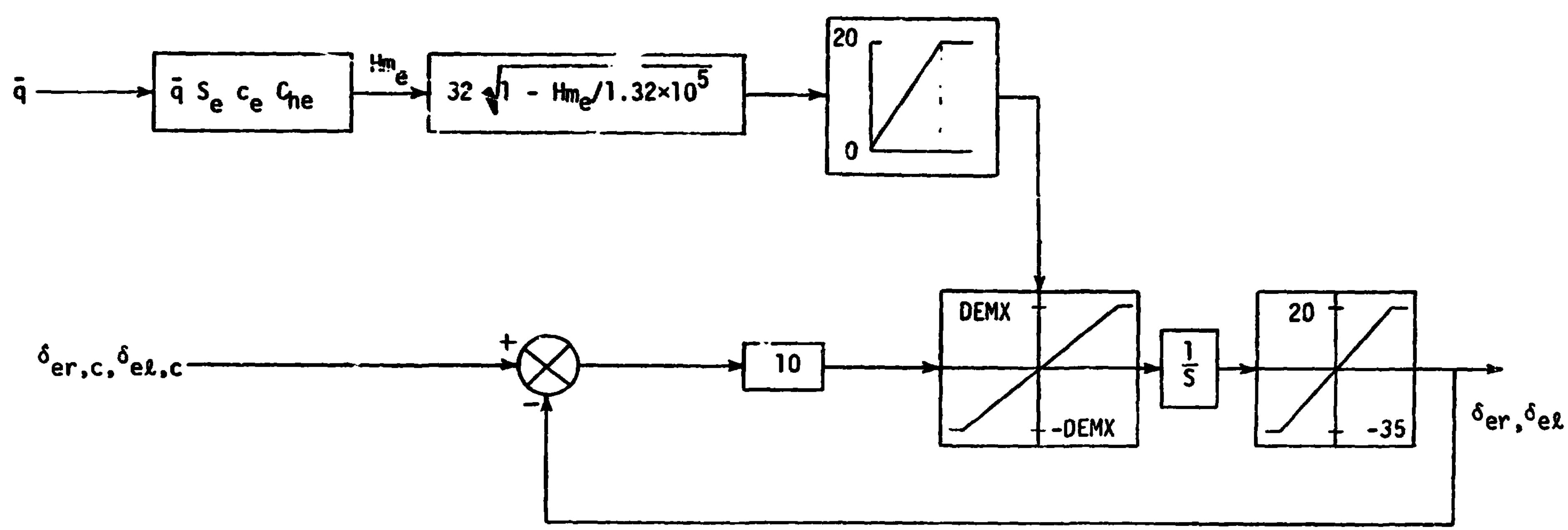

(a) Elevon.

Figure B-11.- Actuator block diagrams.

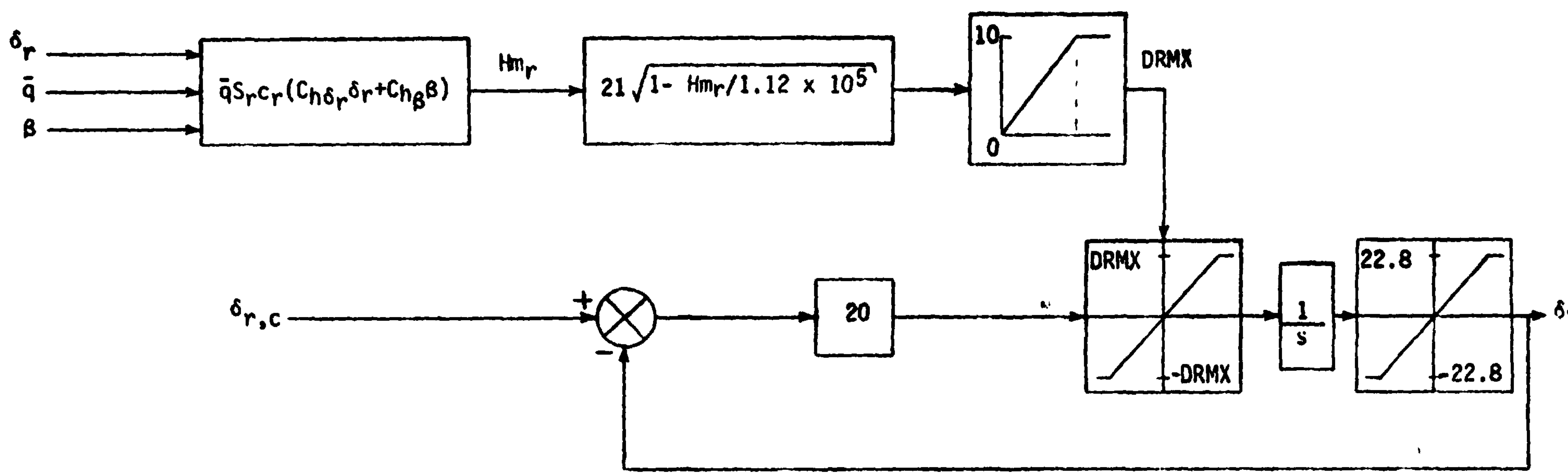

b) Rudder.

Figure B-11.—Concluded.